DANMARKS OG GRØNLANDS GEOLOGISKE UNDERSØGELSE RAPPORT 2011/131

Evaluation and interpretation of geophysical data from the Røros and Meråker districts, Norway

Report prepared for Intex Resources ASA

T. M. Rasmussen

(1 DVD included)

GEOLOGICAL SURVEY OF DENMARK AND GREENLAND
MINISTRY OF CLIMATE AND ENERGY

DANMARKS OG GRØNLANDS GEOLOGISKE UNDERSØGELSE RAPPORT 2011/131

Evaluation and interpretation of geophysical data from the Røros and Meråker districts, Norway

Report prepared for Intex Resources ASA

T. M. Rasmussen

(1 DVD included)

Confidential report

Copy No.

Not to be released

GEOLOGICAL SURVEY OF DENMARK AND GREENLAND
MINISTRY OF CLIMATE AND ENERGY

GEUS

Contents

1. Executive summary

Airborne geophysical survey data from the Røros and Meråker districts are presented and analysed with the purpose of outlining areas of interest for hosting Zn and Cu mineralisations.

Target locations/areas for ground follow-up have been identified from visual inspection of the data. Target areas are presented together with the arguments for the choices made. The locations are provided by a centre/peak location and a polygon encompassing the area of interest. Next, prioritising for a ground follow-up has been based on an evaluation of the data. The locations are provided in digital format in an Excel and ArcView SHP shapefile formats. Maps with target locations are provided in digital format.

In total 72 locations are identified for ground follow-up from the Røros survey data and 44 locations are identified from the Meråker survey data.

2. Introduction

This report is produced for Intex Resources ASA. The purpose is analyses of geophysical data from the Røros and Meråker districts in central Norway in relation to potential mineralisations. The mineralisations of particular interest in these two areas are Zn and Cu (see e.g. Grenne *et al.* 1999). Airborne geophysical survey data are available from both areas and include magnetic field recordings, frequency domain EM (Aerodat system), VLF and gamma-spectrometry. Detailed ground geophysical data are available from a number of areas within the Røros district. Assay data from a number of localities exist within the survey area. Geological information about previous mine sites are accessible from the Geological Survey of Norway (NGU) at www.ngu.no.

The data sets utilised for this report contains a huge amount of information, and the interpretations and processing presented in this report is restricted in terms of applied techniques due to time constraints for the project work. Emphasis has been placed on providing an overview of the entire airborne data set simultaneously with an attempt to provide target areas for ground follow-up work. The exploration model is basically a search for good electrical conductor associated with sulphides. The approach used for target definitions builds on various types of data processing combined with visual inspection and evaluation of the data characteristics. The target definitions are based partly on an analysis of correlation between various data types. Modelling of the electromagnetic data with the aim of providing conductivity-depth sections over target areas is not included for this report due to time limitations, but this type of quantitative analysis should be considered for future work.

The report contains a short description of the data with some comments on data quality that needs to be considered, when processing the data. Then follows descriptions of the applied data processing techniques and results are presented as maps and in tables. Targets areas are presented together with the arguments for the particular choices that are made. Coordinates for target areas are provided digitally on the accompanying DVD. Maps are also provided digitally on DVD.

The data from Røros and Meråker are presented separately and no attempt has been made to integrate and synthesise the interpretations from the two areas. Maps of the surface geology for the two survey areas are shown in Figures 1 and 2 respectively. The lengend for the geological maps is shown in Figure 3. The maps in Figures 1 and 2 have been provided digitally by Intex Resources for this report and are based on maps produced by NGU in scale 1:50 000 (see www.ngu.no).

Some of the data have been analysed using a Self Organised Map (SOM) approach (Kohonen, 2001, Fraser *et al.* 2007). SOM is a technique for visualising and analysing multivariable data. Appendix A includes a description of this technique, which is used here as a classification tool.

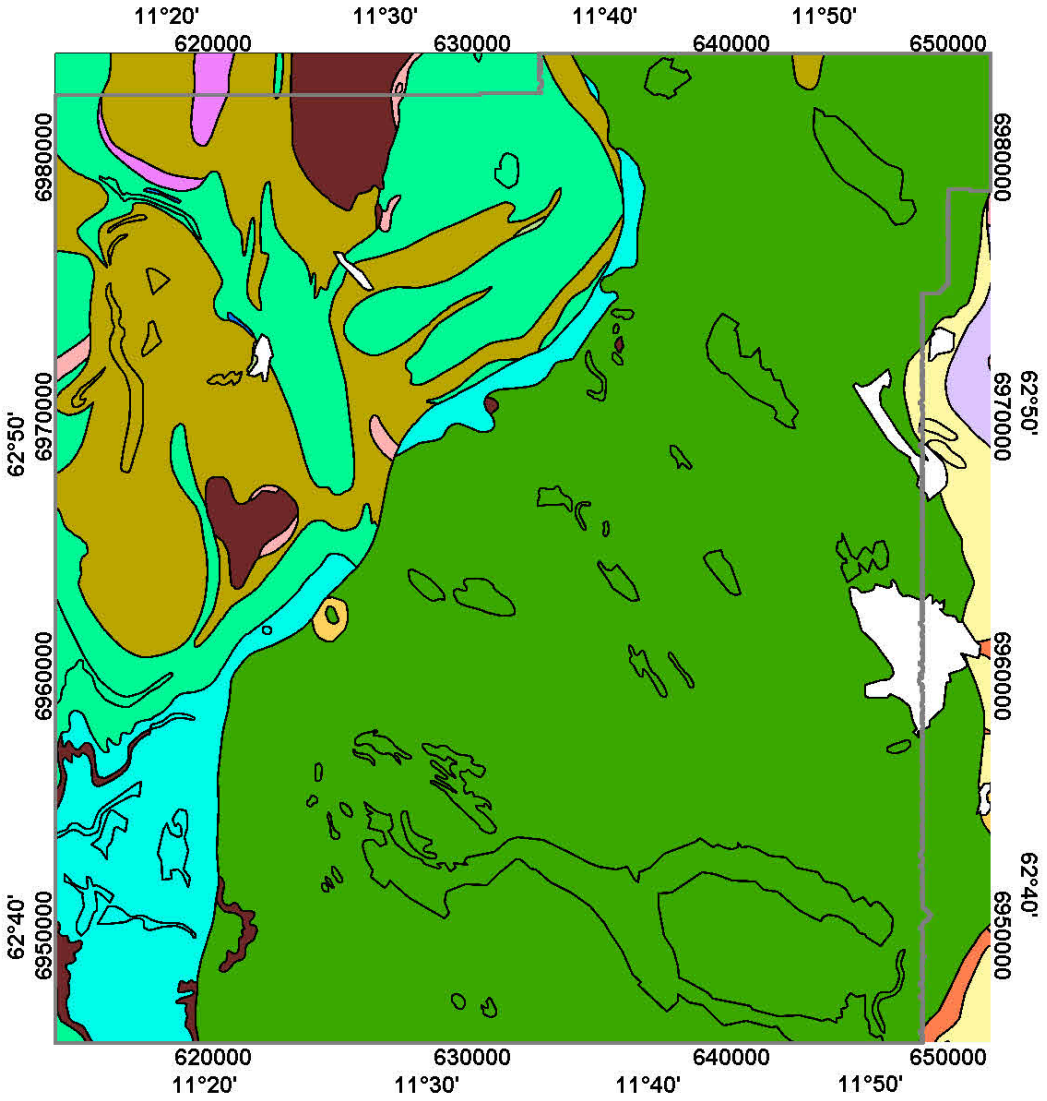

Figure 1. *Geological map of the Røros survey area. The survey boundary is shown by the irregular polygon in grey colour. The legend for the map is displayed in Figure 3.*

Figure 3. *Legend for the geological maps in Figures 2 and 3.*

3. Røros

Appendix B includes an excerpt from a data file description accompanying the airborne survey data. The digital data are provided both as flight line data in ASCII and Geosoft GDB database format, and as interpolated and gridded data of various geophysical parameters. The gridded data are provided in Geosoft map-format. Topographic information (height, rivers and lakes) and information on infrastructure (roads, power lines) are provided as separate layers in the maps.

3.1 Data and data quality

3.1.1 Airborne magnetic data

Total magnetic field intensity (TMI) data were provided for the project as raw and processed line data in both ASCII and Geosoft GDB format. The data base also contains data recordings obtained during flights, when approaching or when leaving the survey target area. The data outside the survey target area are in some cases noisy and survey parameters deviates from the general survey specifications in terms of altitude etc. The average line spacing in the survey area is 200 m and lines are oriented E-W. No tie-lines were available. The magnetic sensor is towed in a bird about 15 m below the helicopter during surveying. The average terrain clearance of the helicopter is about 80 m with a standard deviation of 37 m. Thus, the mean terrain sensor clearance is 65 m. Mean magnetic total field value is 51288 nT for data in the data base and values are in the range from 50145 nT to 98119 nT with a standard deviation of 190 nT. The maximum value of 98119 nT (erroneous data) is found on flight line 1730 at a position outside the target area for the survey.

Interpolated and gridded total magnetic field data are available in Geosoft GRD format with 50 m spatial resolution. A grid of the second vertical derivative of the magnetic field was also provided. Maps in scale 1:50 000 with display of the two grids were provided in digital Geosoft MAP format. The mean value for the total magnetic field grid data is 51283 nT and the data have standard deviation of 163 nT. The data range is from 50416 nT to 53402 nT.

Visual inspections of the maps show that the initial levelling of the magnetic total field data is not optimum. Striations along flight lines can be seen in parts of the maps, which is a clear indication of problems with the levelling. In particular, striations are seen in the northern half of the map. Re-levelling was not possible because no tie-line data are available.

Interpretation of magnetic data often builds on processing of the gridded data by applying filters that enhance short wavelength features. An example is the calculation of the second vertical derivative of the magnetic field. The levelling problems inevitable introduce noise in the output when attempting to enhance short-wavelength features in the data by applying various filters. In order to reduce the influence of the levelling problems, de-corrugation filters were therefore applied to the data in some cases for this report. The de-corrugation filtering is done by subtraction of an error grid from the initial grid, where the error grid is

created by subjecting the initial grid to an 8'th order Butterworth filter with 800 m wavelength high-pass and a cosine directional filter that pass features +/-α degrees from the line direction. The parameters used for the de-corrugation filter were chosen by comparing output for several combinations of parameters. The angle α was chosen to 2 degrees. The de-corrugation filtering implies a trade-off between an attempt to retain short wavelength features and the attempt to remove artefacts. Another method to remove artefacts in the processed data is to apply short-distance (25–50 m) upward continuation simultaneously to the filters that enhance short wavelength features. The processed data presented in this report involved application of de-corrugation and upward continuation jointly as well as separately.

3.1.2 Aerodat frequency domain EM data

The Aerodat frequency domain system used for the Røros survey includes five frequencies for the following receiver-transmitter configurations:

1. 7000 Hz vertical coaxial coils
2. 6600 Hz horizontal coplanar coils
3. 880 Hz vertical coaxial coils
4. 980 Hz horizontal coplanar coils
5. 34000 Hz horizontal coplanar coils

The coil system is towed below and after the helicopter. The vertical distance from the helicopter is about 30 m; i.e. a mean ground clearance of 50 m. Horizontal coplanar coils have optimum electromagnetic coupling to flat lying conductors, whereas vertical coaxial coils are optimum for picking up responses from steeply dipping structures. Penetration depth increases with decreasing frequency. The maximum penetration depth is roughly 150–200 m in a resistive environment.

Estimated half-space conductivities are provided in addition to the in-phase (real) and quadrature (imaginary) parts if the electromagnetic responses. The conductivities in units of Siemens/m [S/m] can be viewed as an approximation to the mean conductivity from the surface to the (variable) penetration depth ∂, where the penetration depth is given by $\partial[m] = 500\ m \cdot \sqrt{\frac{1}{\sigma[\frac{S}{m}] \cdot f[Hz]}}$ and where *f* is the frequency. Conductivity in units of [S/m] is the inverse of resistivity in units of [Ohmm]. De-corrugated half-space conductivities for each of the five frequencies are available as both line data and as grids according to the description in Appendix B. However, gridding of the data in the database did not reproduce the delivered grids. Flight line artefacts are visible in the re-gridded data. Most likely the data in the database are the initial conductivity estimates prior to an applied de-corrugation filtering. Maps with profile data of the in-phase and quadrature components are available, and they are useful for a qualitative evaluation of the electromagnetic responses in combination with the maps of estimated half-space conductivities.

3.1.3 Totem 2A VLF

The VLF-system recorded data transmitted at two frequencies which roughly equals 16 kHz. Data are recorded using triaxial receiver coils but the data are processed into one normalised parameter for each of the two transmitters. The applied processing is unfortunate, because important information has been thrown away. The applied processing technique implies that responses from electrical conductors with strike oriented towards the corresponding transmitter is enhanced compared to structures that are orthogonal to this orientation. Thus, the maps with responses provide a biased representation of the conductivity distribution and a dependency of transmitter position. The data from the two transmitters are classified as ORTHO and LINE with reference to which strike direction is enhanced in relation to the flight line direction; i.e. roughly orthogonal or parallel to the flight path which is oriented E-W.

Techniques for combining data from two transmitters were developed at Uppsala University and at the Swedish Geological Survey in mid 1990'es (Pedersen *et al*., 1994), which give an unbiased parameter presentation and magnetic tipper data which depends on the conductivity distribution only. No raw data are available for applying this technique.

3.1.4 Radiometric data

Estimates of potassium, uranium and thorium concentrations are available but not used for this report. The estimates correspond to variations in concentrations within the upper ½ m of the ground, and these data are therefore difficult to use for target definition. Radiometric data usually show very good correlation to the surface geological units, and these data are therefore mainly useful for geological mapping purposes.

3.2 Processing and interpretation

3.2.1 Magnetic field data

For the purpose of this study, the total magnetic intensity field data (Figure 4) has been decomposed into orthogonal vector component data using an extension of a technique described in Pedersen *et al*. (1989). The extension implies that component data are calculated without assumption of induced magnetisation. Components are shown in Figures 5–7. Information on the presence of strong remanent magnetisations can be revealed from the component data. The declination of the (anomalous) horizontal magnetic field is calculated from the north and east magnetic components and shown in Figure 8. The magnetic east component delineates a very pronounced north-south trending boundary (from east coordinate 620000 m at the southern map boundary to east coordinate 628000 m at the northern part). This lineament merges into an area with strong remanent magnetisation in the northern part of the map, which corresponds to the mapped Fongen-Hyllingen gabbro complex. The lineament is noticed to cut the mapped surface geological structures, and an interpretation of the lineament must involve deep seated structures. The significance of the linea-

ment in terms of mineralisations is not immediately clear, but the location is obviously of interest for a ground follow-up study. The Killingdal mineral occurrence is located at the lineament.

Another indication of remanent magnetisation is at east coordinate 642500 m at the northern map boundary.

The mean declination angle is around 40 degrees east. This value differs significantly from an expected value close to 0 degree. The discrepancy is most likely due to an insufficient description of the regional magnetic field, but the cause for this needs further investigation.

Locations of known mineral occurrences are superimposed on the map showing the east component of the anomalies (Figure 6). A majority of these occurrences are seen to be adjacent to short wavelength magnetic features of low to intermediate amplitudes. Locations with short wavelength feature are obvious targets for a ground-follow up

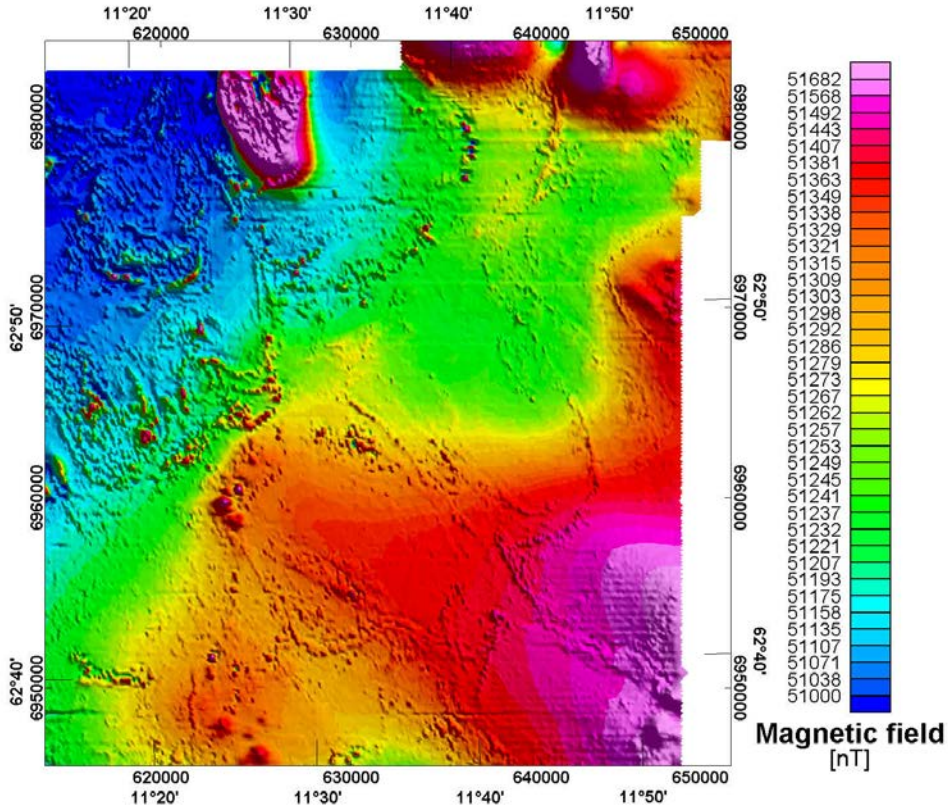

Figure 4. *Magnetic total field data.*

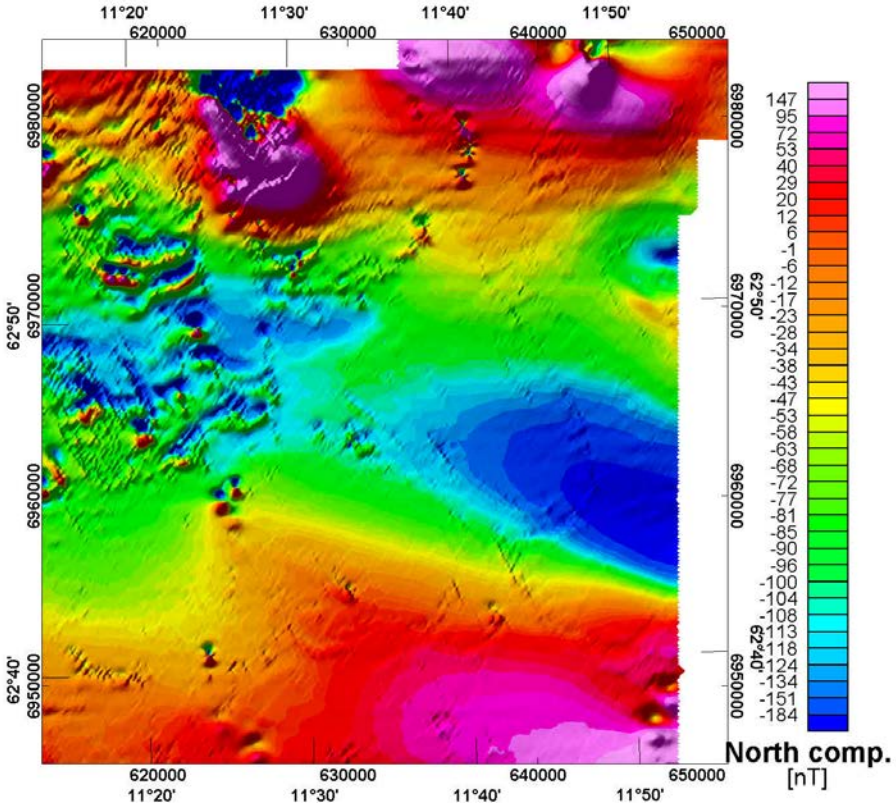

Figure 5. *Calculated anomalous magnetic north component.*

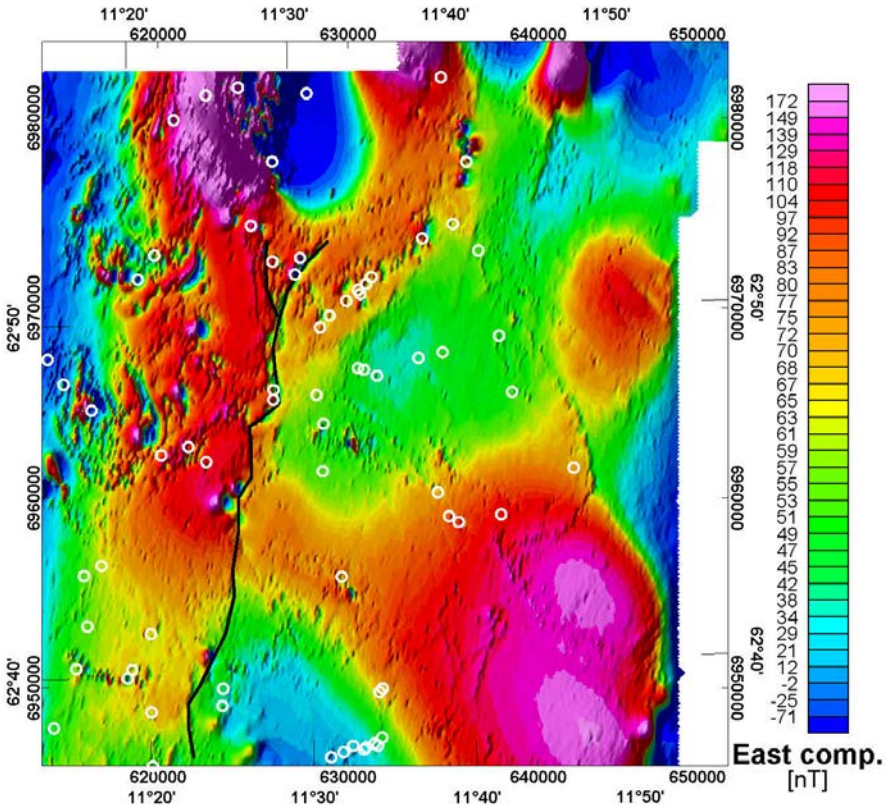

Figure 6. *Calculated anomalous magnetic east component. A major-north south trending lineament is marked by line in black colour. Locations with mineral occurrences and deposits are marked with open white circles.*

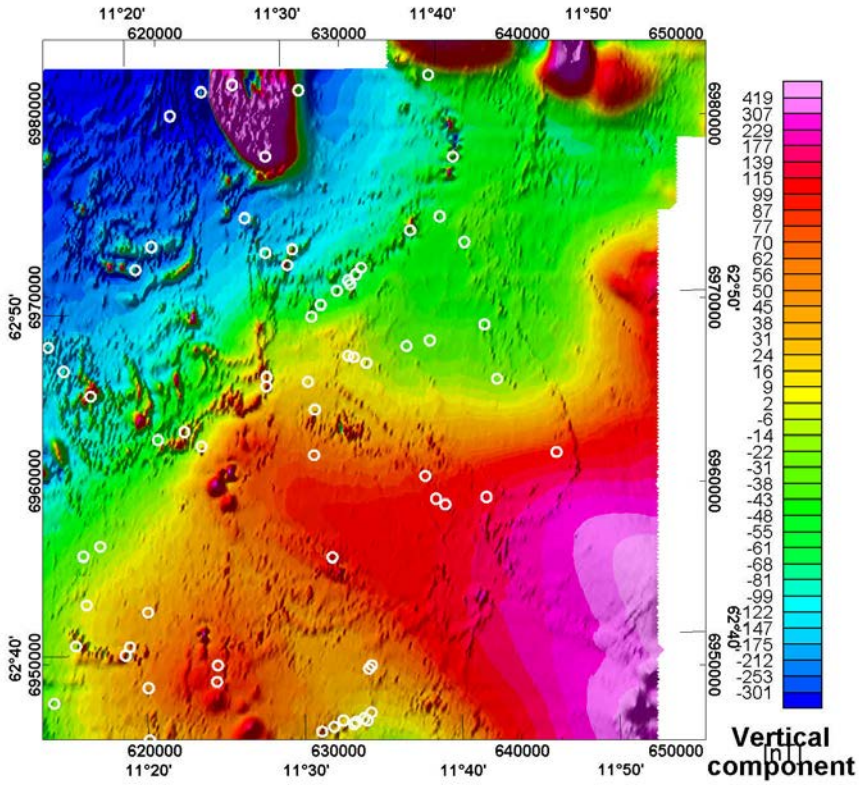

Figure 7. *Calculated anomalous magnetic vertical component.*

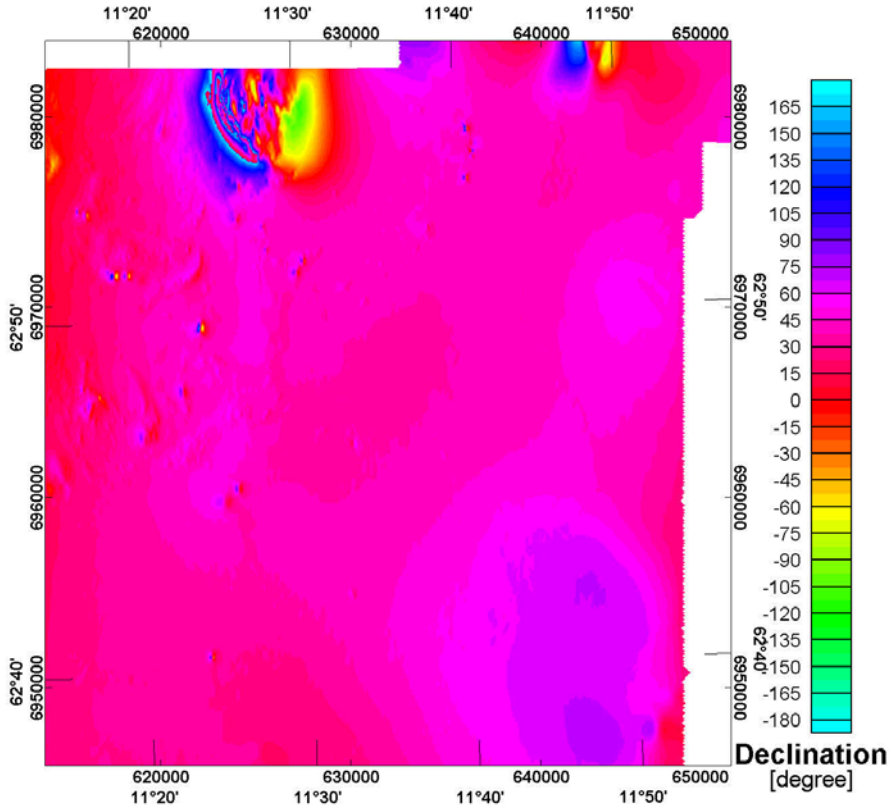

Figure 8. *Calculated anomalous magnetic declination.*

The magnetic component data are processed further by calculating the magnetic gradient tensor and some rotational invariants I_1 and I_2 of the tensor that are useful for describing structures (Pedersen & Rasmussen, 1991). In particular, the invariant I_1 is used for picking of isolated magnetic anomalies. Further enhancement of the data is done by applying the analytic signal filter to the invariant I_1. In short, this technique is useful for providing information of isolated magnetic anomalies. The gradient tensor is symmetric and the upper triangle of the tensor is shown in Figure 9. Invariant I_1 and the analytic signal processed data of I_1 are also shown in Figure 9 together with the logarithm of the norm of I_2. An image of the analytic signal processed invariant I_1 is shown at a different scale in Figure 10. The pronounced lineament picked from the magnetic east component data is superimposed on the image in Figure 10 (black line). It is noticed that several isolated peaks are located along this lineament. Some of the other peaks line up along almost straight lines (grey colour) whereas other peaks follow large scale fold structures. The locations of these peaks are clearly of interest for a ground follow-up study.

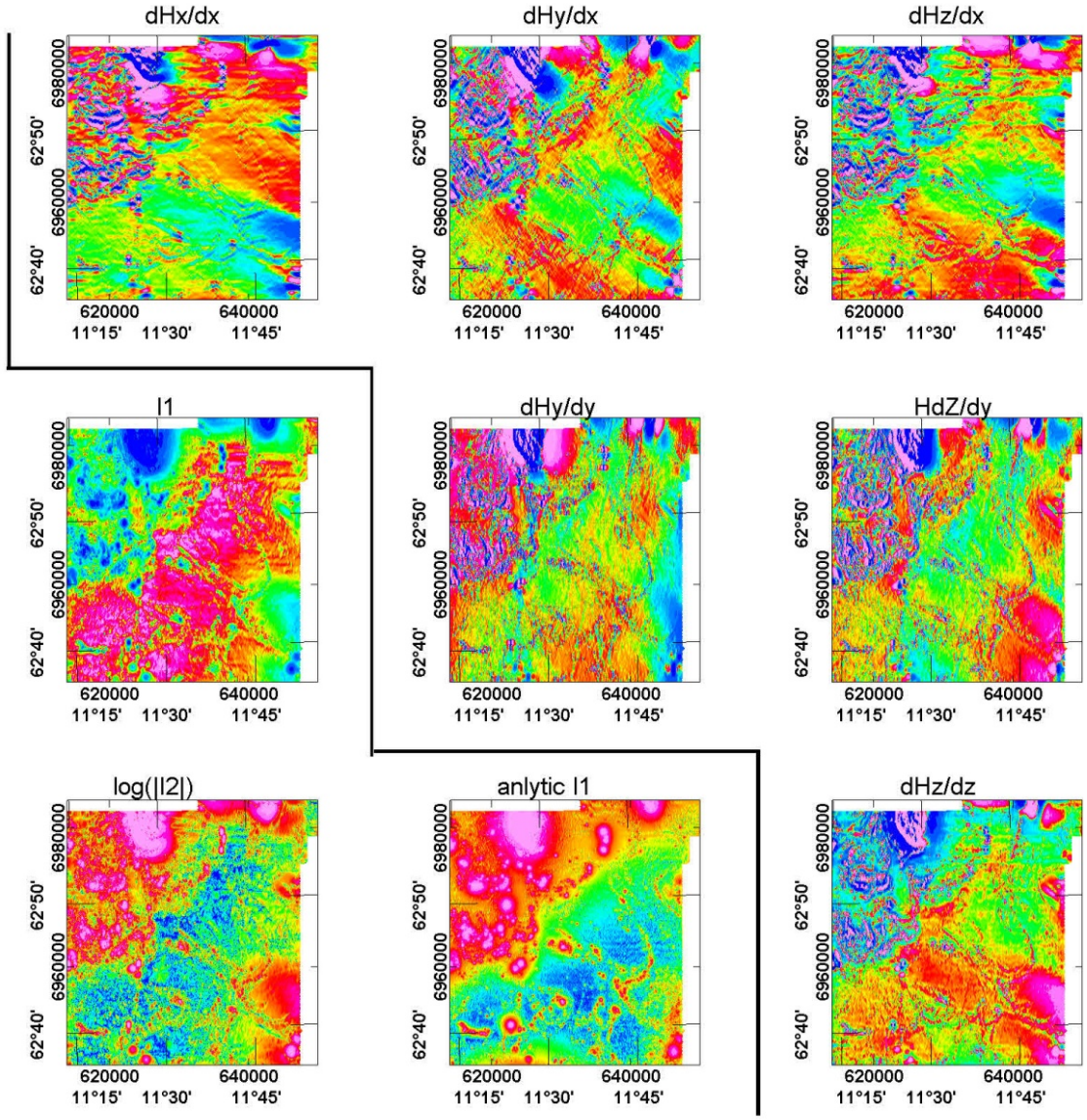

Figure 9. *The upper triangle and diagonal of the magnetic gradient tensor* $\begin{Bmatrix} \partial H_x/\partial x & \partial H_y/\partial x & \partial H_z/\partial x \\ - & \partial H_y/\partial y & \partial H_z/\partial y \\ - & - & \partial H_z/\partial z \end{Bmatrix}$ *and the rotational invariants* I_1 *and* $\log_{10}|I_2|$ *,and the analytic signal filtered* I_1.

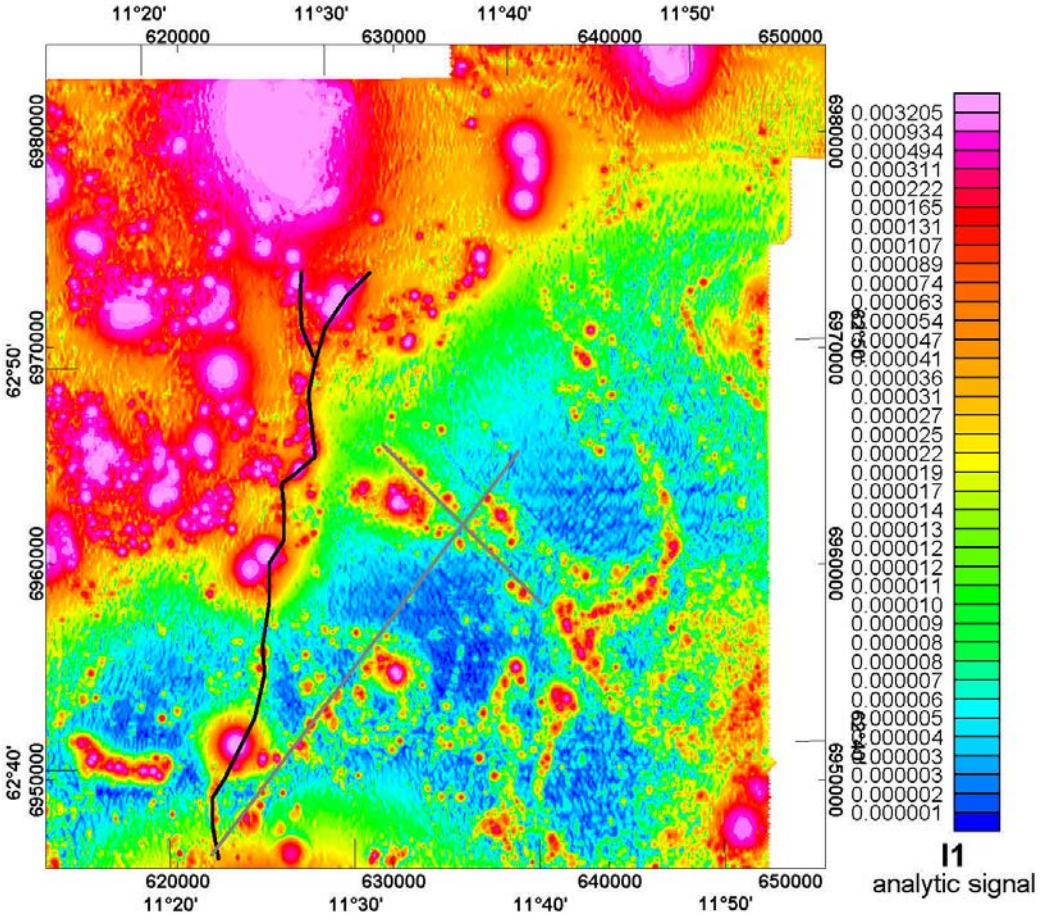

Figure 10. *Rotational invariant I_1 after application of analytic filter to the data. The line in black colour delineates the location of a major regional structure defined from the east magnetic component. The lines in grey colour mark peaks aligned along almost straight lines.*

3.2.2 Frequency domain EM

Profile data were available for the project both as ASCII data and as profile plots in Geosoft maps. The profile data for the 880 Hz vertical coaxial coils and the 980 Hz horizontal co-planar coils were analysed further by extracting information about local peak values (value above background) of the quadrature component and the anomaly width. These estimates were then superimposed on the original maps produced by NGU, and the data were inspected and compared to data in other maps. An example is shown in Figure 11 and 12, which show a subset of the maps from the south-western part of the survey area. The target areas outlined are based on visual inspection of each map individually and a joined target selection is later defined by combining the targets produced from both maps. Note how the peaks from the analytic signal processed tensor invariant I_1 (background image in Figure 12) correlate with the position of the EM peaks in certain areas. Maps for the entire survey area are included in digital format on the accompanying DVD.

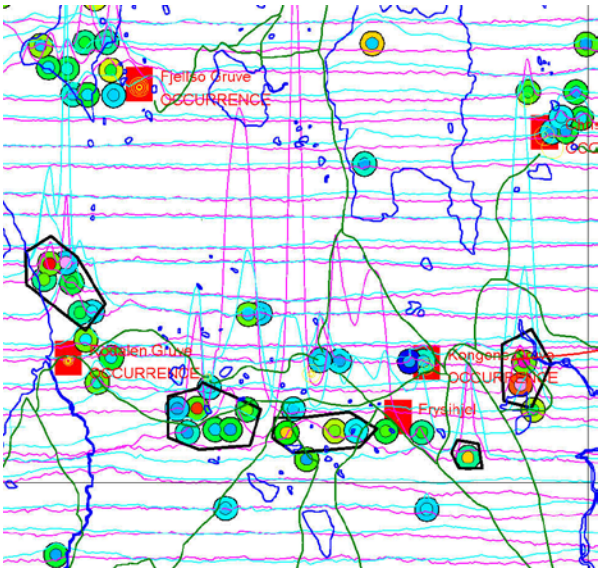

Figure 11. *Example with profile data for 980 Hz including description of peak values and peak width by using circular colour symbols. Profiles in light blue colour describe the quadrature component and profiles in magenta colour show the in-phase part. The inner colour circle describes peak value and is superimposed on a larger circle with colour code indicating peak width. Blue colour indicate low values and red colour indicate large values. Polygons in black colour show areas of particular interest for a ground follow-up. Maps for the entire survey are provided digitally with the report. Power lines (red colour), roads (green colour) and rivers (dark blue) are also shown.*

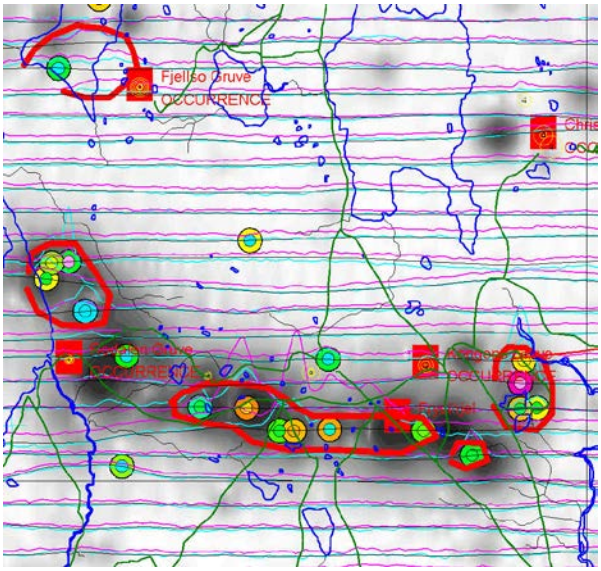

Figure 12. *Example with profile data for 880 Hz including description of peak values and peak width by using circular colour symbols. Profiles in light blue colour describe the quadrature component and profiles in magenta colour show the in-phase part. The inner colour circle describes peak value and is superimposed on a larger circle with colour code indicating peak width. Blue colour indicate low values and red colour indicate large values. Polygons in red colour show areas of particular interest for a ground follow-up. Maps for the entire survey are provided digitally with the report. Power lines (red colour) and roads (green colour) are also shown. The background image in grey scale is the analytic signal processed tensor invariant I_1.*

A few locations are seen to have negative in-phase responses, which is attributed to strong magnetic permeability (see e.g. Huang & Fraser, 2000). In these cases, the magnetic field anomaly is also observed to be high.

3.2.3 Totem 2A VLF

Grids of the VLF data from the Ortho and Line directions were produced. The VLF data were used in prioritising the target areas defined from the frequency domain EM system. The maps are shown in Figures 13 and 14.

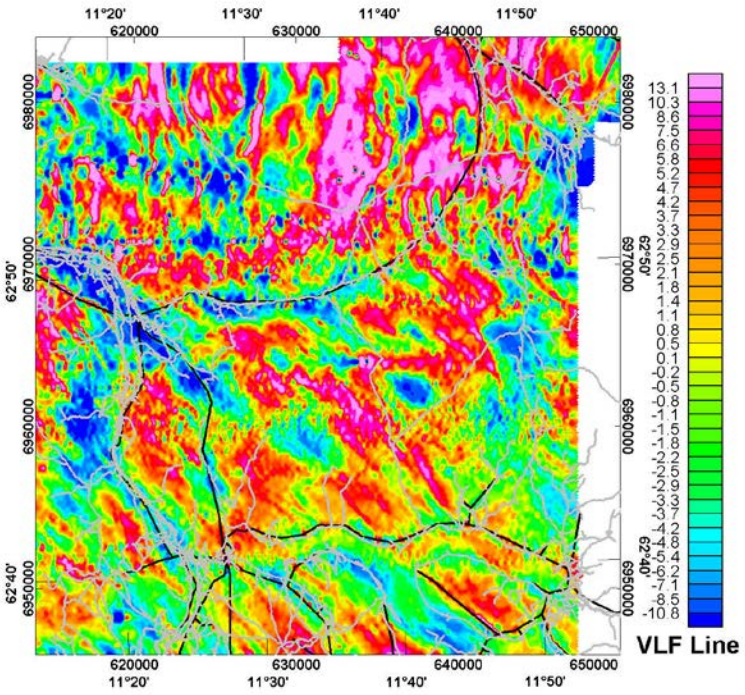

Figure 13. *The VLF Line data with superimposed locations of power-lines (black lines) and roads (grey).*

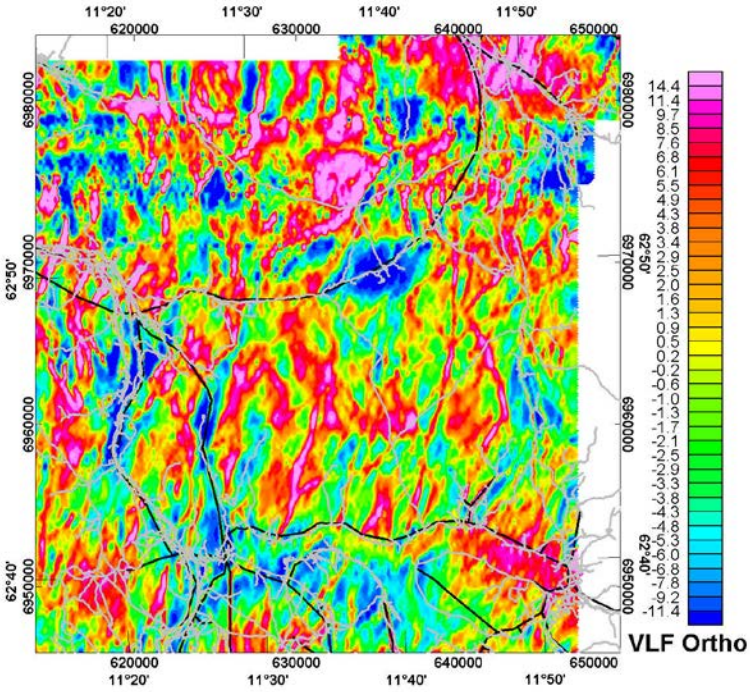

Figure 14. *The VLF Ortho data with superimposed locations of power-lines (black lines) and roads (grey).*

3.3 Ground follow-up targets and descriptions

The locations with high amplitude frequency domain EM response should in general be prioritised for a ground follow-up, but also the magnetic field data should be used in guiding the prioritisation of target areas. Note that the lineament picked from the east component of the magnetic field show almost no coincidence with targets defined solely from the EM data. Note, however, that the Killingdal occurrence located at the lineament is associated with an EM anomaly. It was mentioned above in the discussion of data in Figure 12 that many of the EM peaks are coincident with the peaks obtained from the analytic signal processed tensor invariant I_1.

Locations with coincidence of high VLF response and frequency domain EM anomalies should be prioritised.

Three types of magnetic features are of particular interest:

- the two locations with remanent magnetisation. In particular the western most area is associated with very strong in-phase EM anomalies. At the westernmost location with remanent magnetisation, both a strong in-phase and quadrature anomaly is observed and this should also be checked
- locations of magnetic break lines - in particular if associated with any local peaks
- isolated peaks - in particular if associated with any adjacent EM anomalies

A total of 72 target locations/areas (see Figure 15 and 16) have been identified from visual inspection of the presented data. The locations are provided in digital format in an Excel format and in ArcView SHP shapefile format. The locations are provided by a centre/peak location and a polygon encompassing the area of interest. Prioritising (1 [highest] – 5 [lowest]) has been done based on an evaluation of the maps shown above. Maps with target locations are provided in digital format. Appendix C include screen dumps with polygons outlining target areas from visualisations of geophysical anomalies

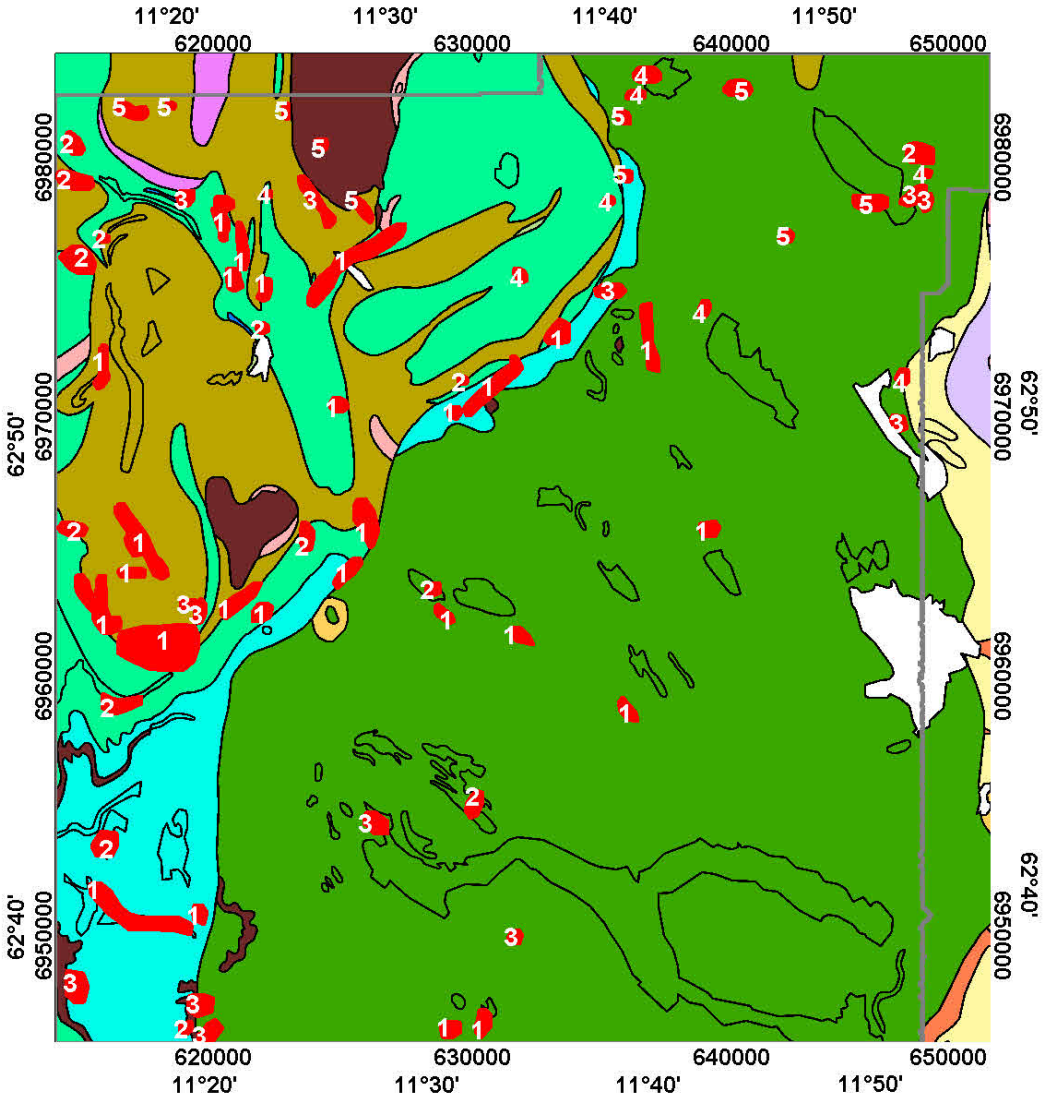

Figure 15. *Priority of target areas (filled red polygons) superimposed on the geological map of the Røros district. Legend for the map is shown in Figure 3.Target priority number in the range 1-5 is indicated. Priority 1 is highest.*

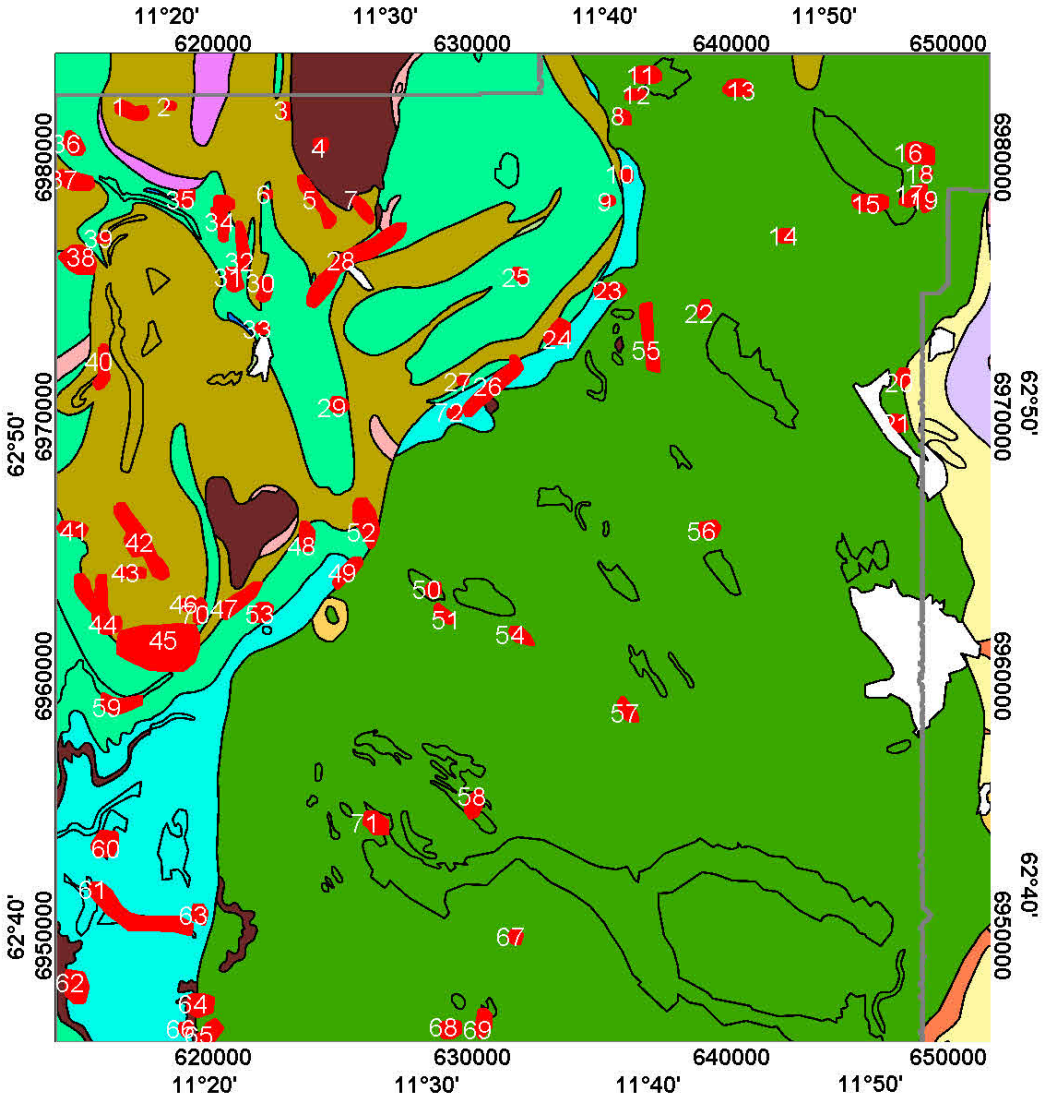

Figure 16. *Target areas (filled red polygons) superimposed on the geological map of the Røros district. Legend for the map is shown in Figure 3.Target numbering is superimposed.*

5. Conclusions and recommendations

The airborne geophysical data from the Røros and Meråker districts analyzed are in general of good quality and contain valuable information for a general understanding of the geology. A high degree of correlation to mapped geological units is observed. Targets areas for a ground follow-up in a search for mineralisations can be identified from both magnetic and electromagnetic data.

Quantitative modeling of the electromagnetic data has not been done for this report, but should be considered for further work. In particular, insight from modeling of data from locations with known and mapped mineralisations is expected to be useful for a more refined prioritizing of targets. An integrated interpretation in which geochemical data is included may further improve the prioritizing of target areas. The self organizing map analysis presented in this report is considered a feasible approach for data integration.

6. References

Grenne, T., Ihlen, P. M. & Vokes, F. M., 1999: Scandinavian Caledonide Metallogeny in a plate tectonic perspective. Mineralium Deposita **34**, 422-471.

Fraser, S.J. & Dickson, B.L., 2007: A New Method for Data Integration and Integrated Data. Interpretation: Self-Organising Maps. In "Proceedings of Exploration 07: Fifth Decennial International Conference on Mineral Exploration" edited by B. Milkereit, 2007, p. 907-910.

Huang, H. & Fraser, D.C. 2000: Airborne resistivity and susceptibility mapping in magnetically polarizable areas. Geophysics, 65, NO. 2, p. 502–511.

Kohonen, T, 2001: Self-Organizing Maps. Third Extended Edition, Springer Series in Information Sciences, Vol. 30, Springer, Berlin, Heidelberg, New York, 2001.

Pedersen, L.B., Qian, W., Dynesius, L., and Zhang, P., 1994. An Airborne Tensor VLF System.From Concept to Realisation. Geoph. Prosp., **42**, 863-883.

Pedersen, L.B. & Rasmussen, T.M., 1990. The gradient tensor of potential field anomalies. Geophysics, 55, 1558-1566.

Pedersen, L.B., Rasmussen, T.M. & Dyrelius, D., 1989. Construction of component maps from aeromagnetic total field anomaly maps. Geophys. Prosp., 38, 795-804.

7. Appendix A – Self Organised Map (SOM) analysis

Three data types, d1, d2 and d3, are analysed in the example with synthetic data. The data values and geographic locations are shown (Fig. 34abc) for each data type using a colour code presentation for each data point value. The values are in the range from 1–16. In short the data fall in four sub ranges:

- Very low (VL) – blue colour
- Low (L) – light blue and green colours
- Intermediate (I) – orange colour
- High (H) – purple colour

A listing of the three data types in terms of sub ranges reveals the following combinations from south (1) to north (4) when inspecting the three data types in Fig 30abc:

1. VL-L-L
2. VL-I-L
3. L-L-L
4. VL-L-H

The listing above give four different combinations of data and it is clear immediately that the data define four groups. In this simple synthetic example with only a few types of data, it is straightforward to distinguish the four groups. However, an analysis by visual inspection becomes much more difficult when both more data types and more complex data distributions are added. The SOM is useful in these complicated cases. The basic principles are described below.

The SOM processing finds an approximation to the data by mapping the input data into another data set with fewer data than the initial amount of data. This approximation referred to as the best matching units (BMU) has the same amount of data types (same dimensionality) as the input data. The BMU's are presented in the SOM which is a two-dimensional map, and referred as the SOM-space (see Fig. 34 lowermost panels). The SOM is discretized in a pre-selected number of rows and columns (matrix-representation). Thus, the original multi-dimensional data are mapped into a new data space with only two-dimensions and fewer data. In the synthetic example, the number of rows and columns are 21 and 16 respectively. The number of cells or elements defines the data reduction applied to the initial data. In this synthetic case, a reduction from 998 initial data to 21x16=336 data is used. Each BMU is associated with a cell in the matrix or SOM-space, and they are ordered in the matrix such that similar BMU's are adjacent to each other in the two-dimensional map. Although the SOM is two-dimensional, the multidimensionality of the input data is retained by the dimensionality of BMU. Each of the input data has a BMU to which the data are most similar to. Several input data may be associated with the same BMU, in which case the SOM presentation may be viewed as a classification of the input data. An example of a link between initial data and a BMU is indicated in Figure 34, where six data points are represented by one BMU in the matrix. Some BMU's may not have any of the initial data associated to it. The matrix presentation is utilised in two ways:

- U-matrix presentation: similarity between adjacent BMU's
- Component presentation: relationship between components for subsets (i.e. data associated with one or several cells in the matrix) of the data

The U-matrix describes the deviation for a particular cell to the surrounding cells by using a colour scale representation of the "distance" between the associated BMU's. The component presentation simply shows the value of the BMU at each cell and for each component.

The BMU's may be analysed further with respect to clustering of data. A standard k-mean clustering procedure is used. The result for the synthetic data example is that the data cluster into four distinct groups, as displayed in Figure 34d. Thus, a data reduction or simplification from 998 initial data to 4 is obtained.

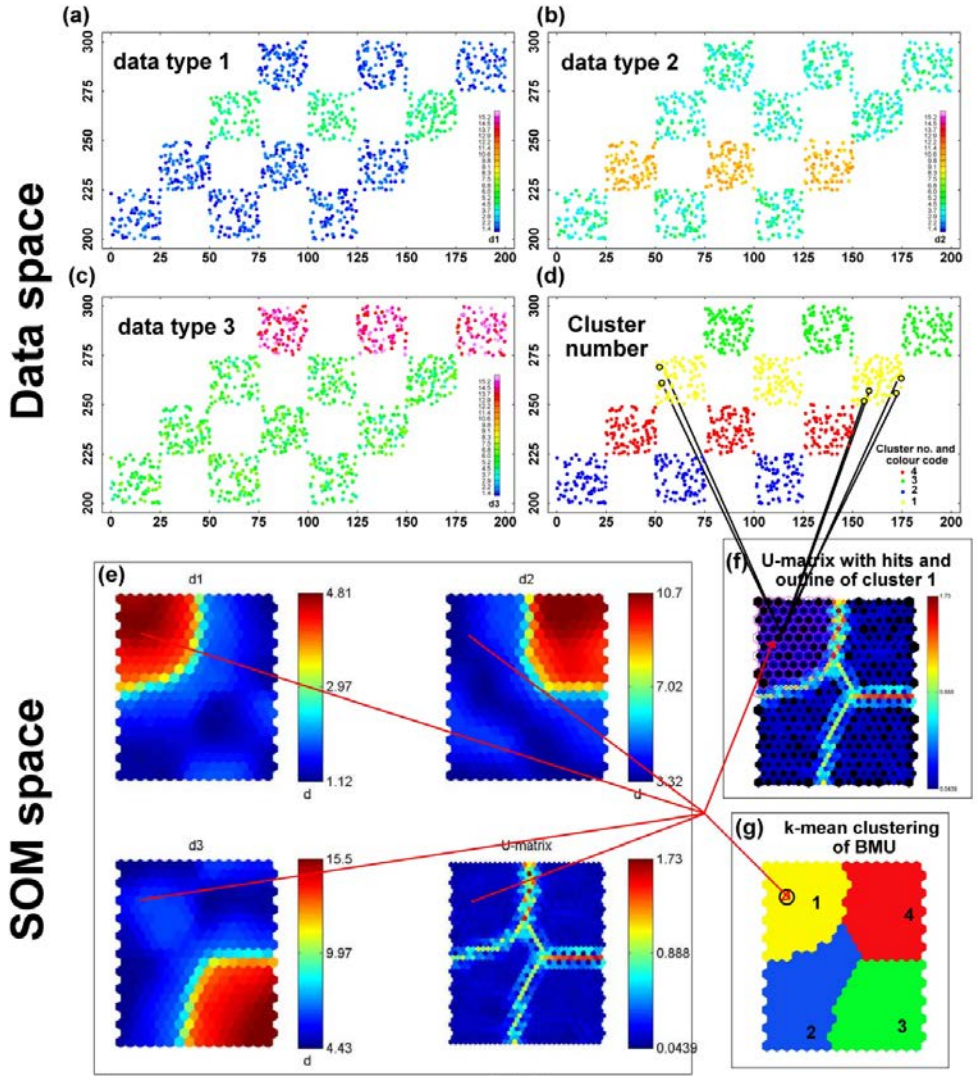

Figure 34. *SOM-presentation of synthetic data consisting of 998 locations with 3 data types at each position: (a) values of data type d1 at each geographic location; (b) values of data type d2; (c) values of data type d3; (d) results of k-mean cluster analysis displayed in a geographic map ; (e) components in SOM-space; (f) U-matrix representation of BMU with colour code showing distance to neighbouring cells; (g) k-mean clusters of BMU's in SOM-space. An example of link between data space and SOM-space is indicated by the lines pointing to one of the cells in the matrix representation.*

8. Appendix B – Røros data files

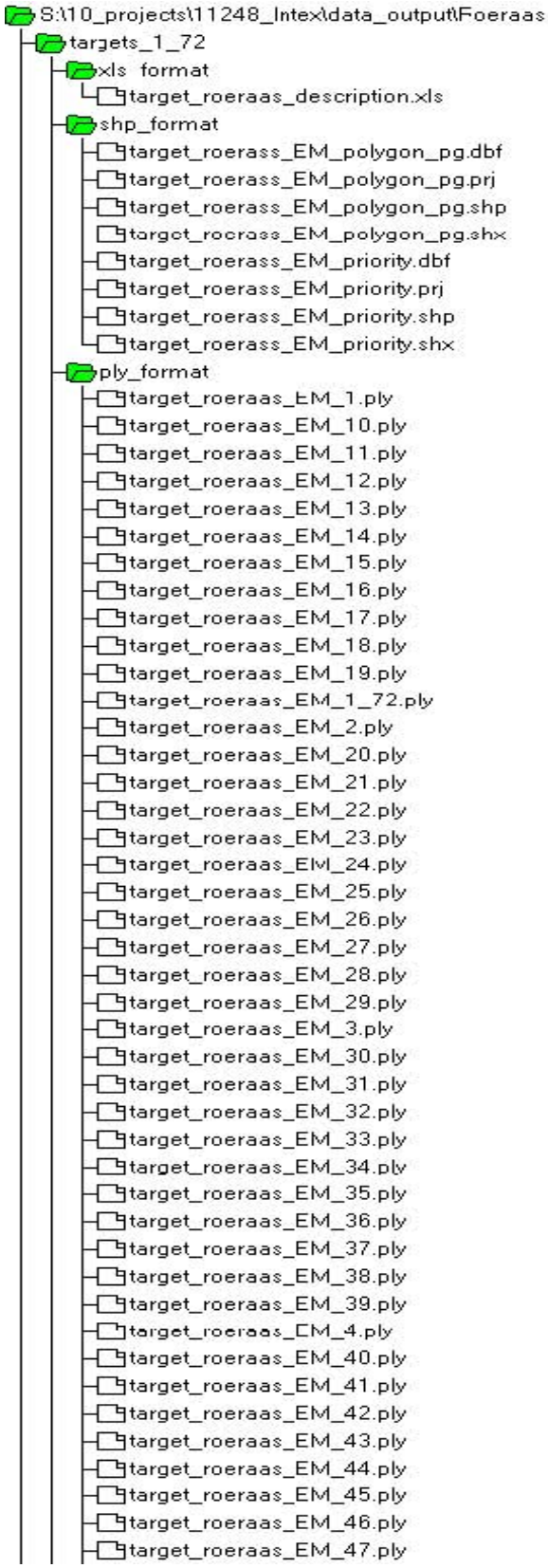

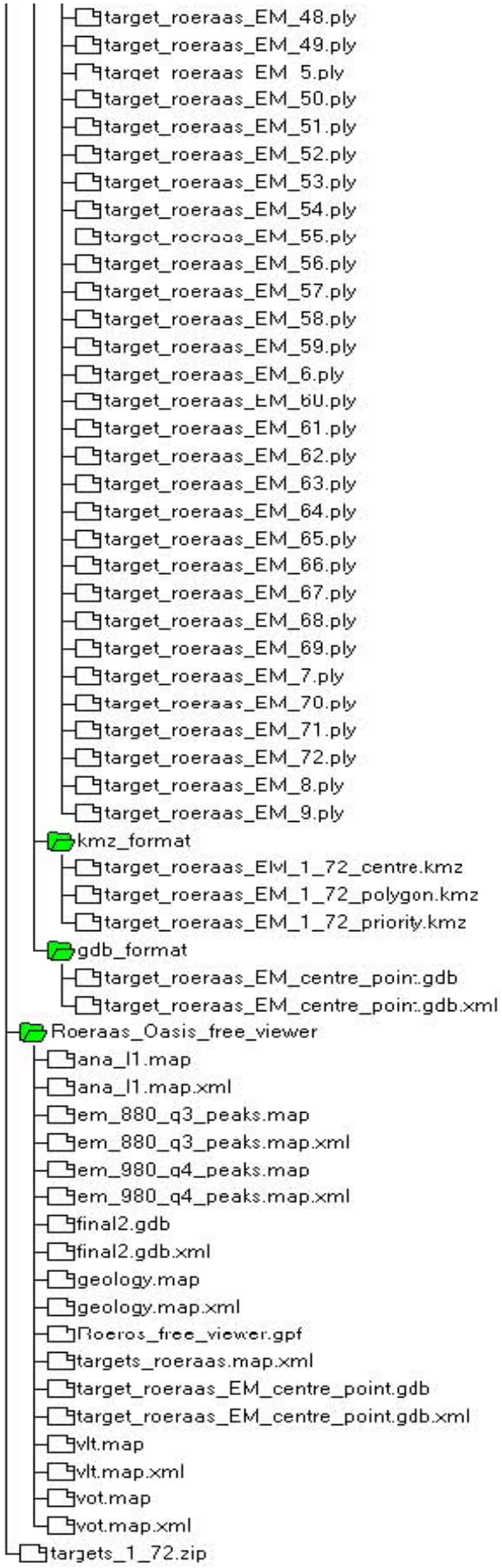
target_roeraas_EM_48.ply
target_roeraas_EM_49.ply
target_roeraas_EM_5.ply
target_roeraas_EM_50.ply
target_roeraas_EM_51.ply
target_roeraas_EM_52.ply
target_roeraas_EM_53.ply
target_roeraas_EM_54.ply
target_roeraas_EM_55.ply
target_roeraas_EM_56.ply
target_roeraas_EM_57.ply
target_roeraas_EM_58.ply
target_roeraas_EM_59.ply
target_roeraas_EM_6.ply
target_roeraas_EM_60.ply
target_roeraas_EM_61.ply
target_roeraas_EM_62.ply
target_roeraas_EM_63.ply
target_roeraas_EM_64.ply
target_roeraas_EM_65.ply
target_roeraas_EM_66.ply
target_roeraas_EM_67.ply
target_roeraas_EM_68.ply
target_roeraas_EM_69.ply
target_roeraas_EM_7.ply
target_roeraas_EM_70.ply
target_roeraas_EM_71.ply
target_roeraas_EM_72.ply
target_roeraas_EM_8.ply
target_roeraas_EM_9.ply
kmz_format
target_roeraas_EM_1_72_centre.kmz
target_roeraas_EM_1_72_polygon.kmz
target_roeraas_EM_1_72_priority.kmz
gdb_format
target_roeraas_EM_centre_poin:.gdb
target_roeraas_EM_centre_poin:.gdb.xml
Roeraas_Oasis_free_viewer
ana_l1.map
ana_l1.map.xml
em_880_q3_peaks.map
em_880_q3_peaks.map.xml
em_980_q4_peaks.map
em_980_q4_peaks.map.xml
final2.gdb
final2.gdb.xml
geology.map
geology.map.xml
Roeros_free_viewer.gpf
targets_roeraas.map.xml
target_roeraas_EM_centre_point.gdb
target_roeraas_EM_centre_point.gdb.xml
vlt.map
vlt.map.xml
vot.map
vot.map.xml
targets_1_72.zip

9. Appendix C –Røros targets

This appendix includes screen dumps (Figures 36–107) from displays of target areas superimposed on maps with frequency domain EM profiles (EM_880_Q3_peaks.map & EM_980_Q4_peaks.map), grids of VLF anomalies (VLT.map & VOT.map) , grids of analytic signal filtered versions of magnetic gradient tensor invariant I_1 (ana_I1.map). Superimposed on the profile images are coloured symbols for anomaly EM peak values and anomaly width. The colour scales used are shown below in Figure 35. A separate window shows profile data (final2.gdb), where a fixed range for ordinate values is used.

Target areas are shown by polygons and the target number is displayed on the VLT.map. Occurrences/deposits are shown by red square boxes on the EM profile maps. Coordinates for target positions (position within highest peak value within polygon) are shown by black dots and by the + cursor position. The corresponding position in the window for final2.gdb is shown by a square box. Coordinates are provides digitally on the enclosed DVD together with the target description and priority number in the range from 1 to 5. A priority of 1 is highest priority. Locations with Zn-assay data are shown by white circles on the ana_I1.map.

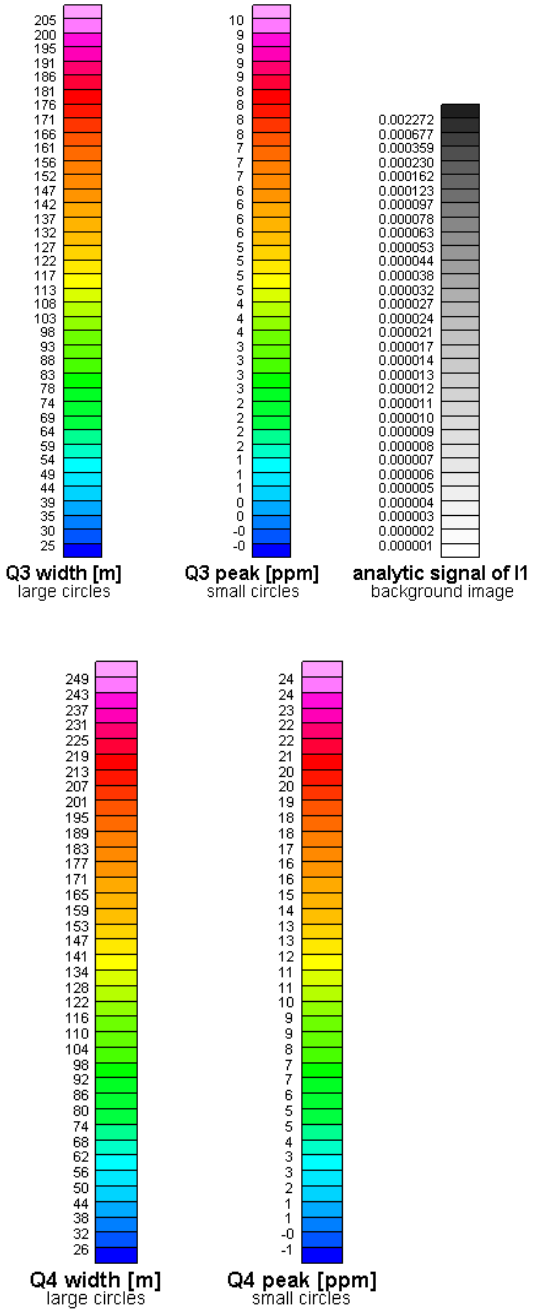

Figure 35. *Legend for maps in Figures 36–107.*

(a)

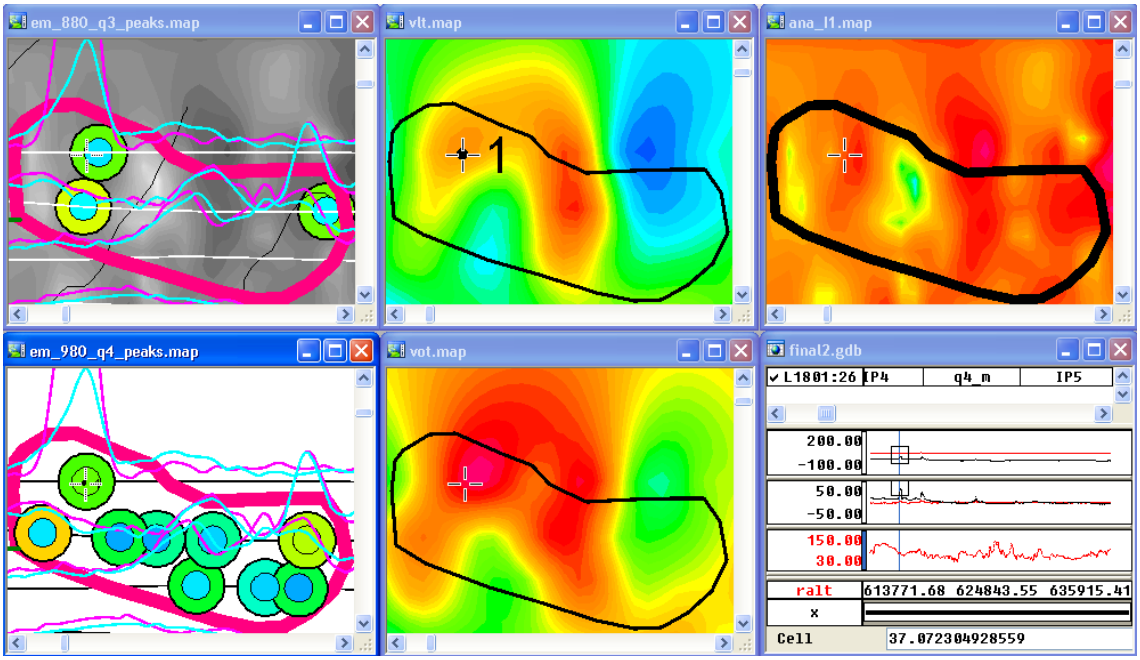

(b)

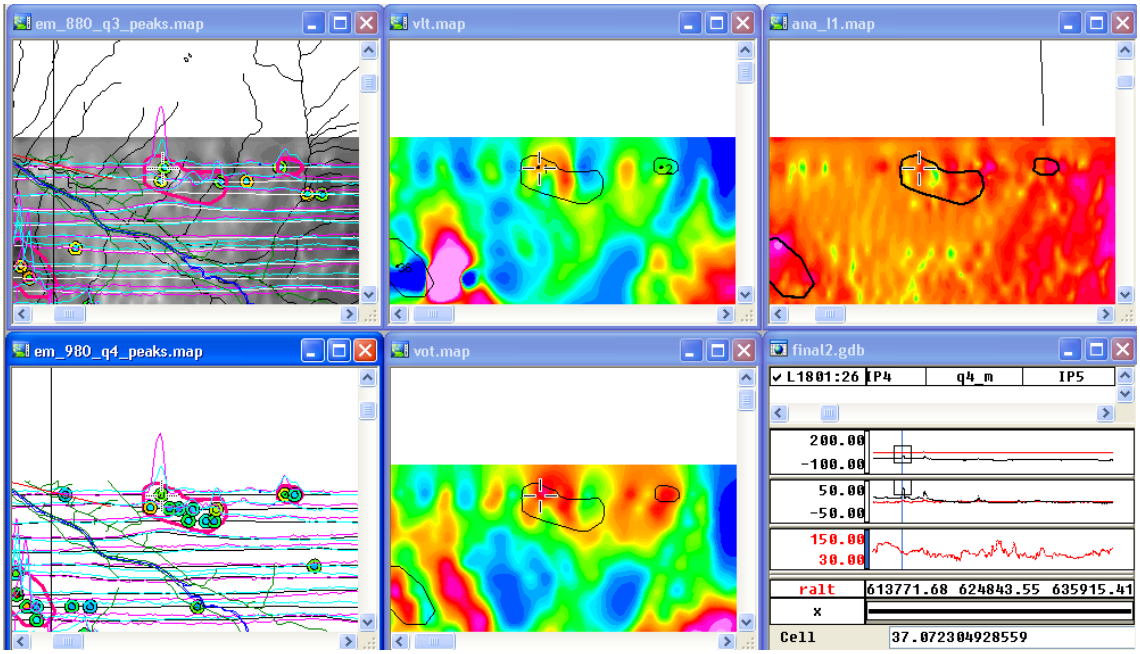

Figure 36. *Target Røros 1; small group of medium EM peaks; weak VLF anomalies; magnetic anomaly uncertain due to levelling problems but most likely weak; priority 5*

(a)

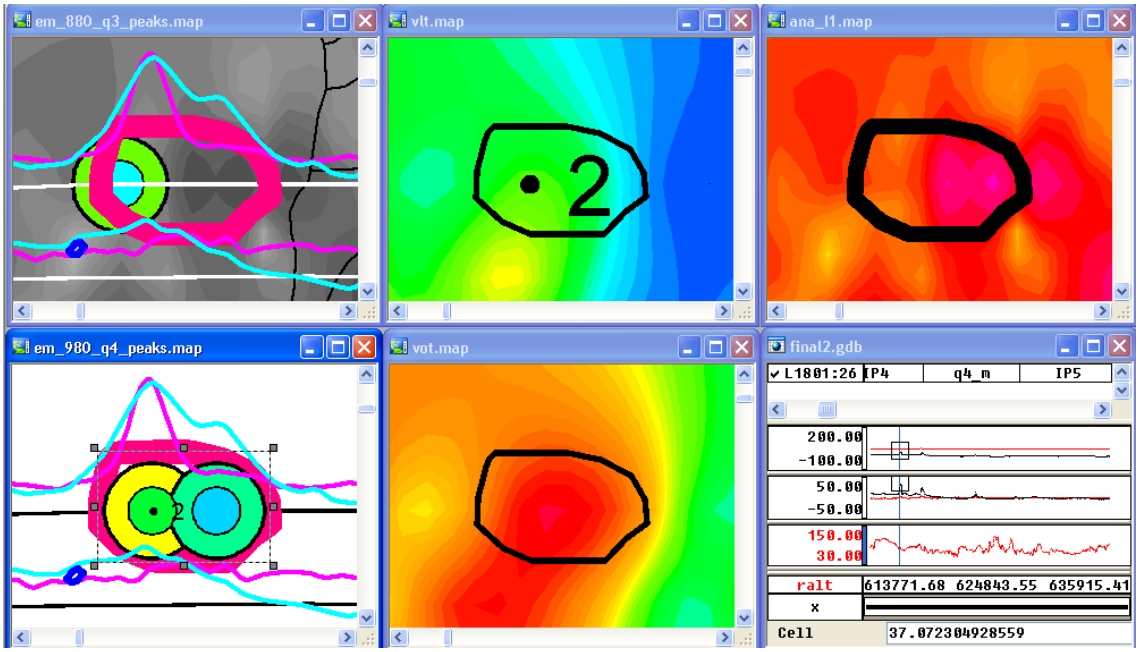

(b)

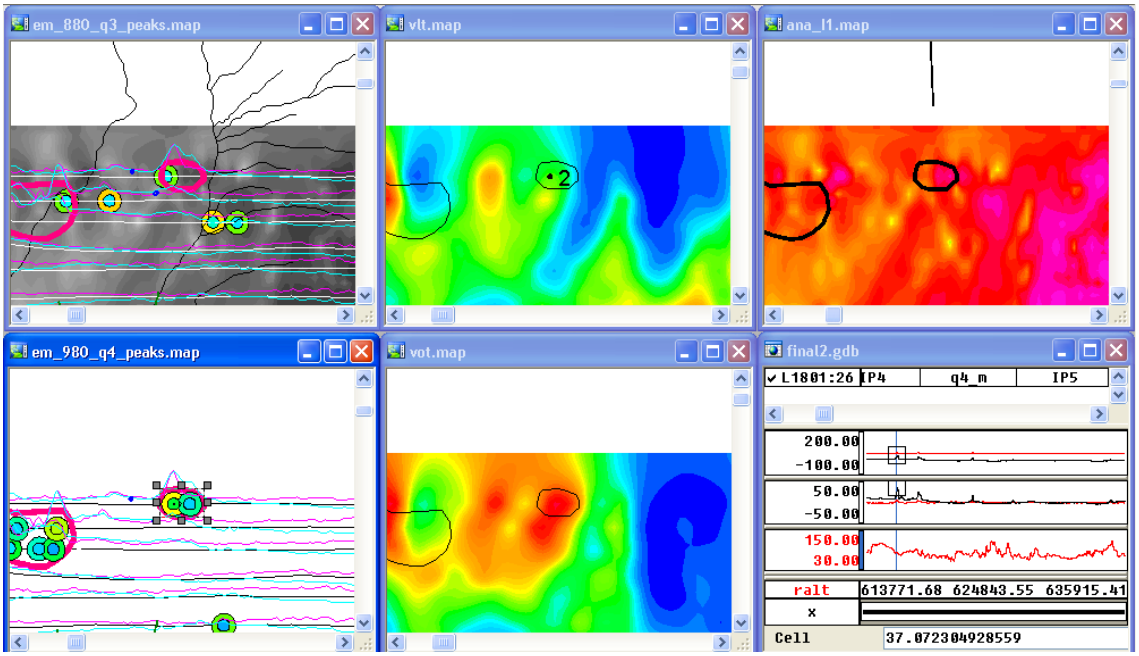

Figure 37. *Target Røros 2; a few medium EM peaks; weak VLF anomalies; weak short wavelength magnetic anomalies; priority 5*

(a)

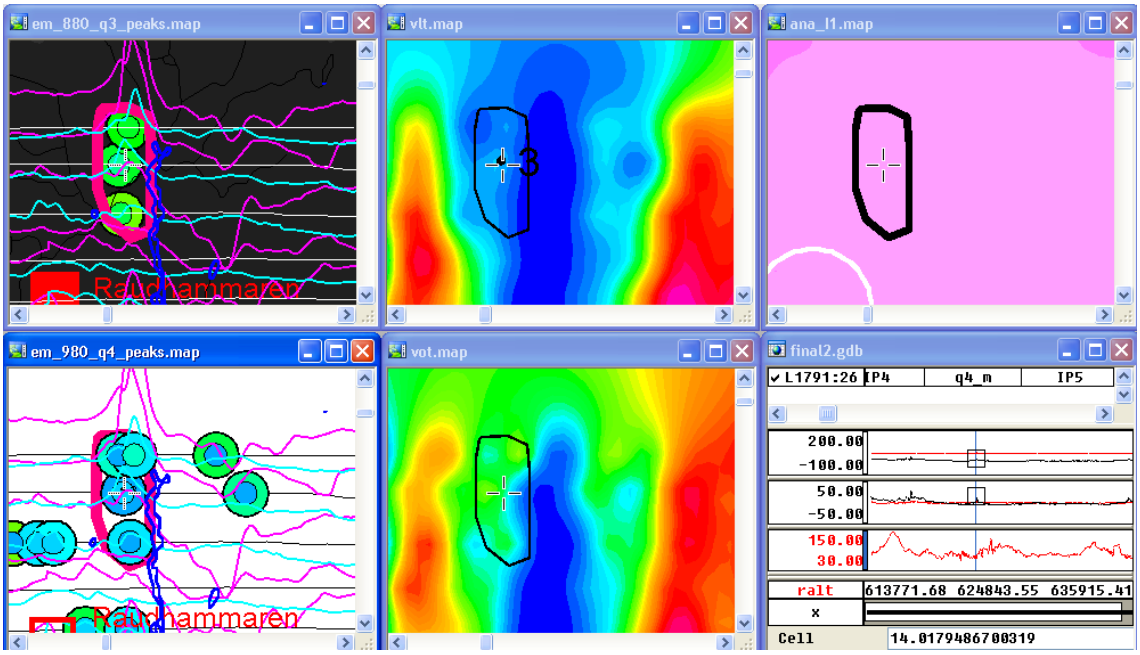

(b)

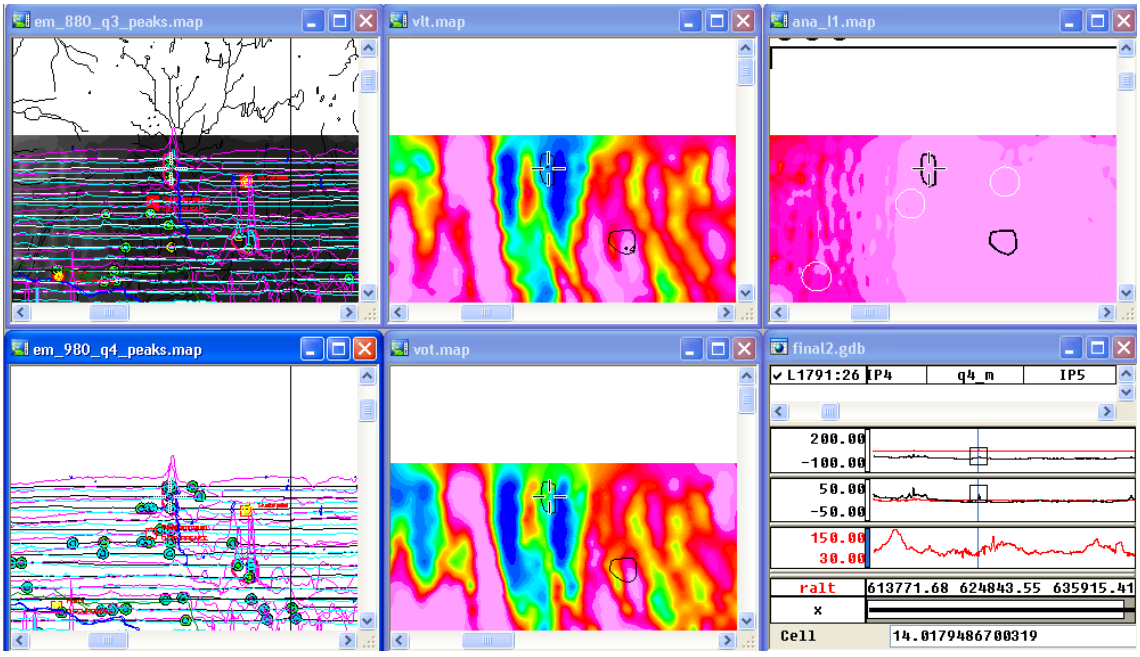

Figure 38. *Target Røros 3; a few medium EM peaks; no VLF anomalies; strong long wavelength magnetic anomaly; priority 5*

(a)

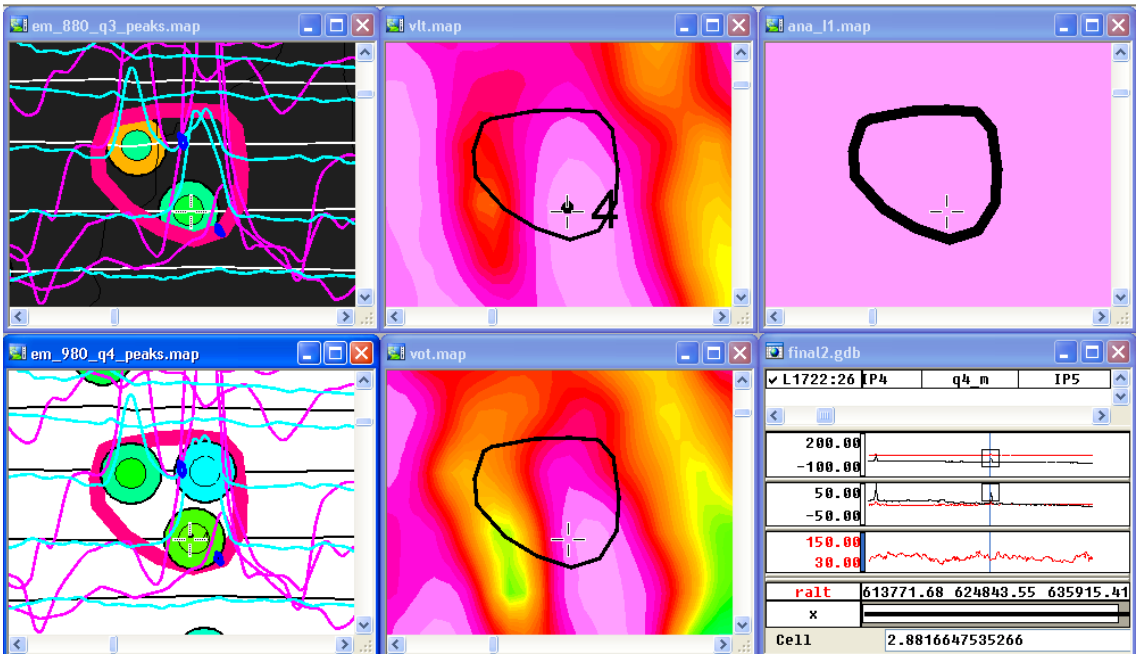

(b)

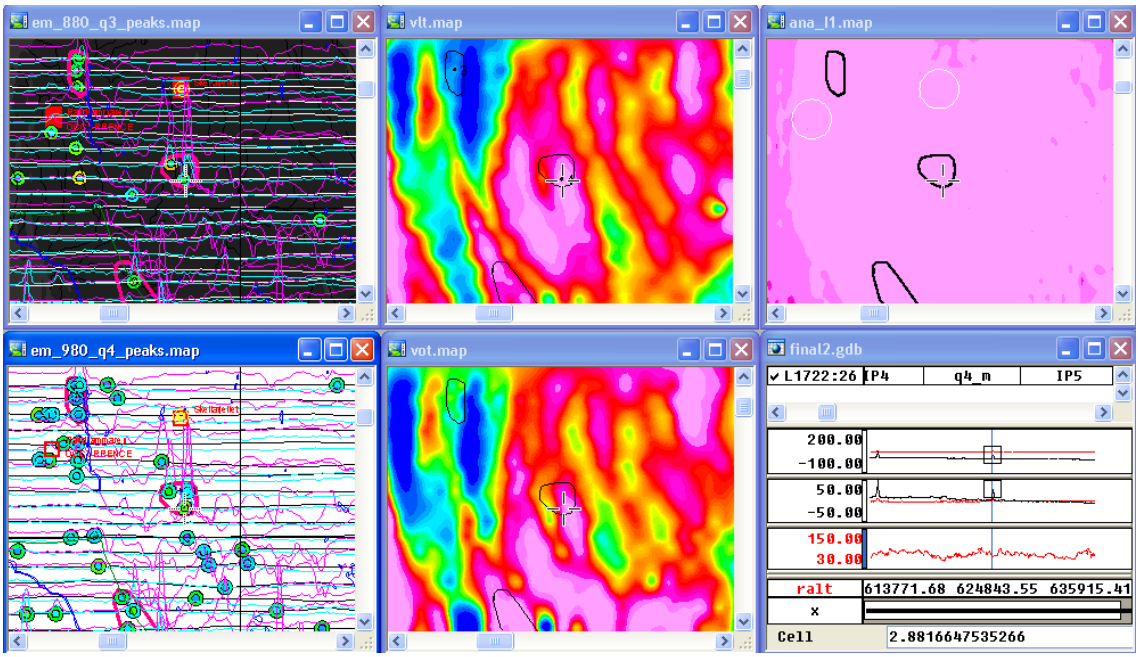

Figure 39. *Target Røros 4; a few medium EM peaks; positive VLF anomalies; strong long wavelength magnetic anomaly; priority 5*

(a)

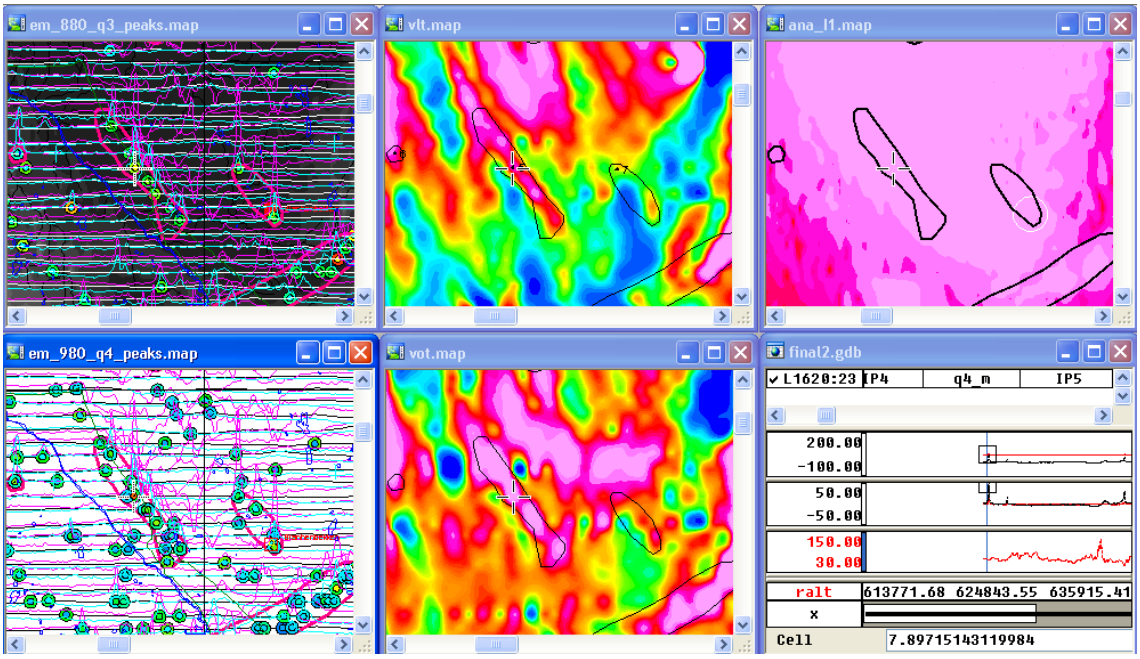

(b)

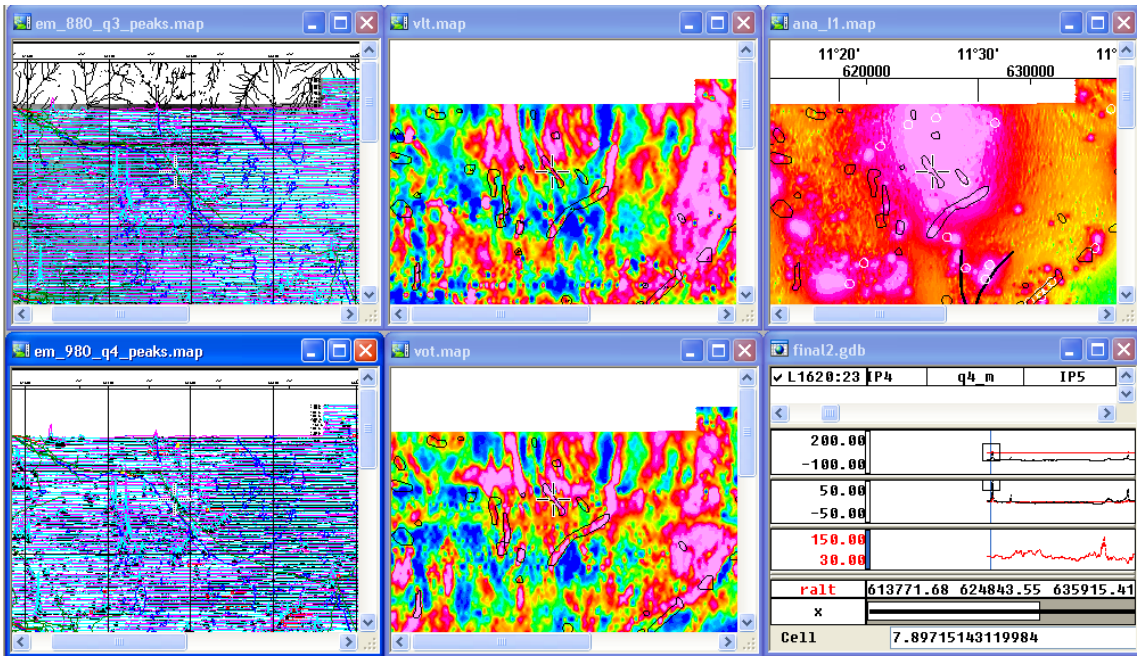

Figure 40. *Target Røros 5; elongated group of medium EM peaks; positive VLF anomalies; strong long wavelength magnetic anomaly; priority 3*

(a)

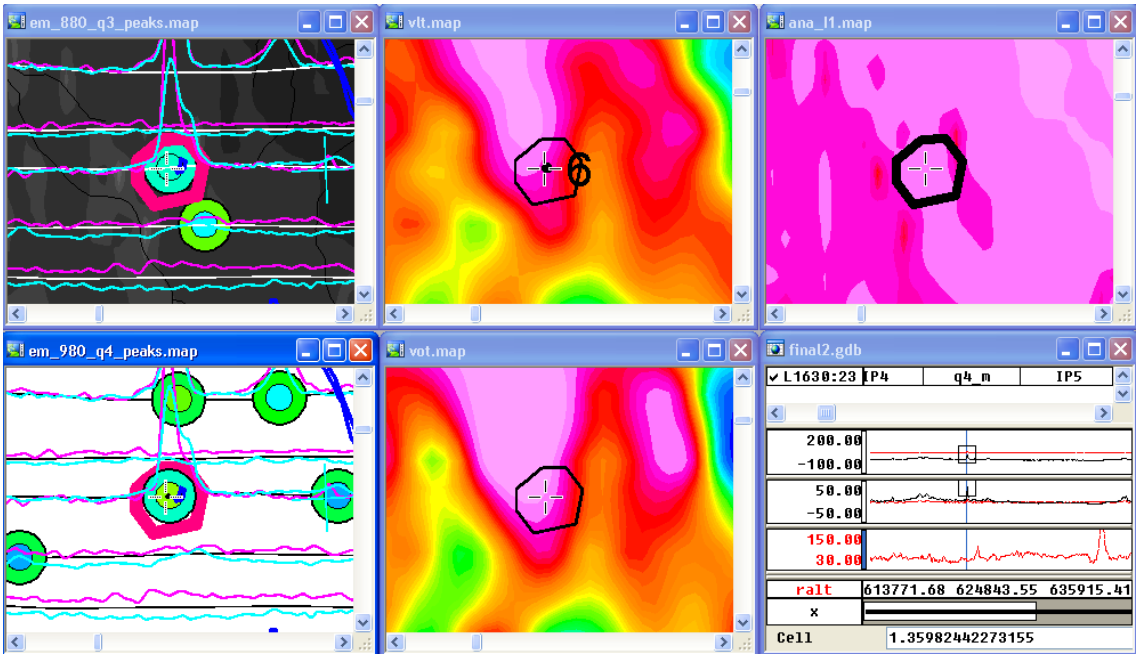

(b)

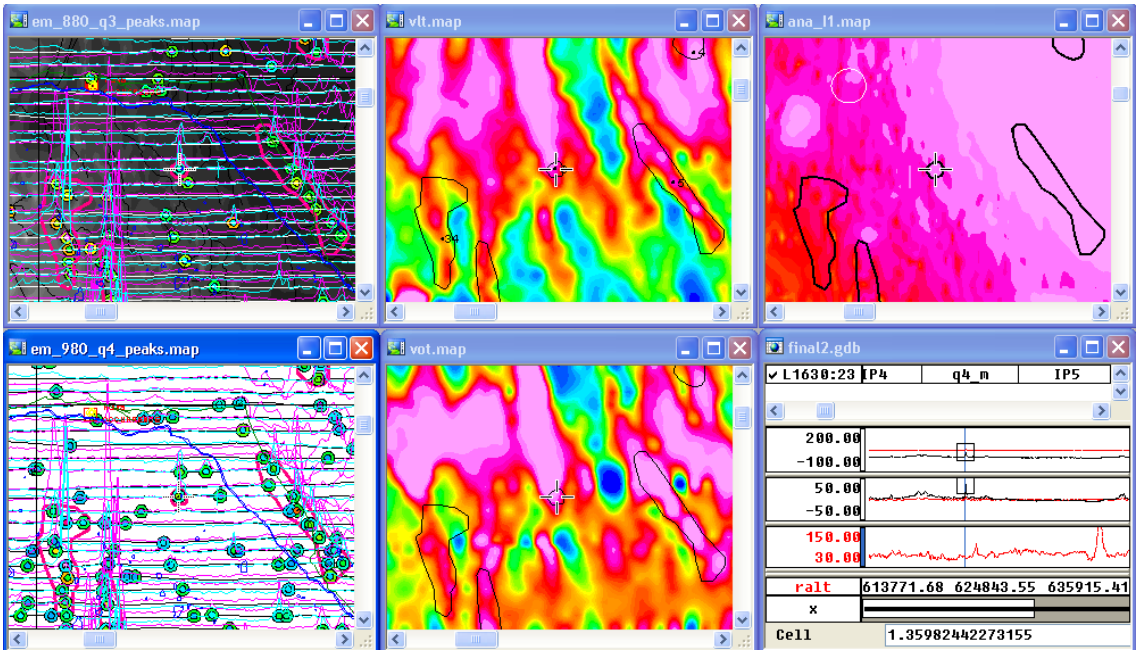

Figure 41. *Target Røros 6; a few medium EM peaks; positive VLF anomalies; at boundary of strong long wavelength magnetic anomaly; priority 4*

(a)

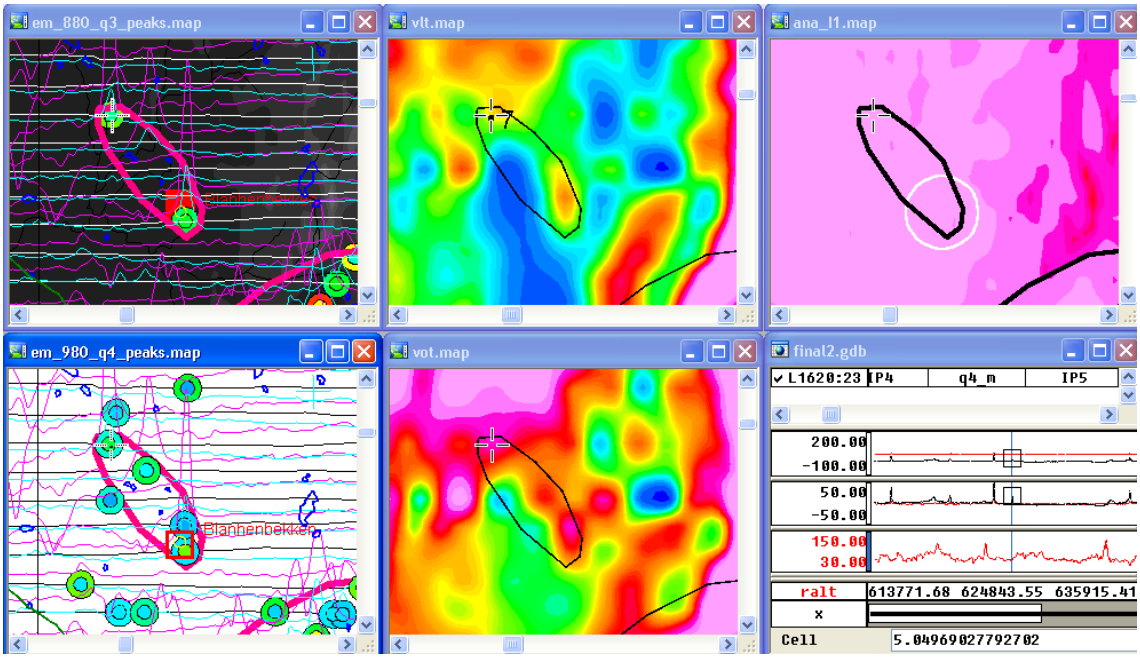

(b)

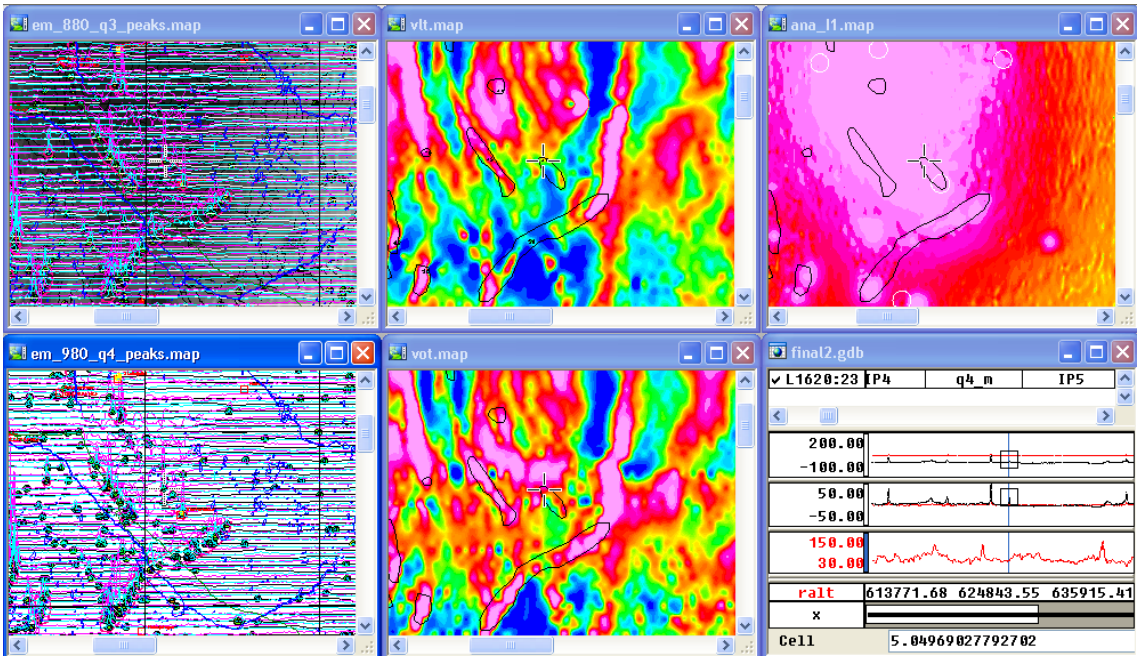

Figure 42. *Target Røros 7; a few medium EM peaks; weak VLF anomalies; strong long wavelength magnetic anomaly; priority 5*

(a)

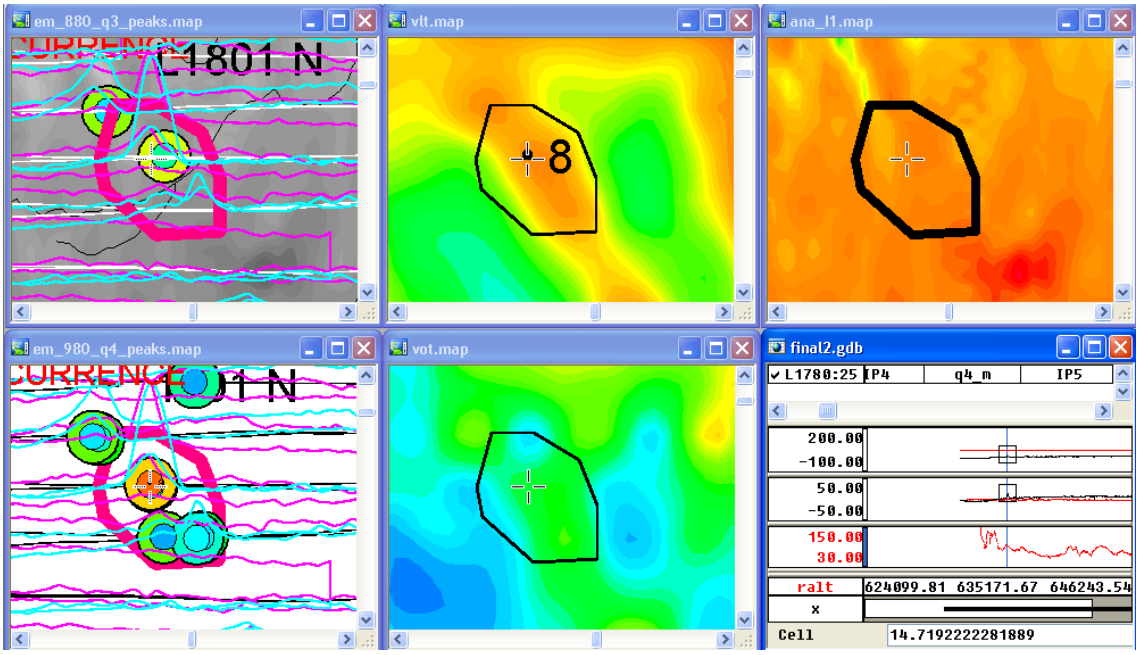

(b)

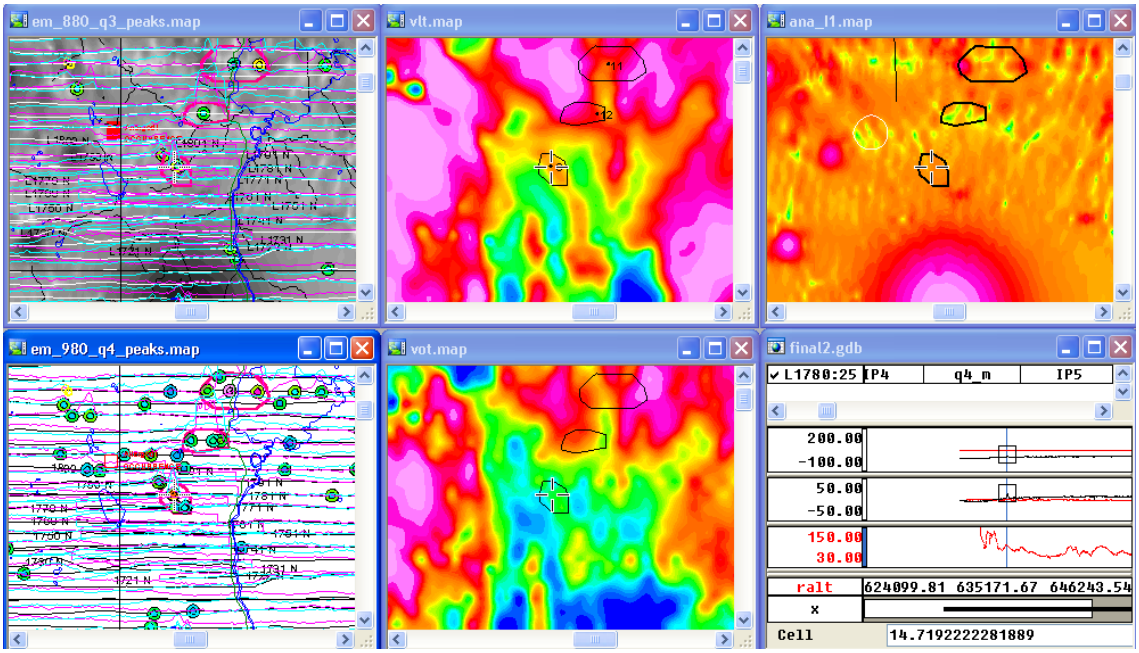

Figure 43. *Target Røros 8; a few medium EM peaks; weak VLF anomalies; no significant magnetic anomaly; priority 5*

(a)

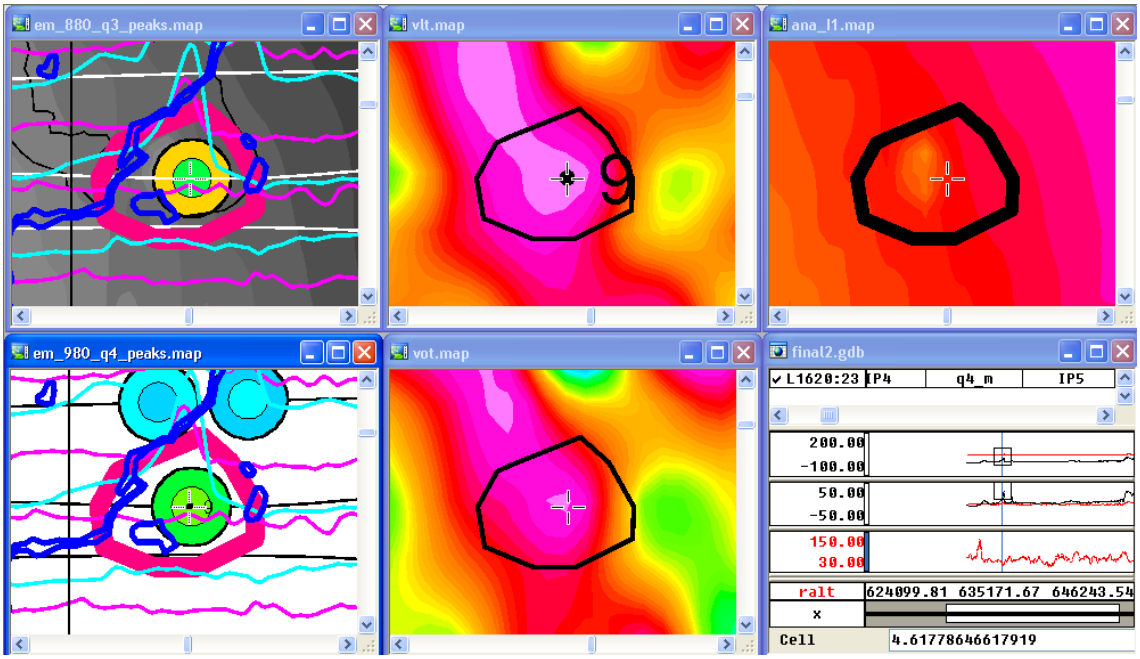

(b)

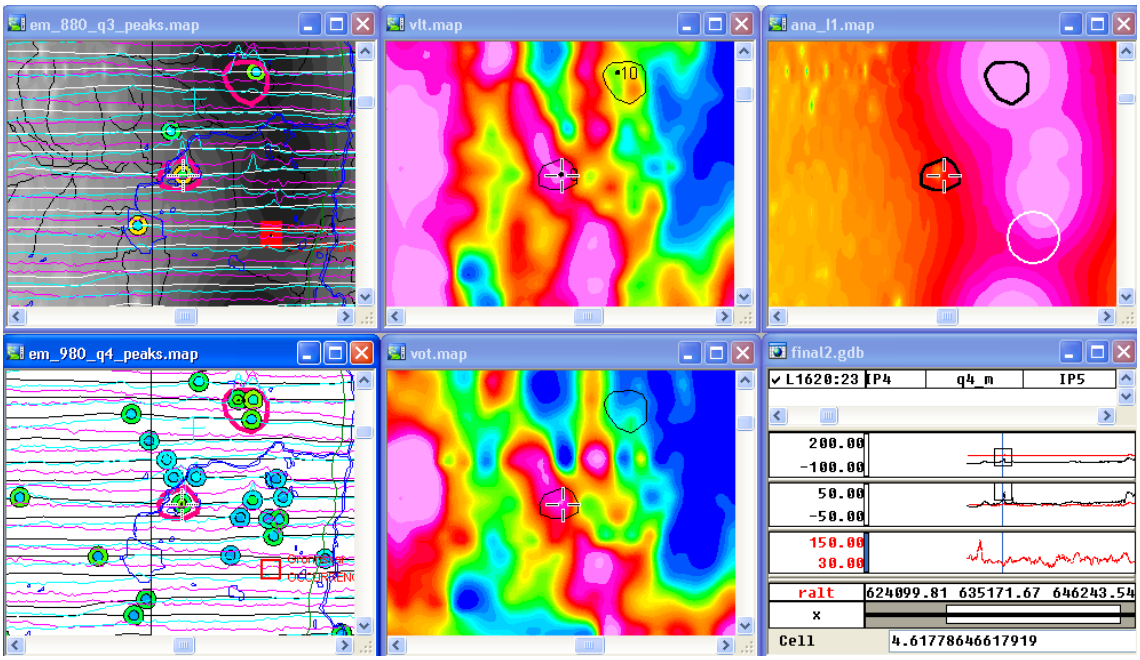

Figure 44. *Target Røros 9; an isolated EM peak; positive VLF anomalies along same trend of weak EM further north; adjacent to magnetic anomaly; priority 4*

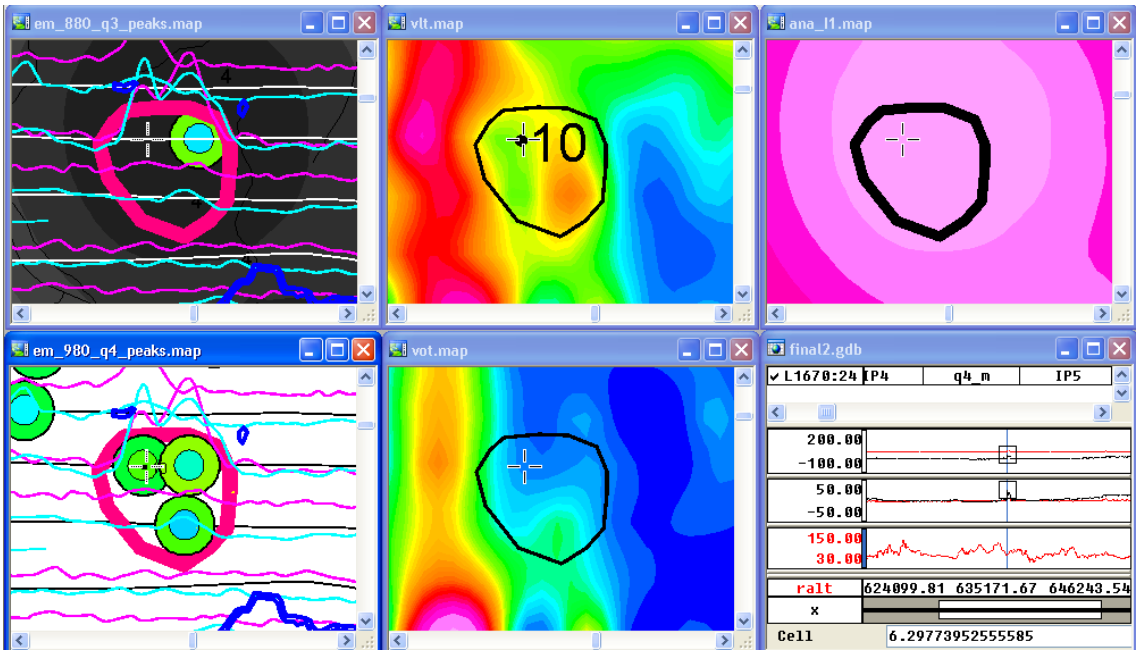

(b)

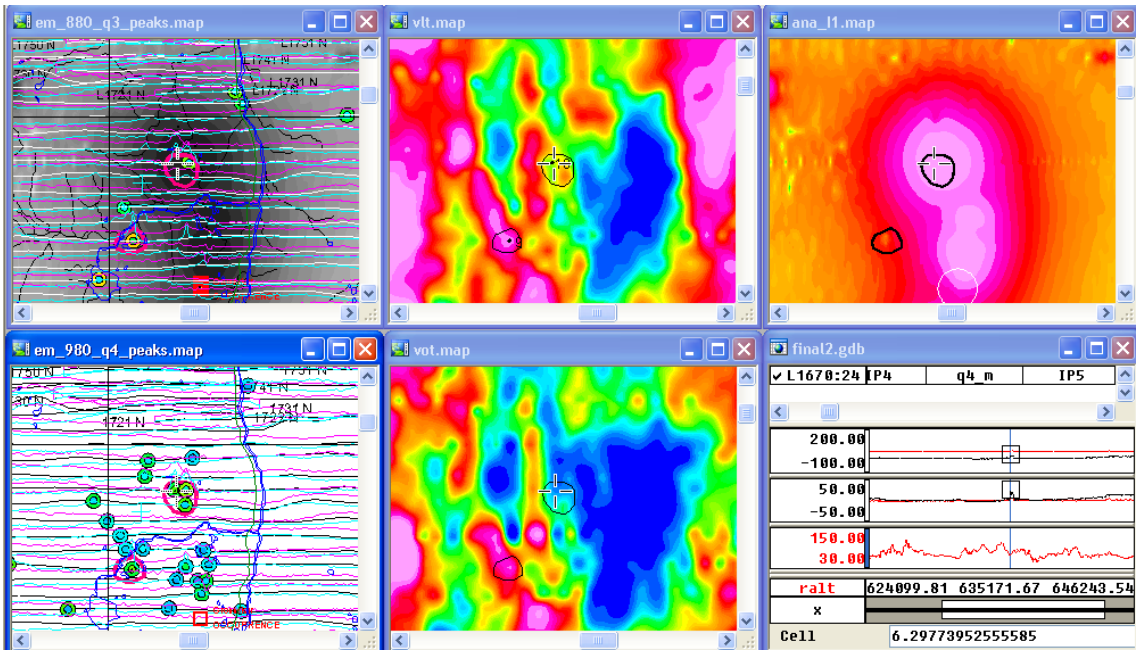

Figure 45. *Target Røros 10; a few medium to weak EM peaks; no VLF anomalies; short wavelength magnetic anomaly; priority 5*

(a)

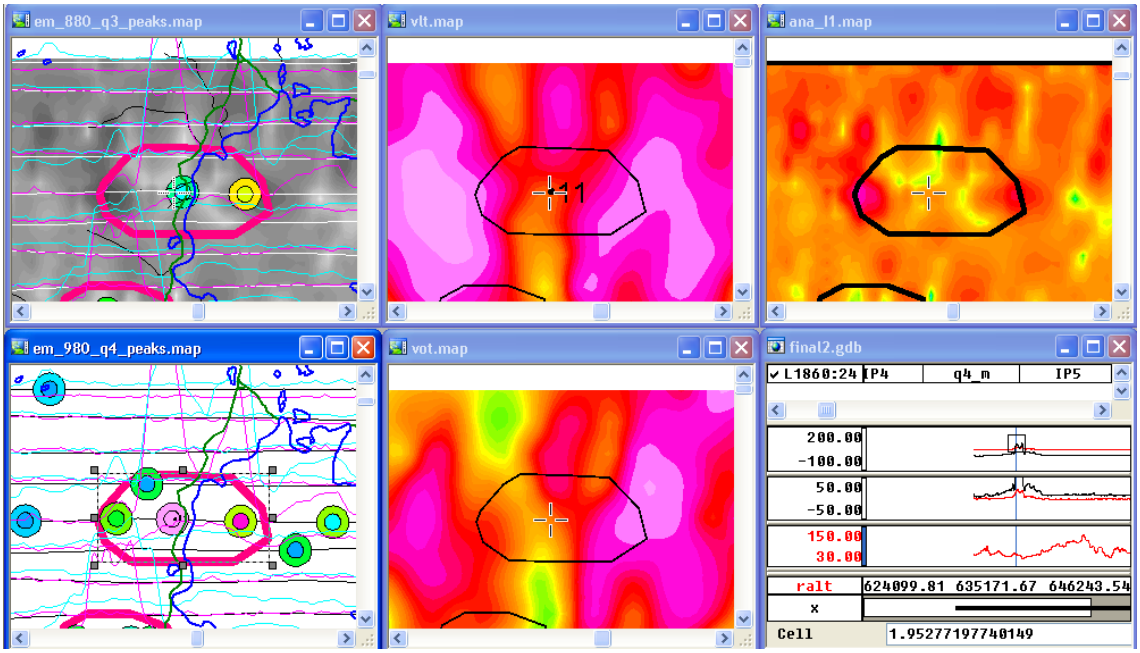

(b)

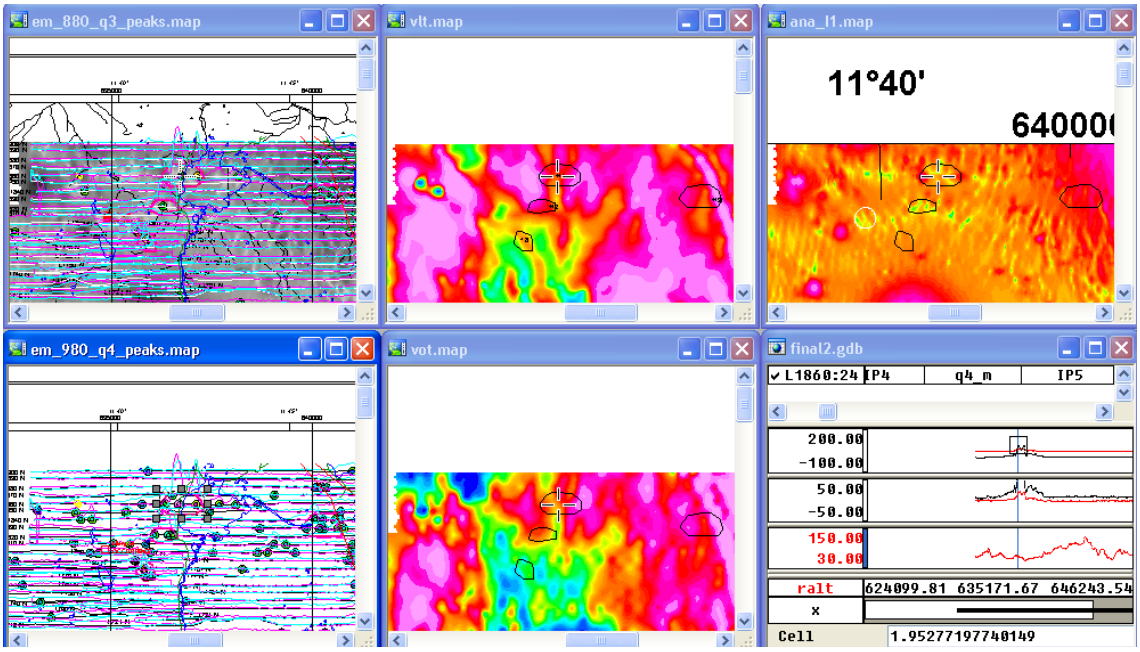

Figure 46. *Target Røros 11; a group of medium EM peaks; positive VLF anomalies at western and eastern boundary of polygon; no pronounced short wavelength magnetic anomaly; priority 4*

(a)

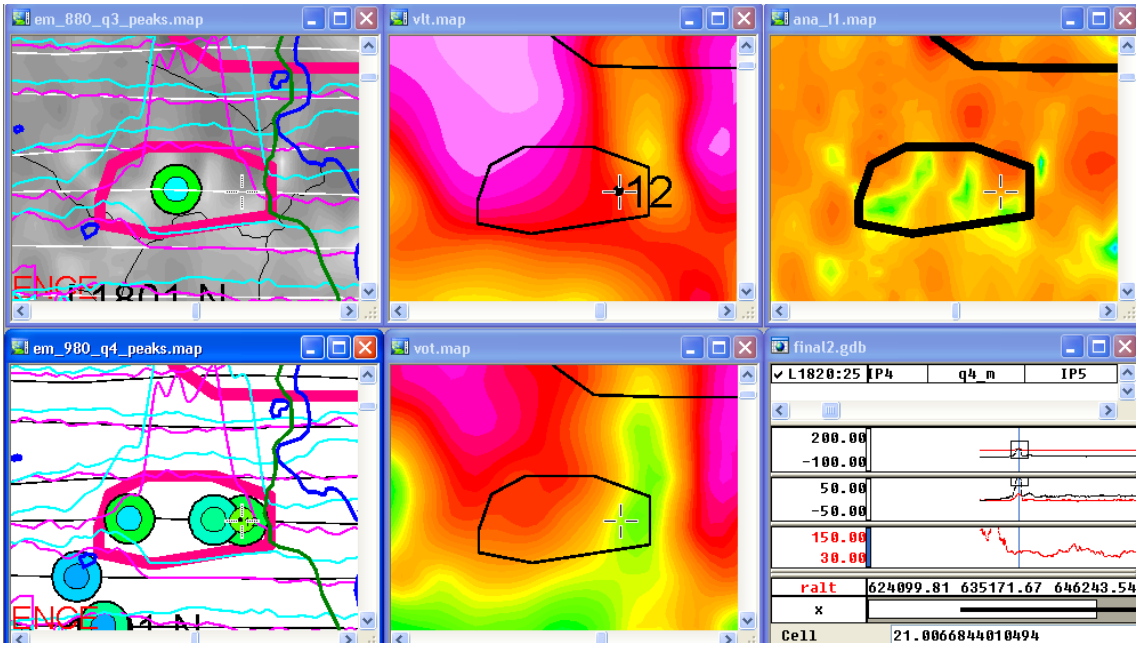

(b)

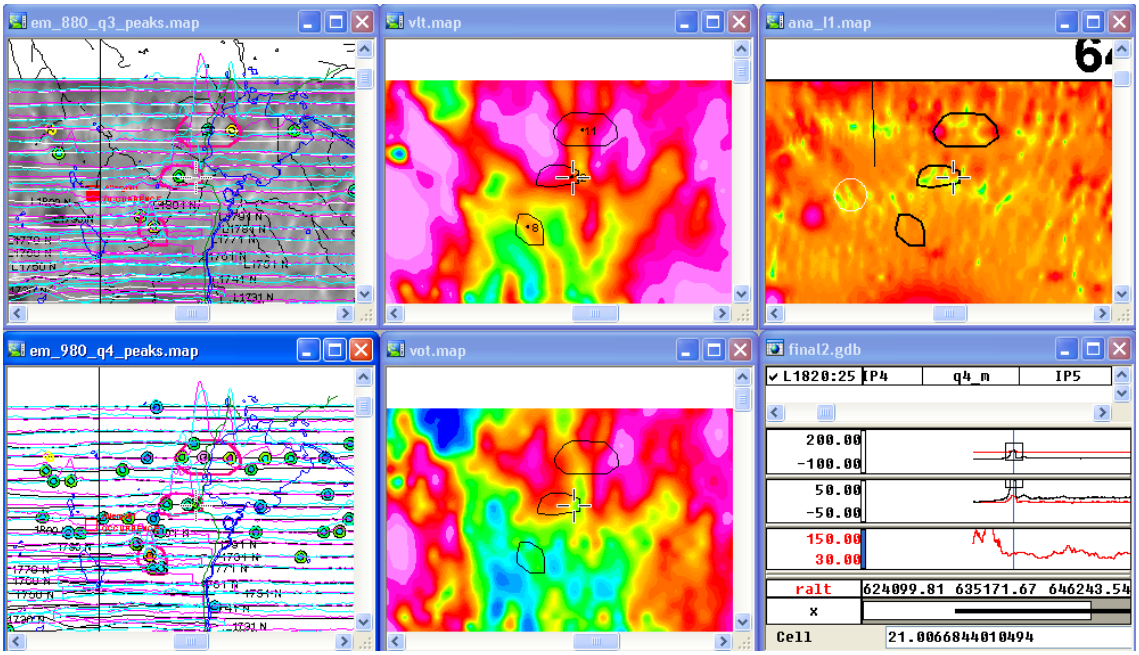

Figure 47. *Target Røros 12; a few medium EM peaks; positive VLF anomalies at western boundary of polygon; some weak short wavelength magnetic anomaly; priority 4*

(a)

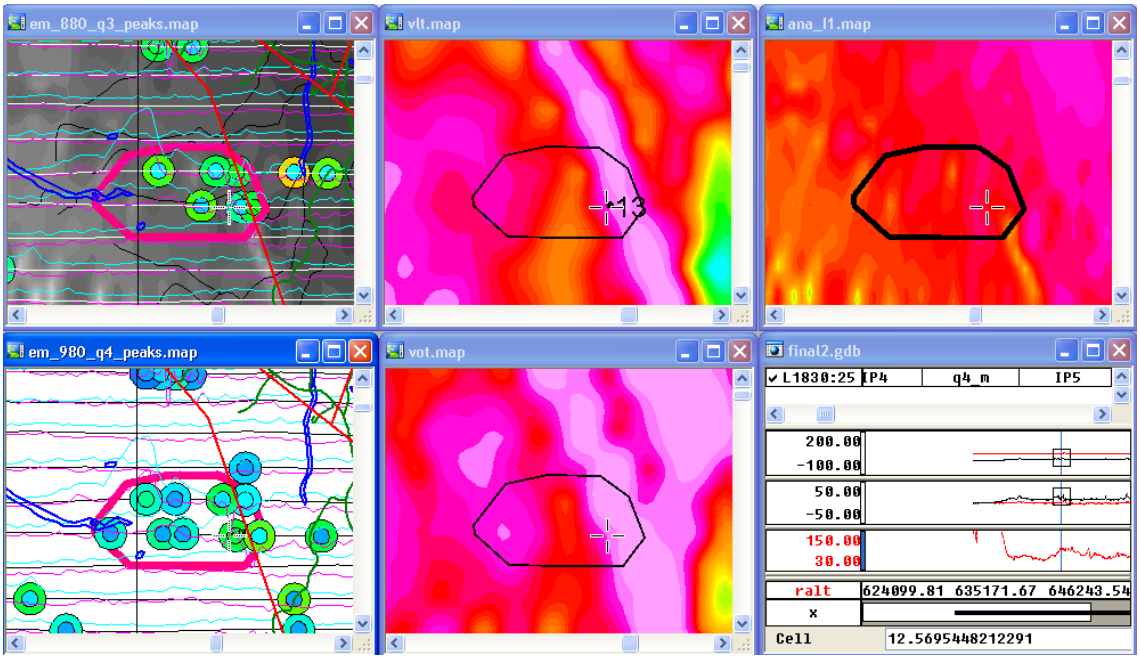

(b)

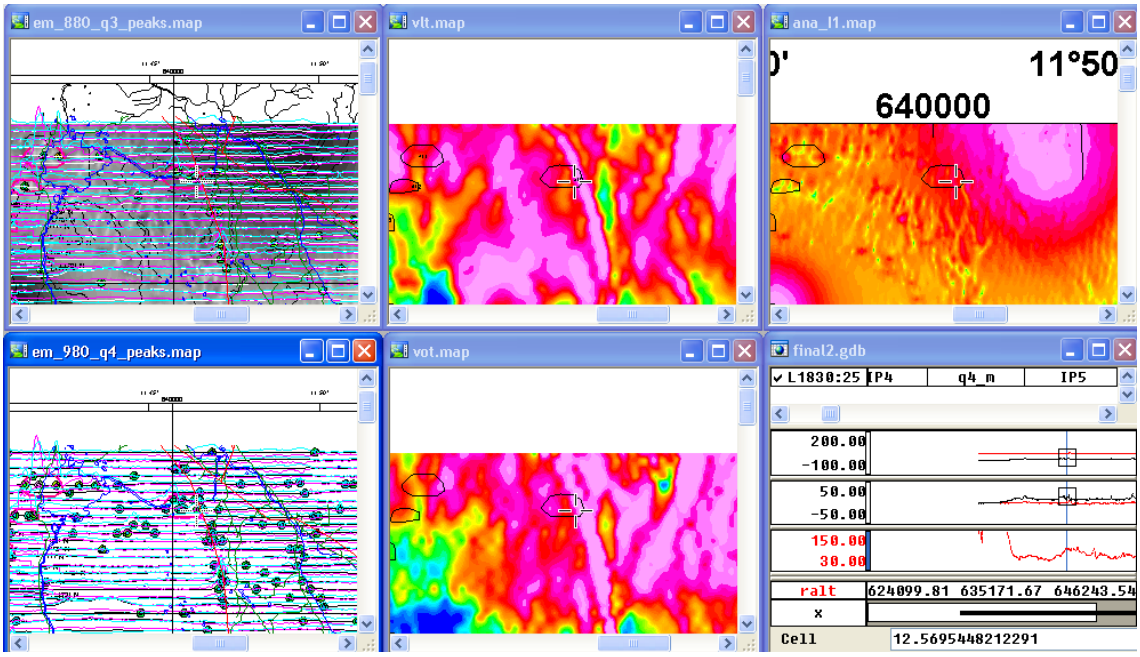

Figure 48. *Target Røros 13; a group of medium EM peaks; medium positive VLF anomalies at western boundary of polygon – probably disturbed by power line; weak short wavelength magnetic anomaly; priority 5*

(a)

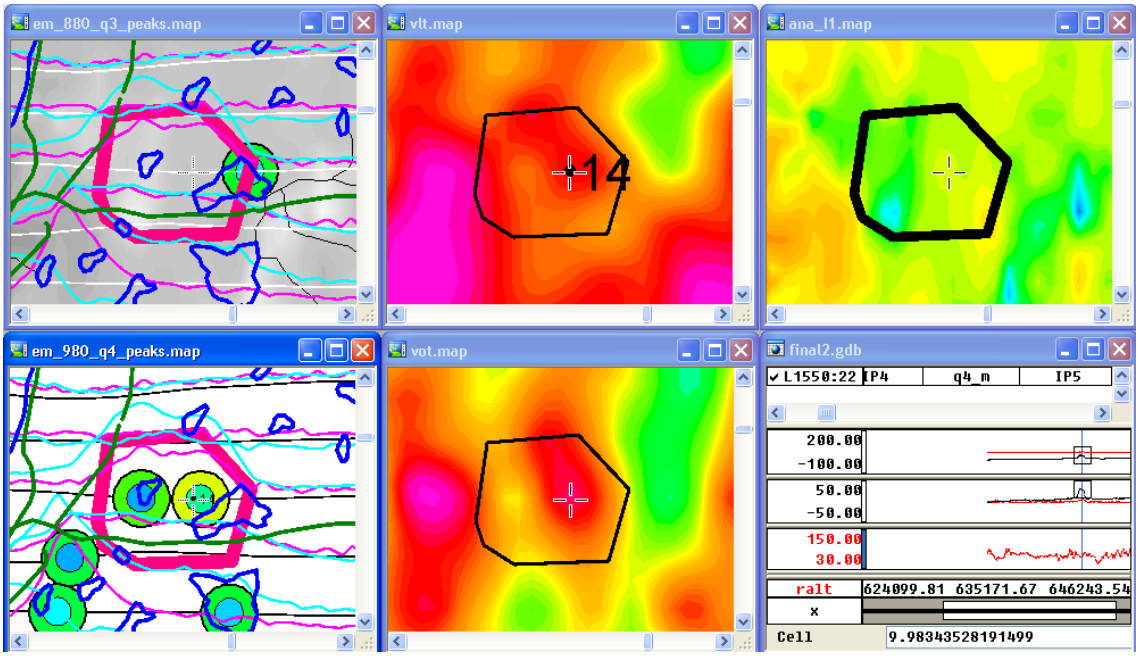

(b)

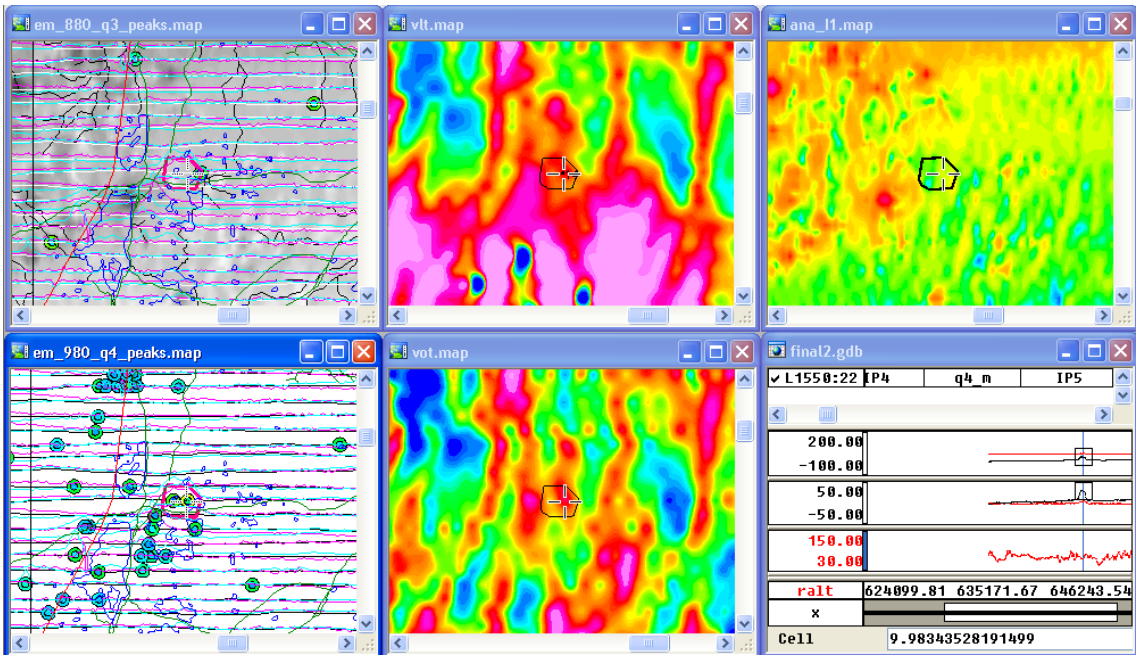

Figure 49. *Target Røros 14; a few medium EM peaks; weakpostive VLF anomalies at western and eastern boundary of polygon; adjacent weak short wavelength magnetic anomaly; priority 5*

(a)

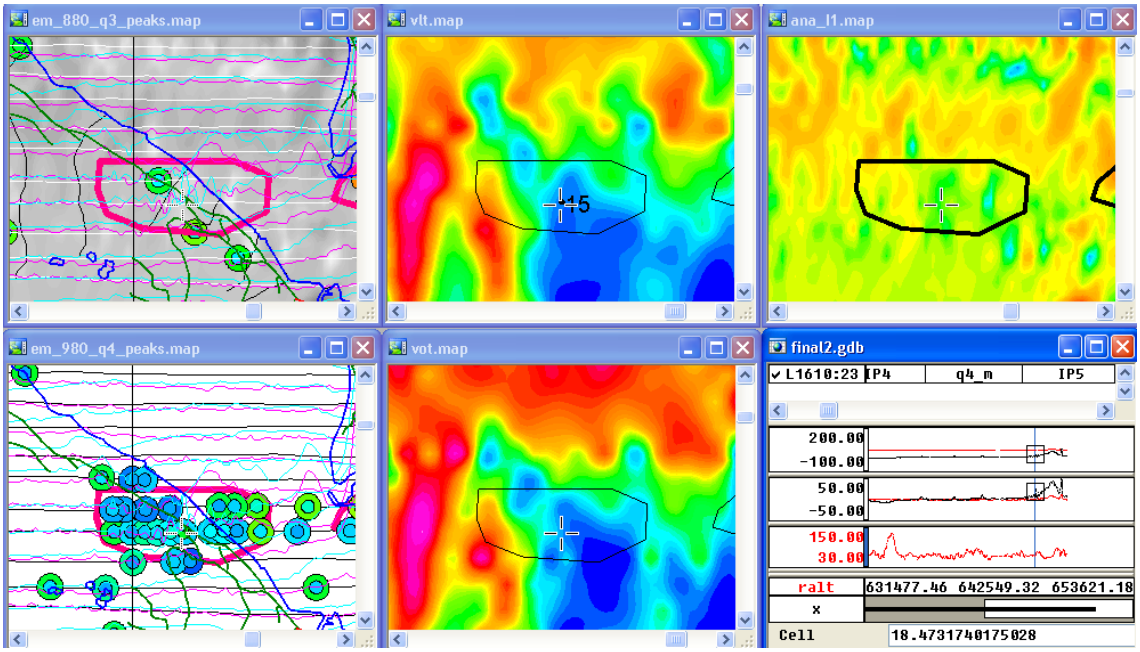

(b)

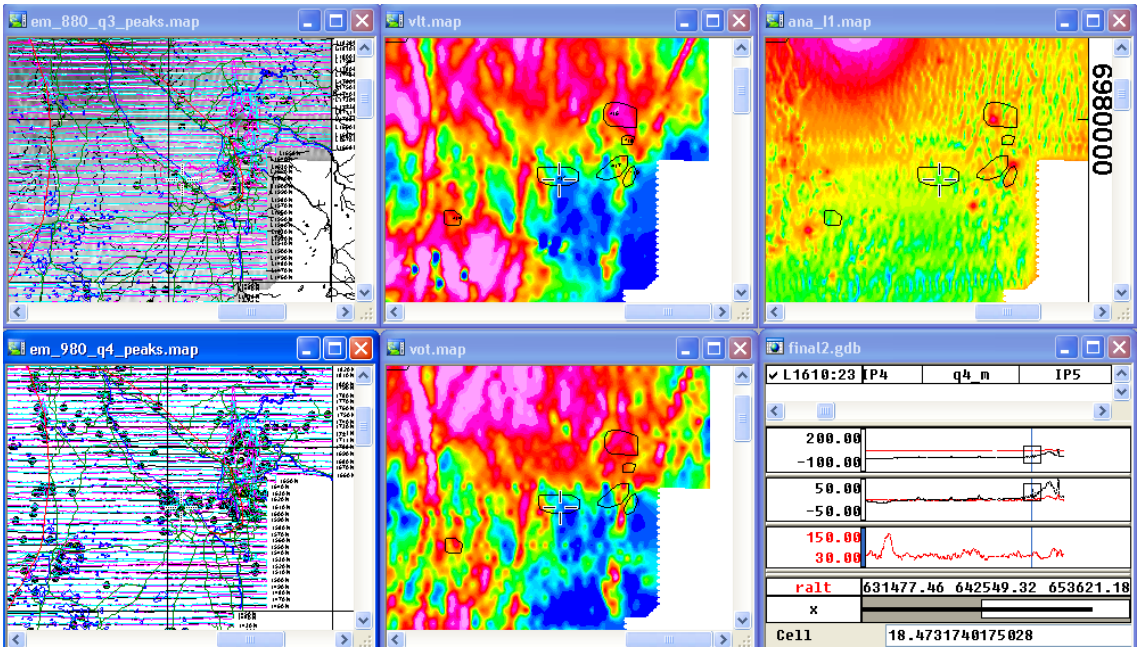

Figure 50. *Target Røros 15; a group of medium to weak EM peaks; no VLF anomalies; no pronounced short wavelength magnetic anomaly; priority 5*

(a)

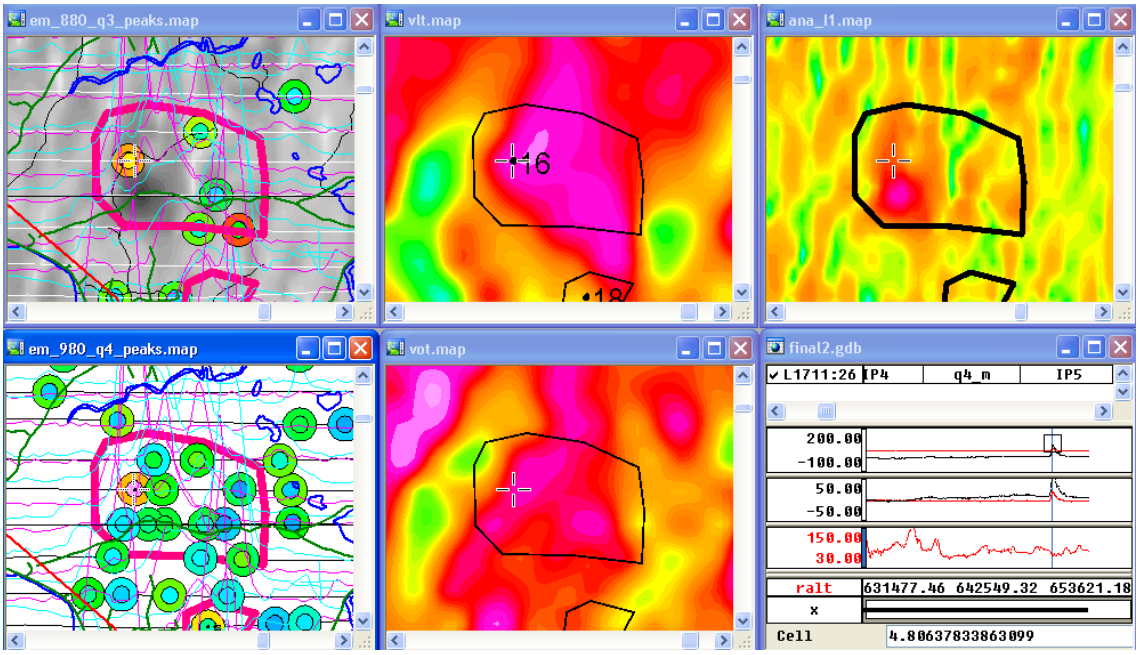

(b)

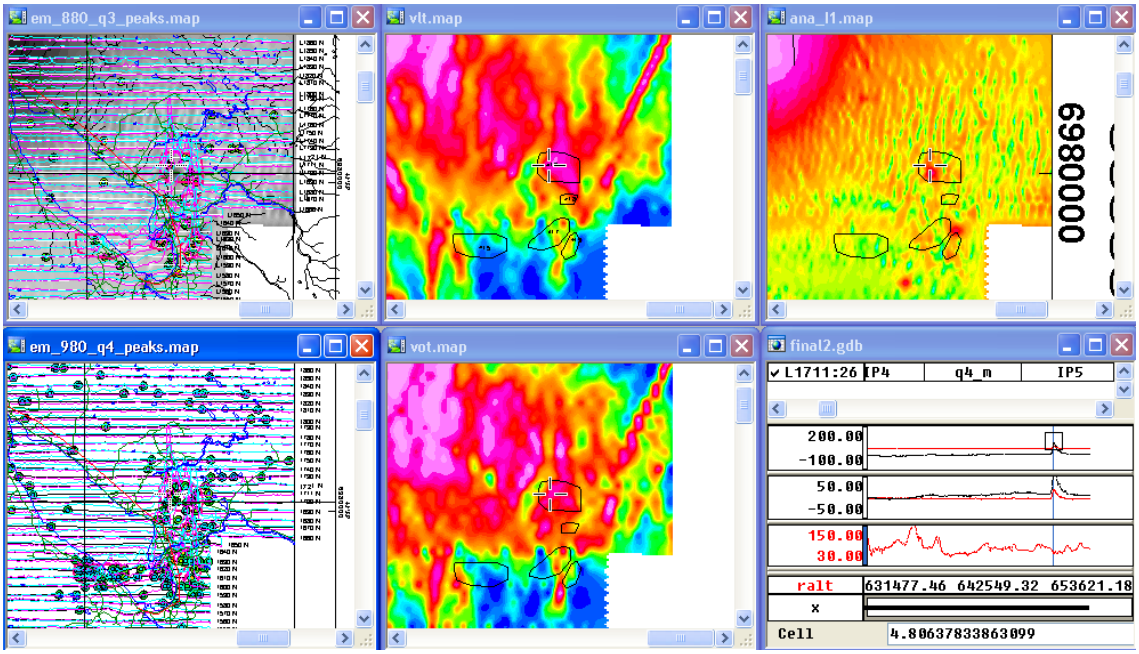

Figure 51. *Target Røros 16; a group of medium to large EM peaks; clear VLF anomalies; clear short wavelength magnetic anomaly; priority 2*

(a)

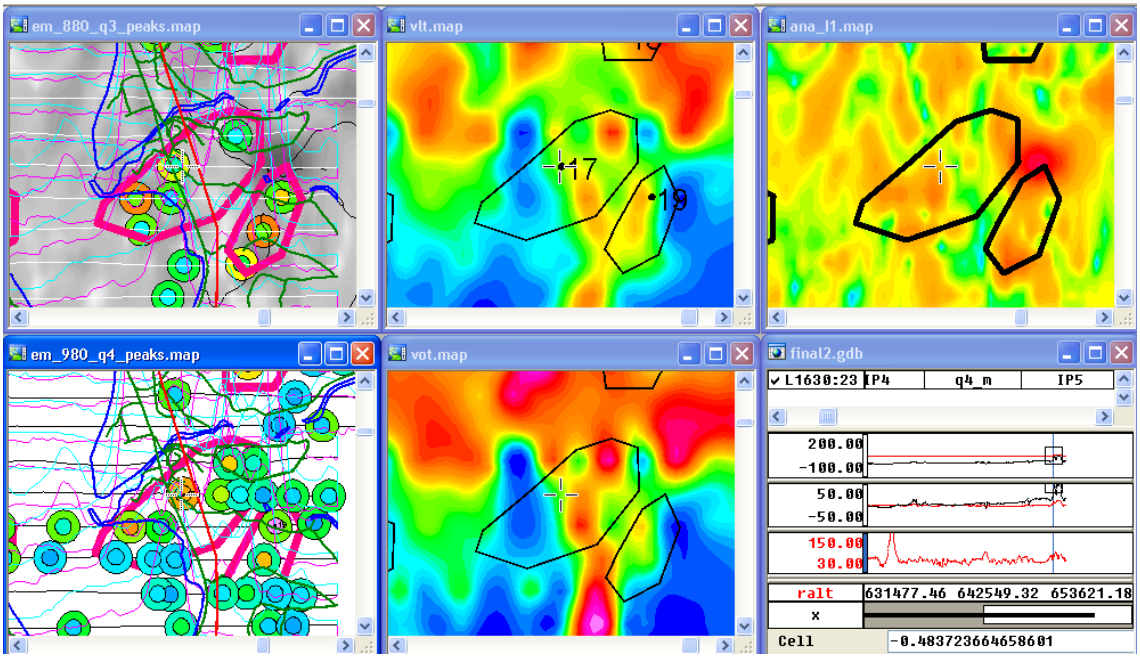

(b)

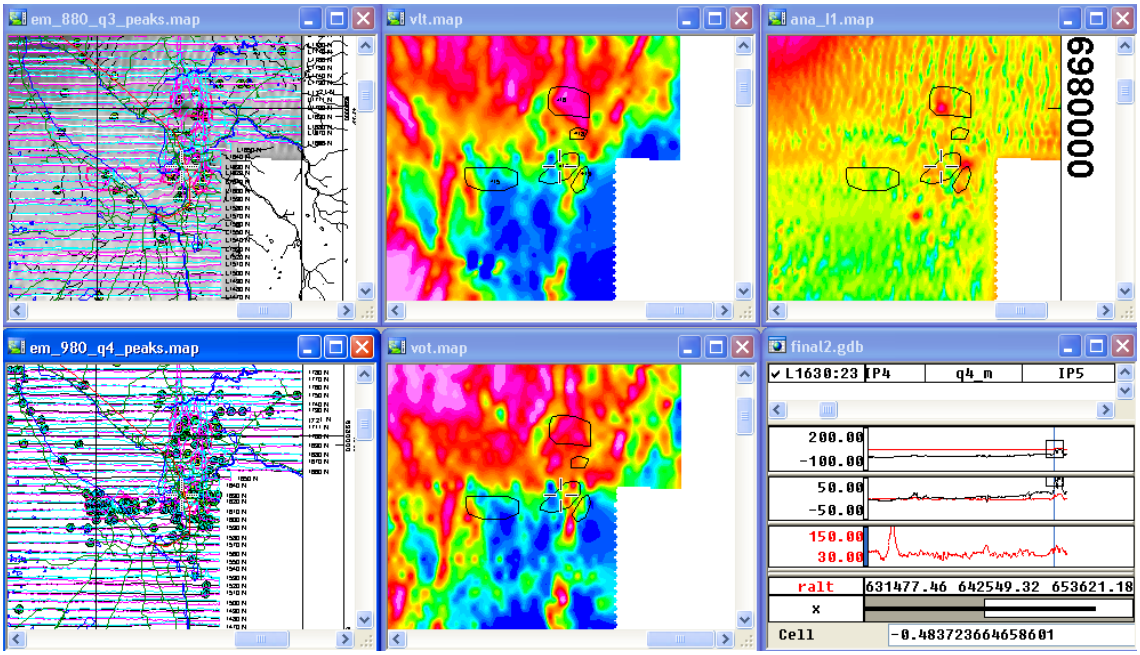

Figure 52. *Target Røros 17; a group of medium EM peaks; weak VLF anomalies; clear short wavelength magnetic anomaly; priority 3*

(a)

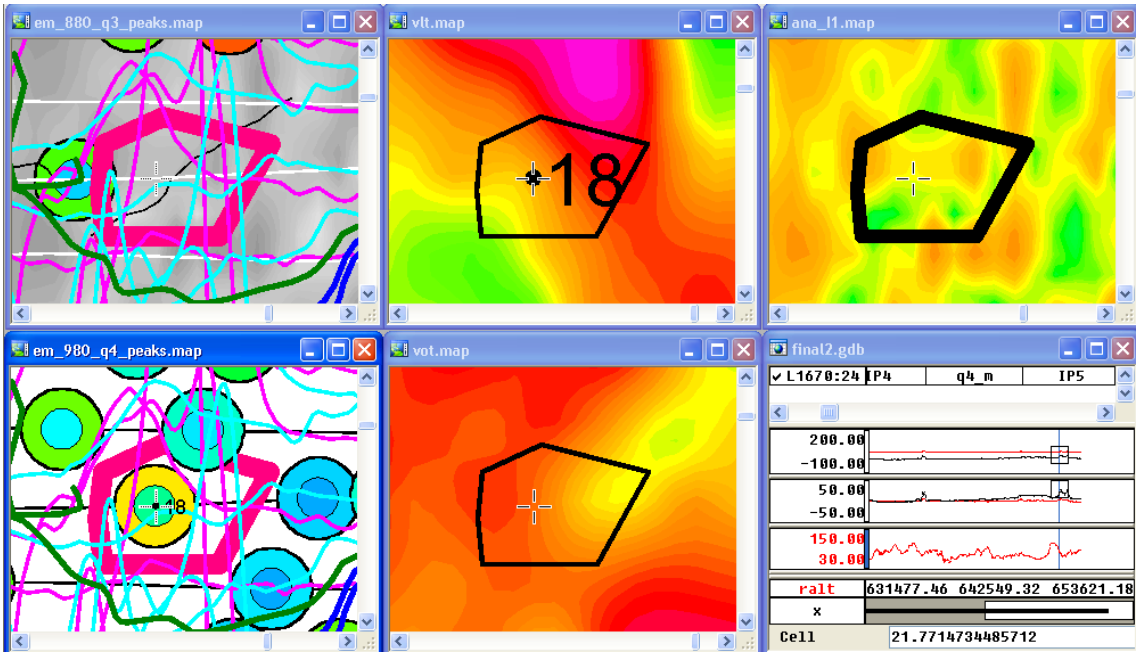

(b)

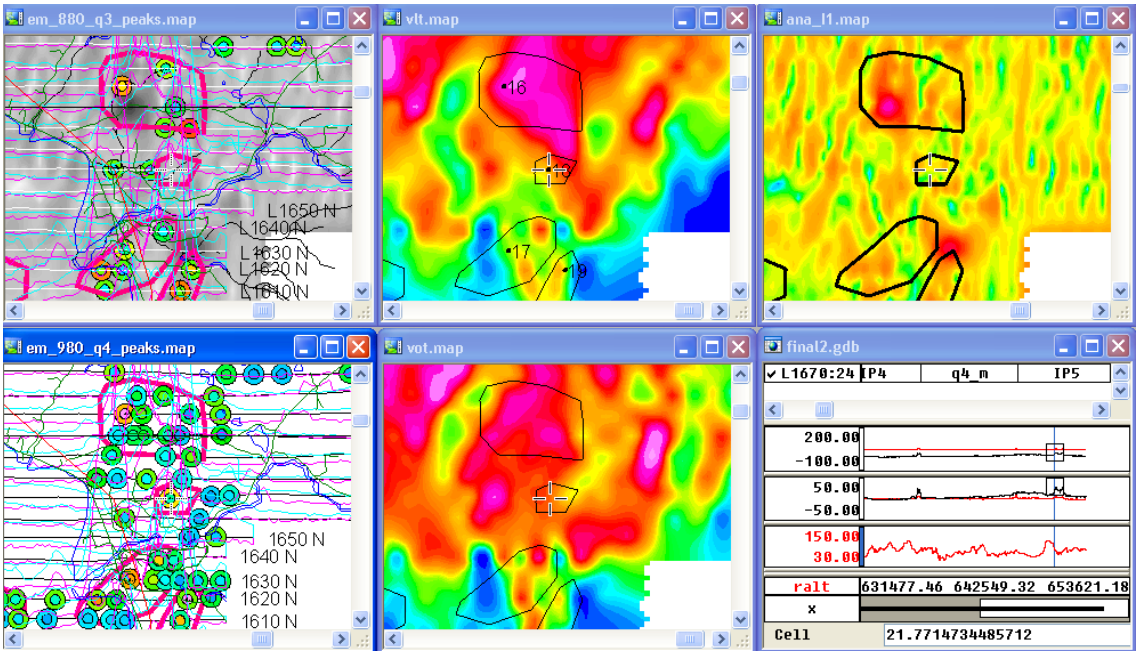

Figure 53. *Target Røros 18; a single medium EM peak but surrounded by a large group of other EM peaks; medium VLF anomalies; weak short wavelength magnetic anomaly; priority 4*

(a)

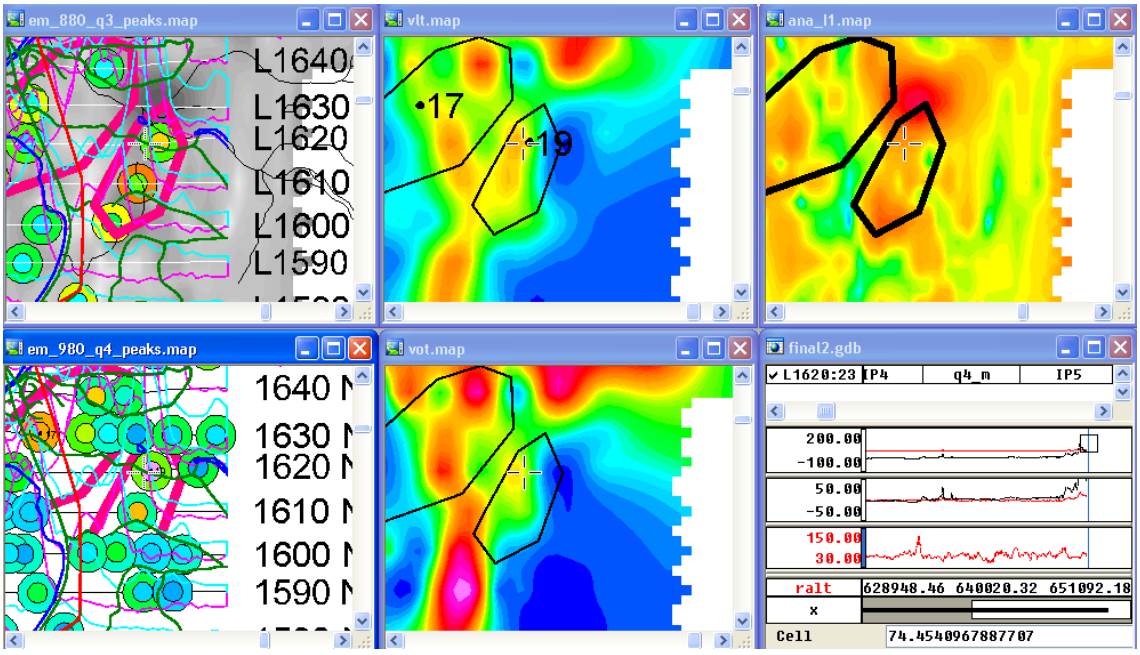

(b)

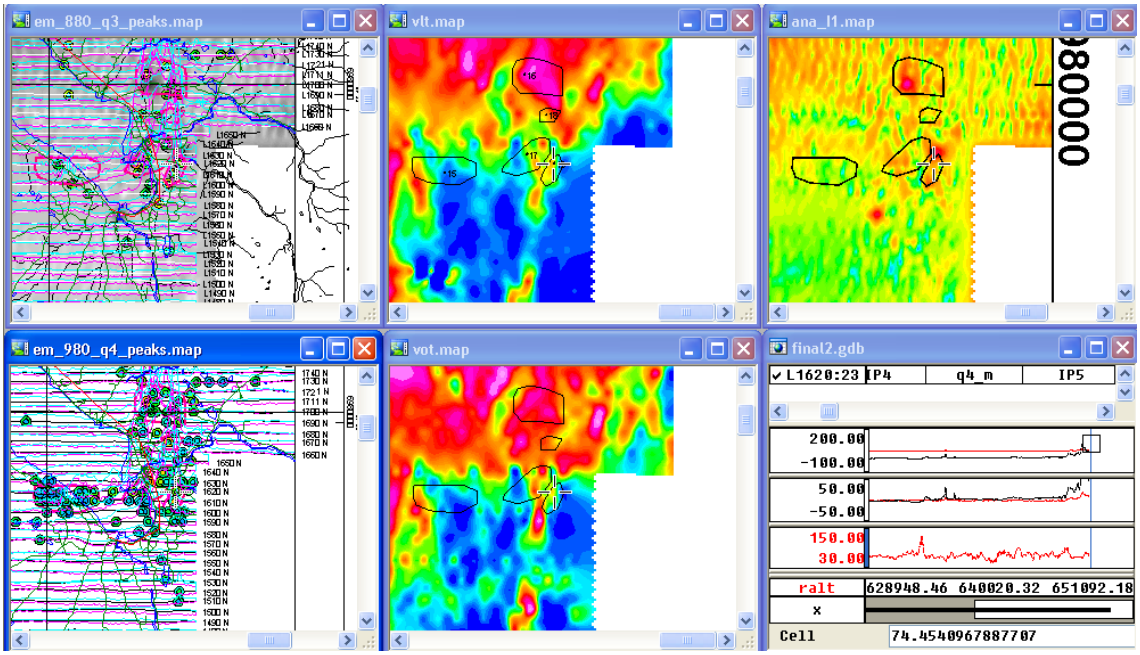

Figure 54. *Target Røros 19; a small group of medium EM peaks; mediumr VLF anomalies; adjacent short wavelength magnetic anomaly; priority 3*

(a)

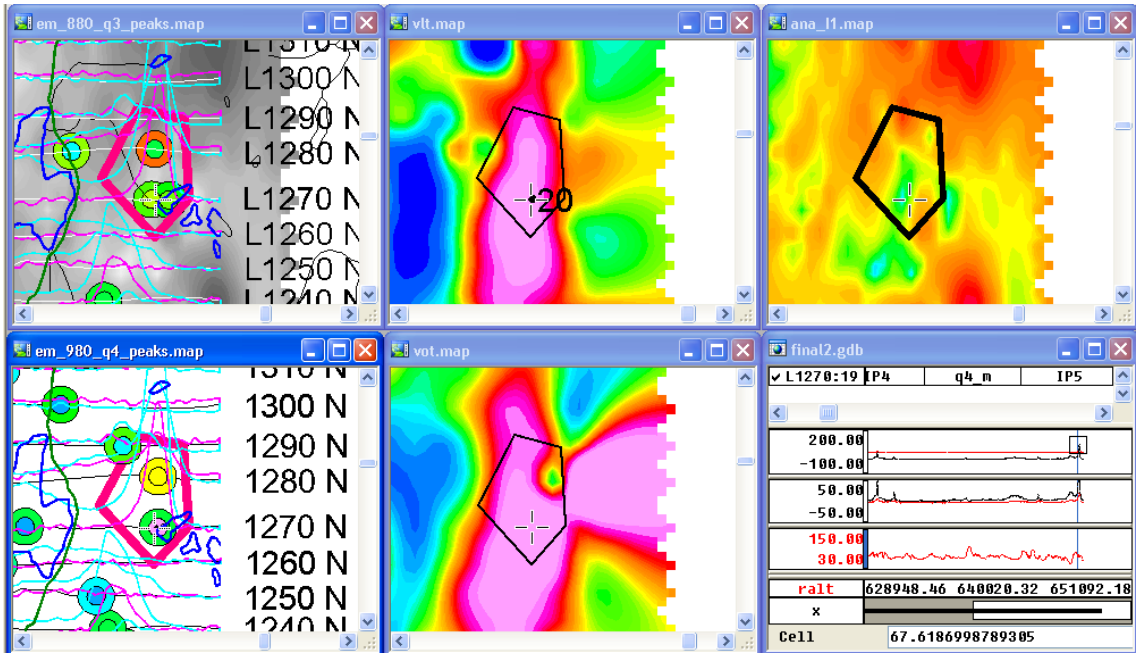

(b)

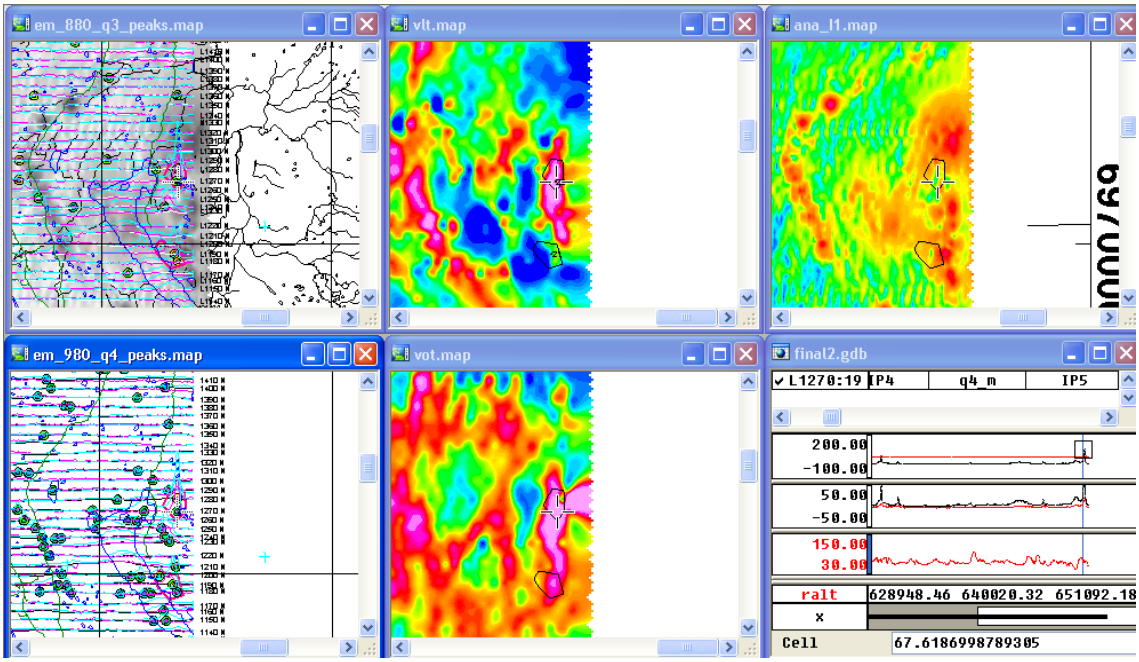

Figure 55. *Target Røros 20; two medium to large EM peaks; clear VLF anomalies; clear short wave-length magnetic anomaly; priority 4*

(a)

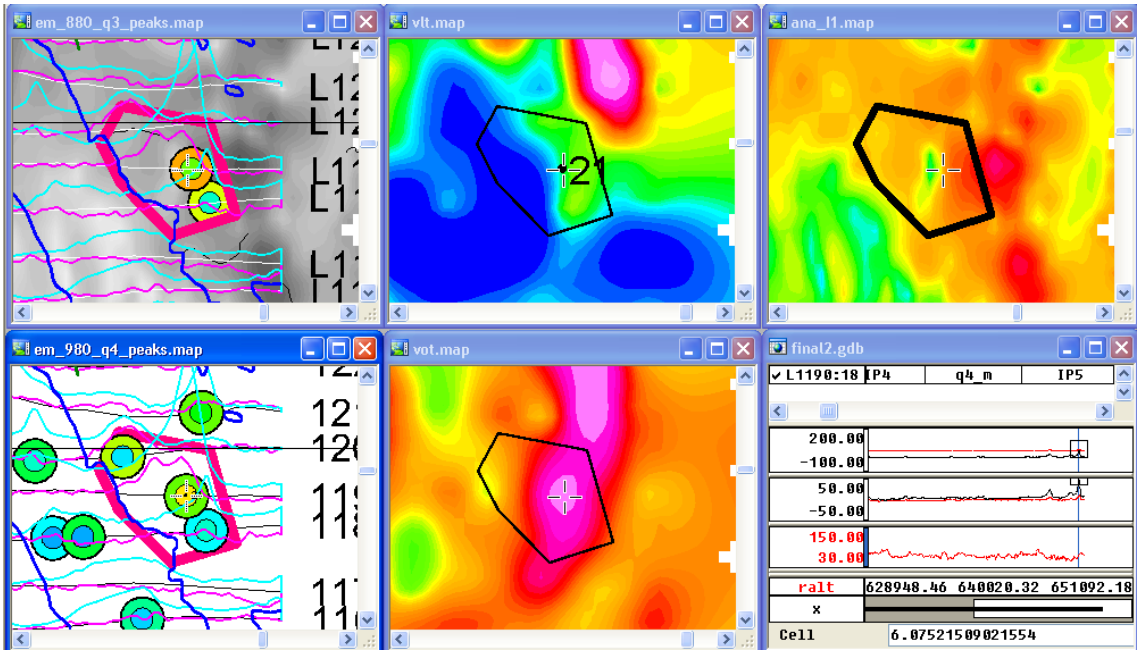

(b)

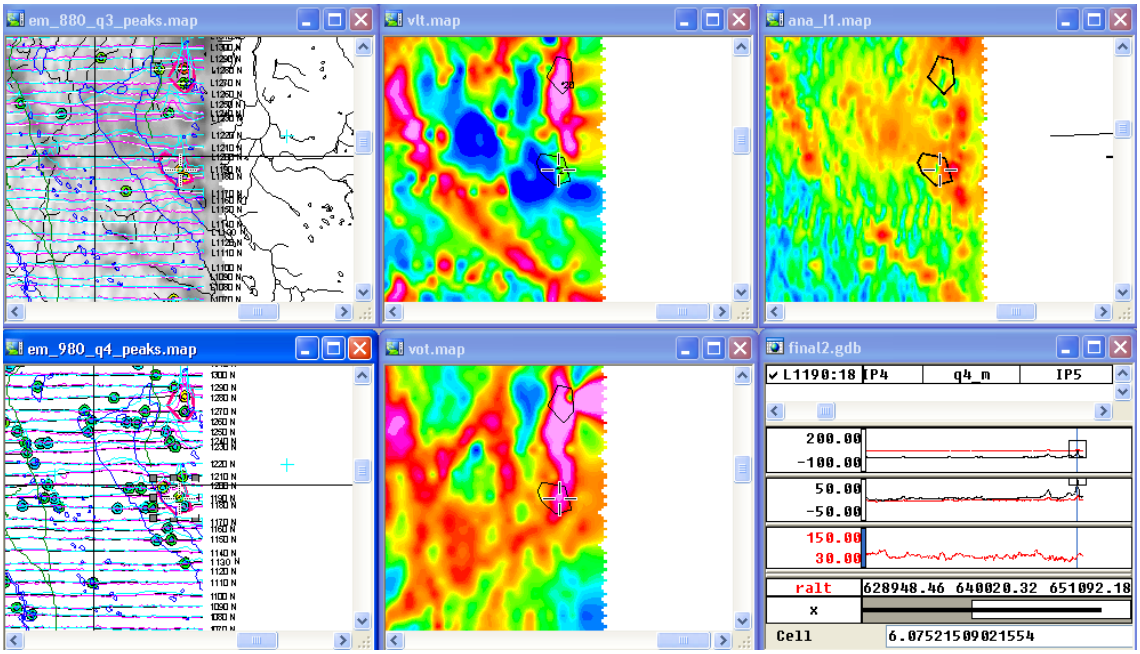

Figure 56. *Target Røros 21; a few medium to large EM peaks; clear VLF anomalies for one direction; clear short wavelength magnetic anomaly; priority 3*

(a)

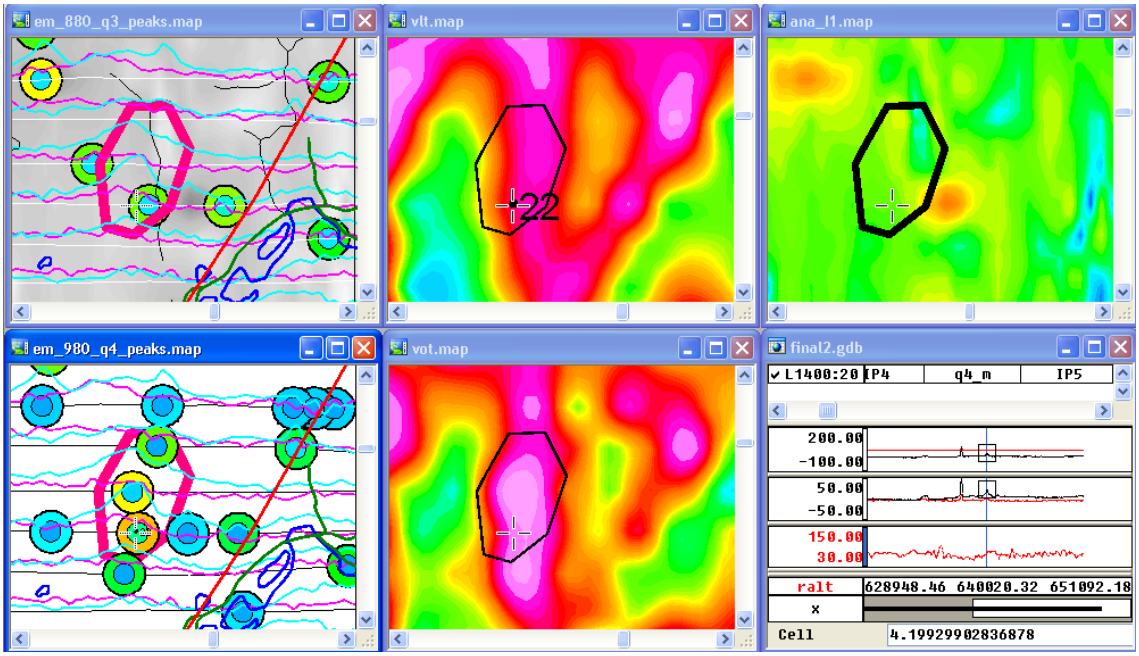

(b)

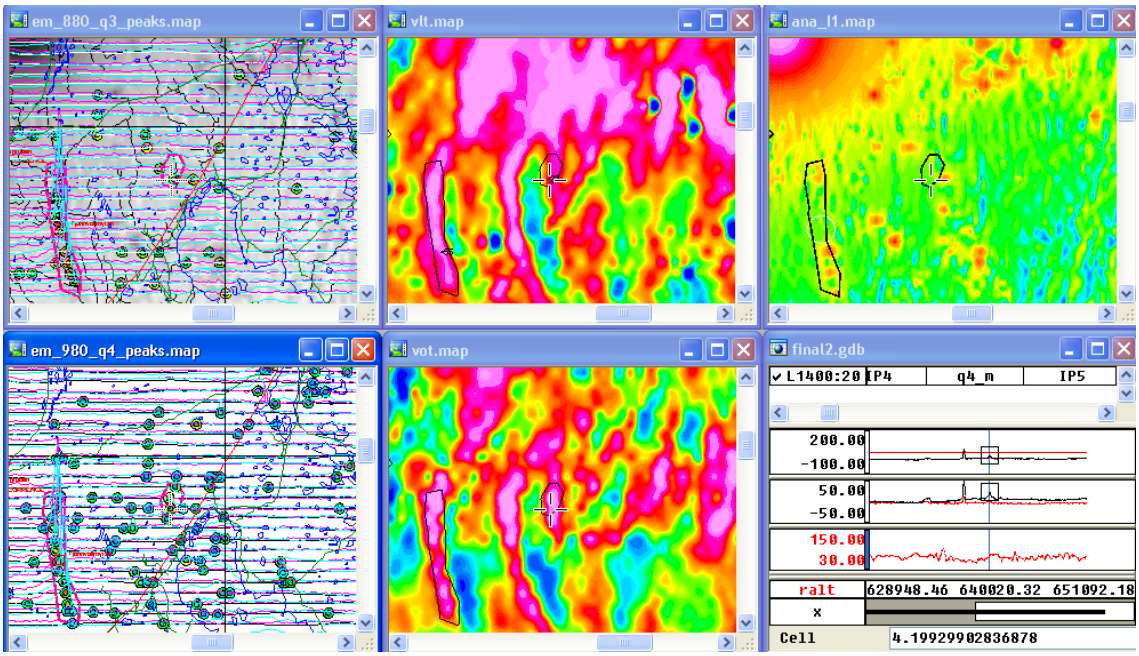

Figure 57. *Target Røros 22; a small group of medium EM peaks; clear VLF anomalies; within trend of medium short wavelength magnetic anomalies; priority 4*

(a)

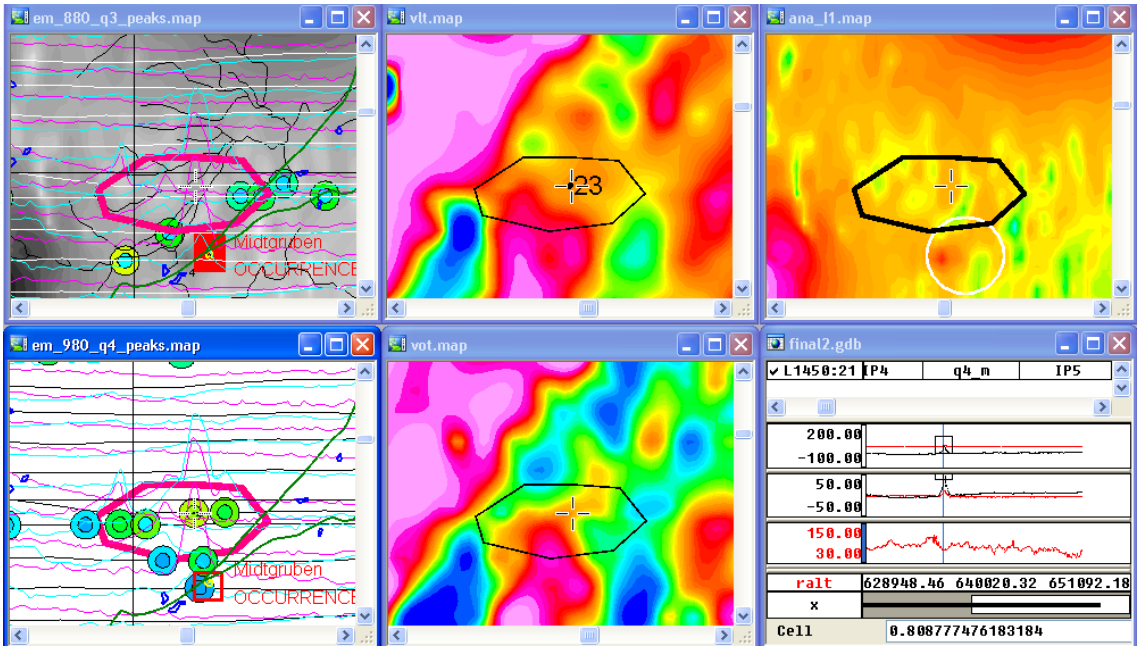

(b)

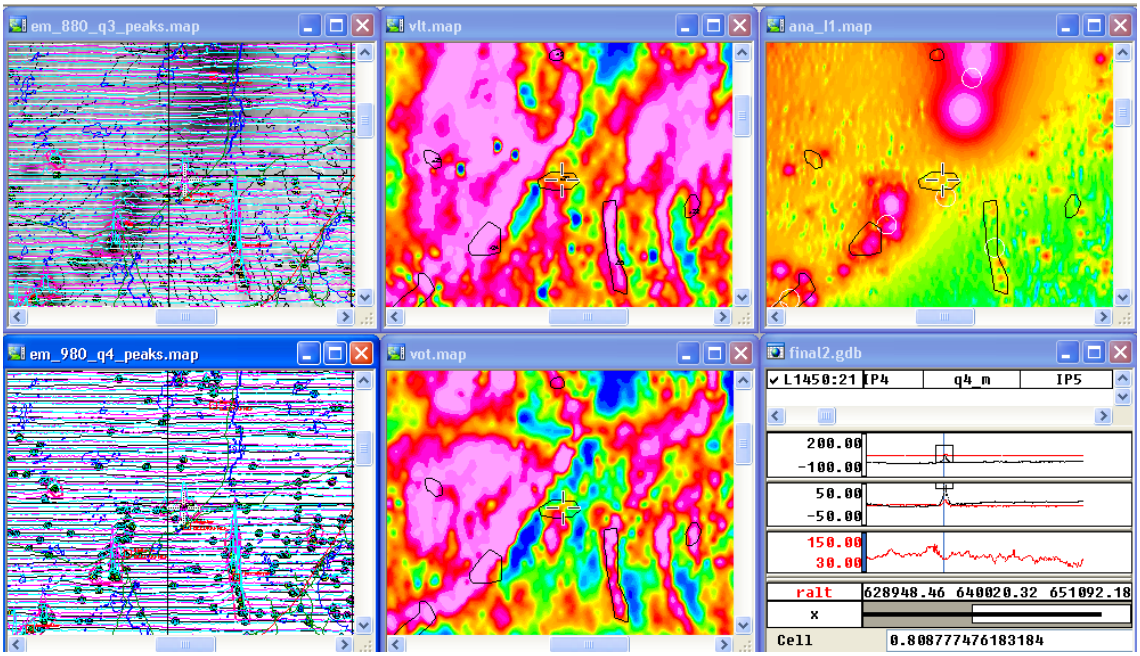

Figure 58. *Target Røros 23; a small group of medium EM peaks; medium to weak VLF anomalies; within trend of short wavelength magnetic anomaly; priority 3*

(a)

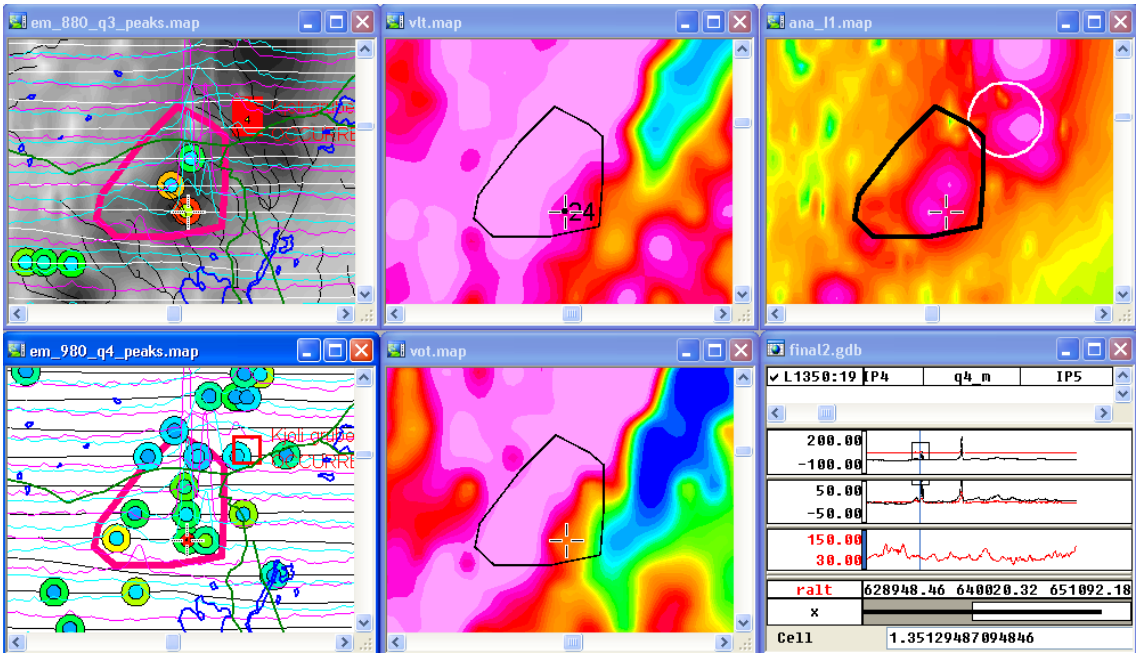

(b)

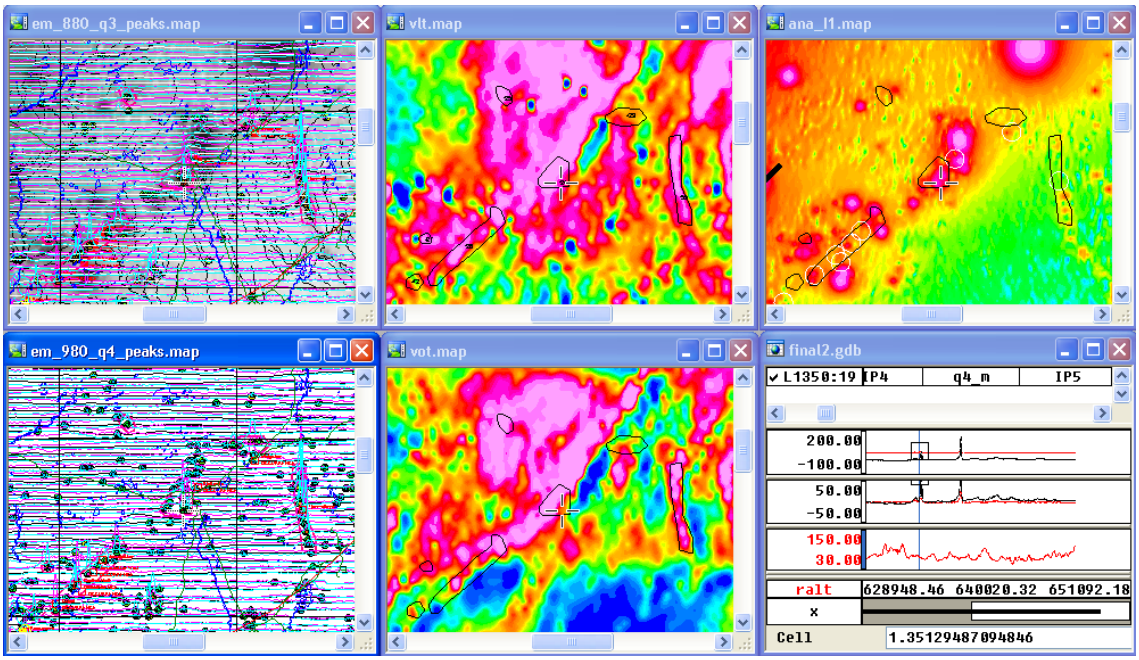

Figure 59. *Target Røros 24; a group of medium to large EM peaks; clear VLF anomalies; within trend of short wavelength magnetic anomaly; priority 1*

(a)

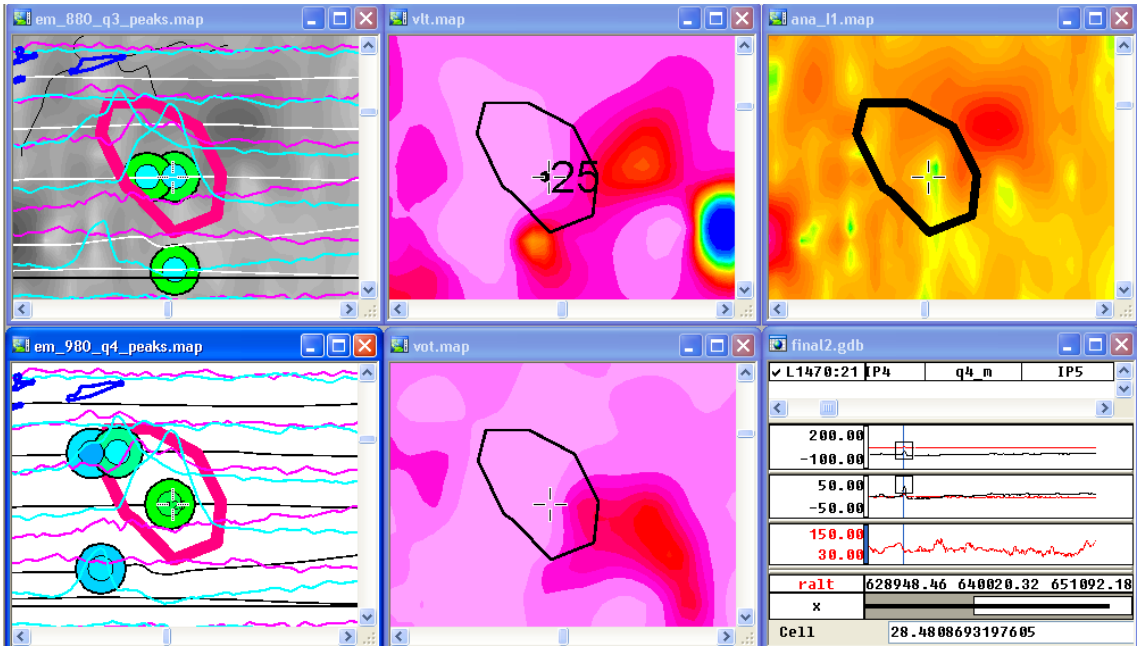

(b)

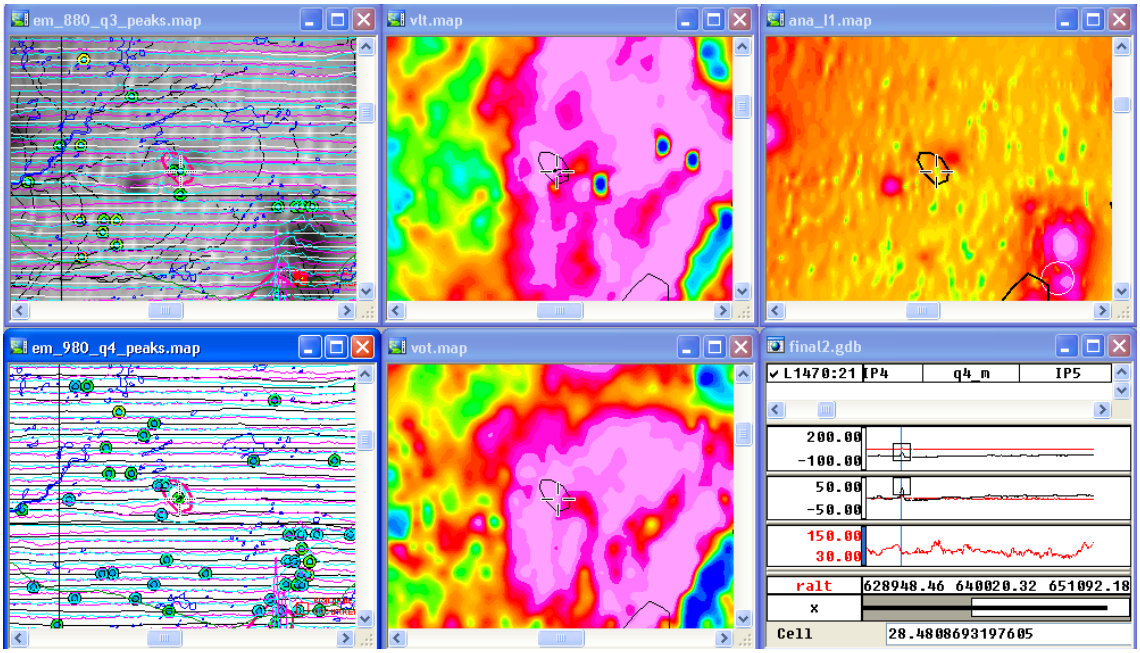

Figure 60. *Target Røros 25; a few medium EM peaks; large and broad VLF anomalies which do not have a clear correlation to the EM anomalies – the VLF may correspond to shallow surface conductivity structure; adjacent short wavelength magnetic anomaly; priority 4*

(a)

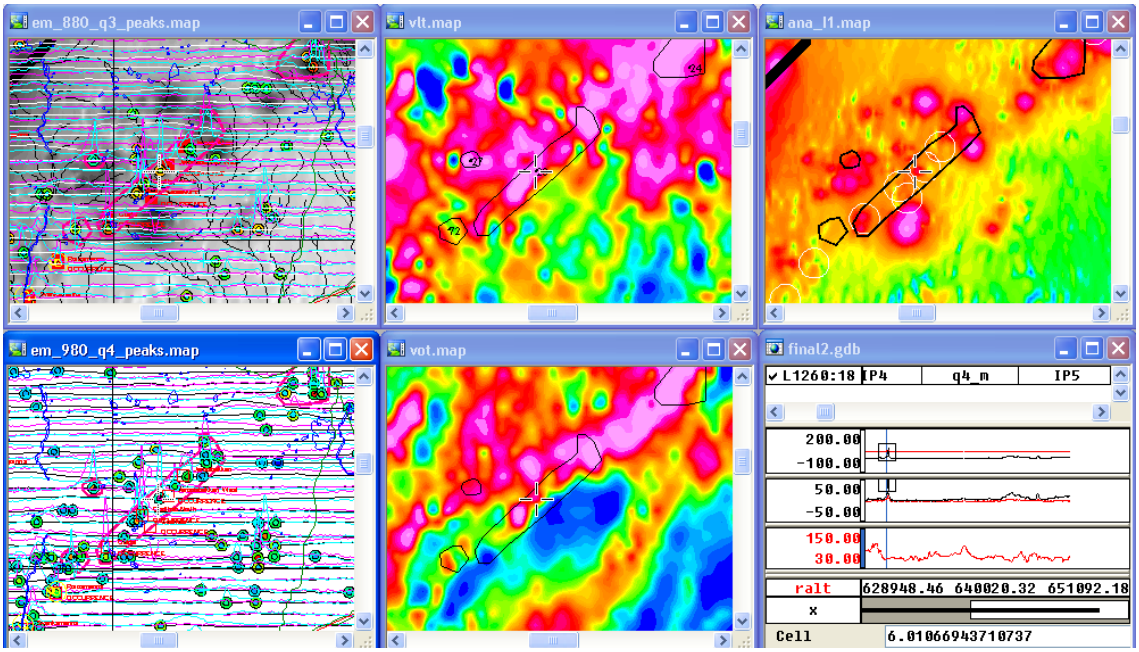

(b)

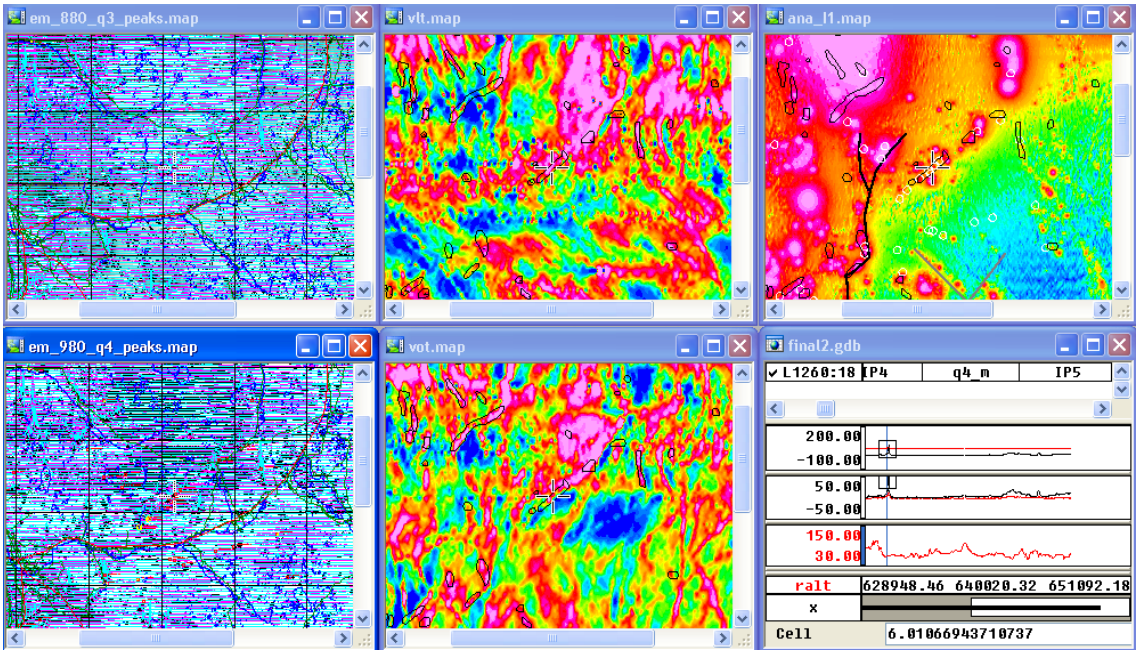

Figure 61. *Target Røros 26; an elongated group of medium EM peaks; coincident medium VLF anomalies; adjacent short wavelength magnetic anomaly; priority 1*

(a)

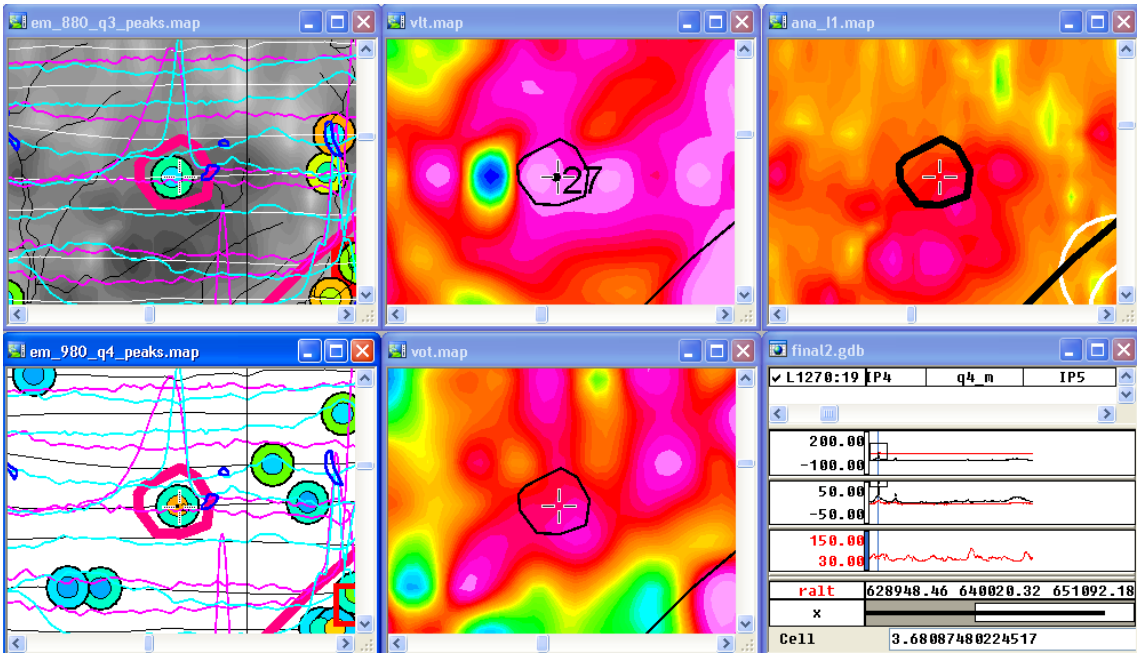

(b)

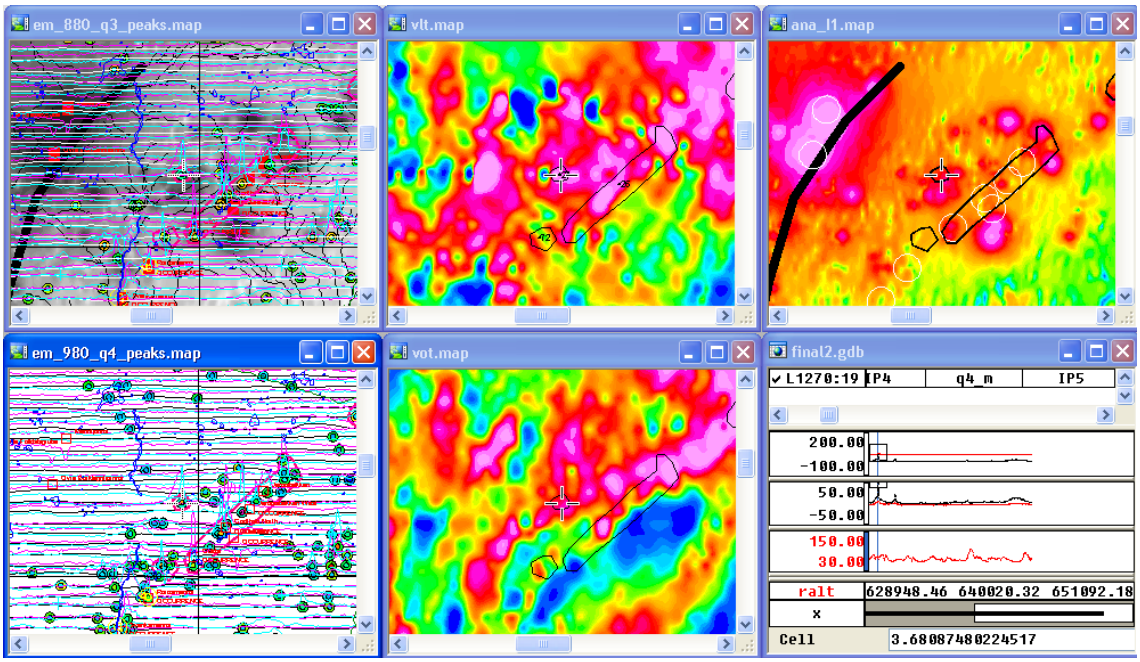

Figure 62. *Target Røros 27; a single large EM peak; coincident VLF anomalies; adjacent short wave-length magnetic anomaly; priority 2*

(a)

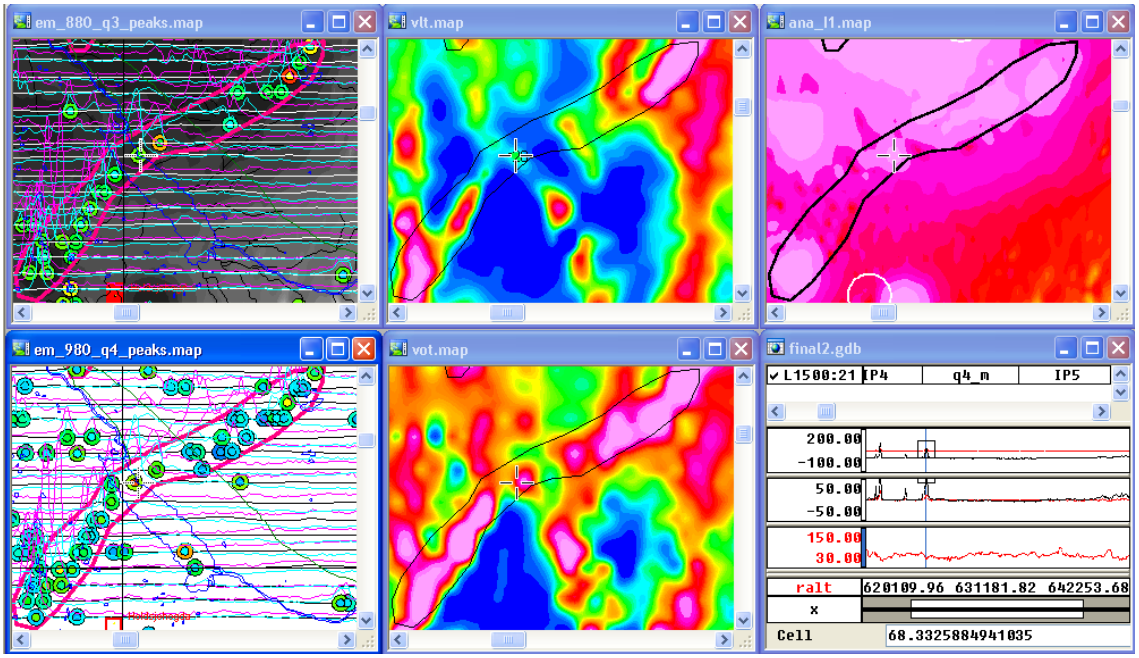

(b)

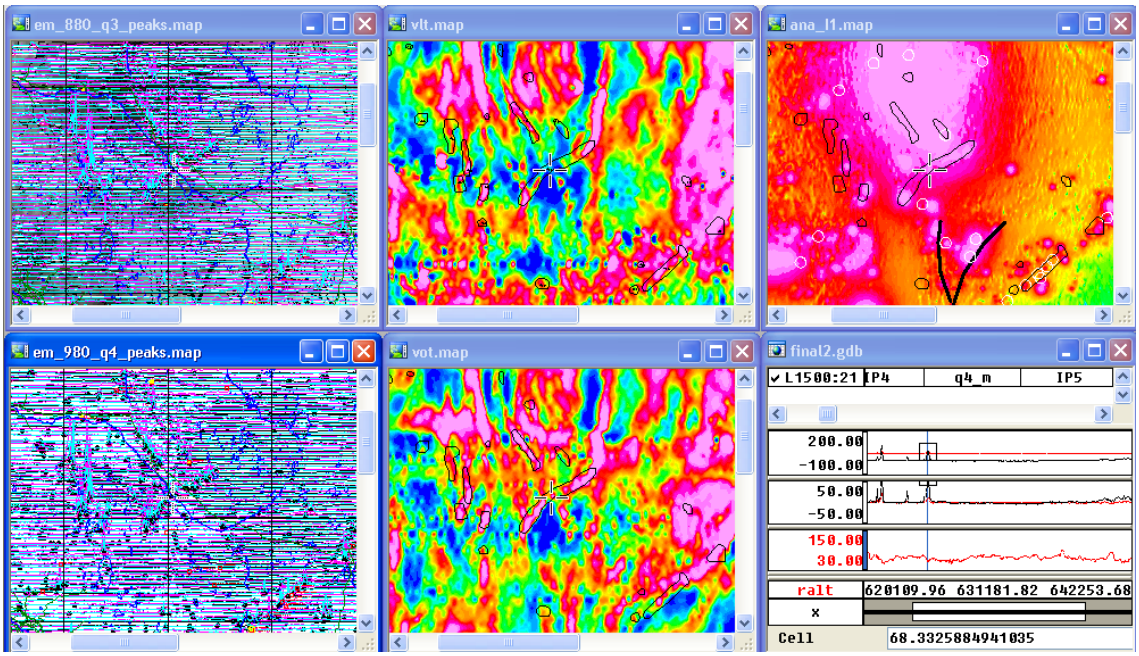

Figure 63. *Target Røros 28; an elongated group of medium to large EM peaks; coincident VLF anomalies; adjacent short wavelength magnetic anomaly; priority 1*

(a)

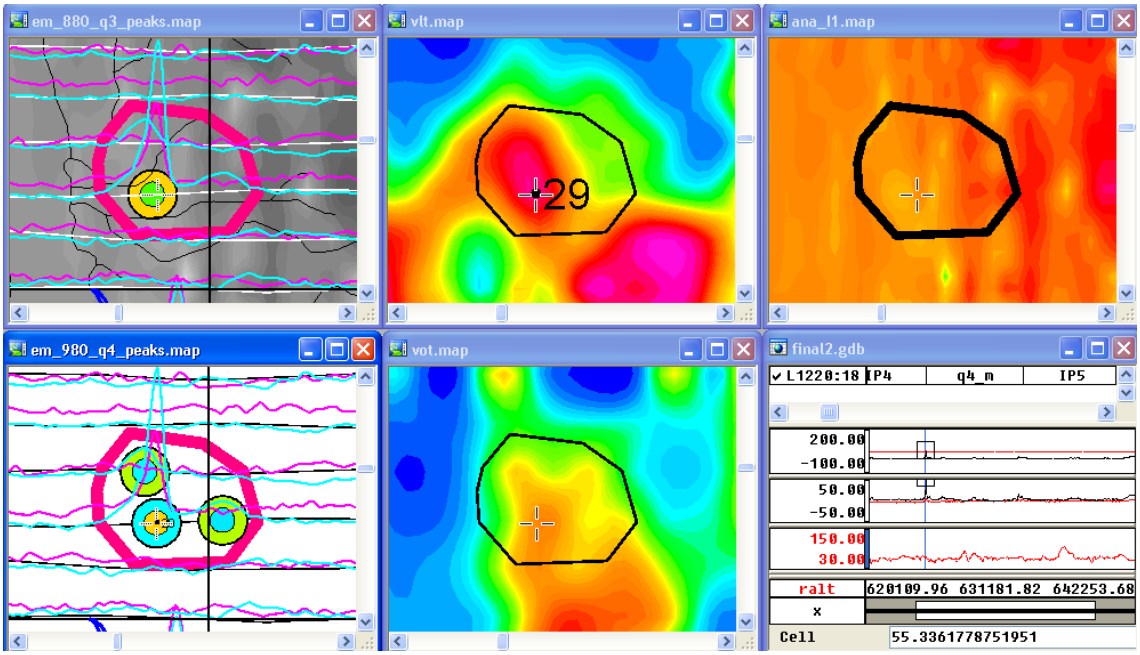

(b)

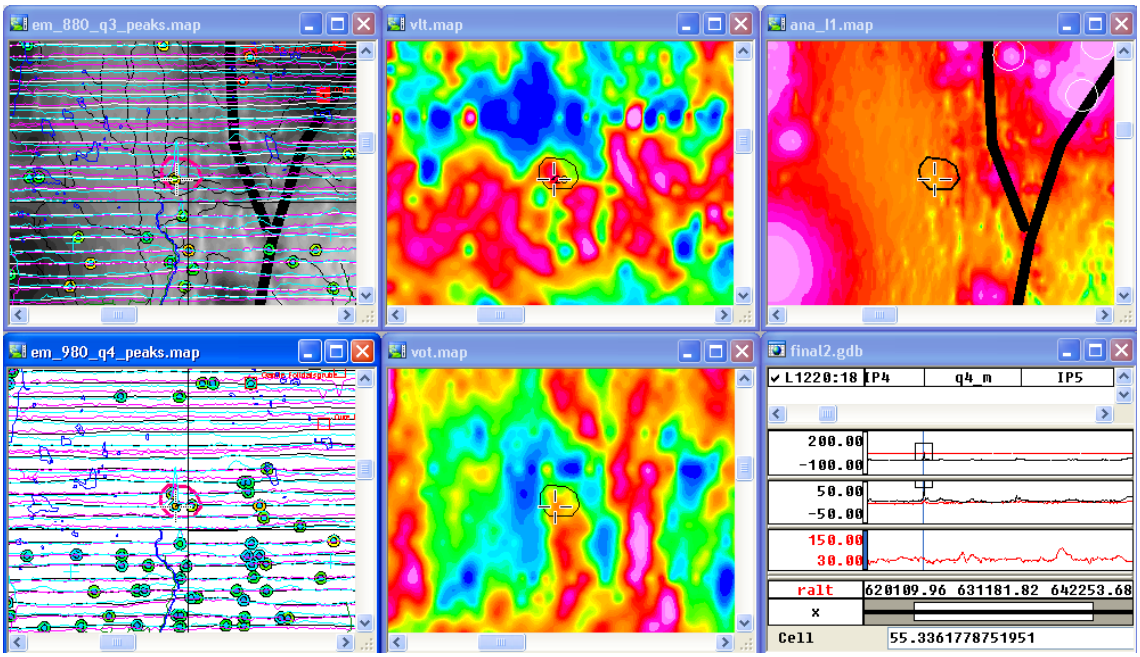

Figure 64. *Target Røros 29; small group of medium to large EM peaks; coincident medium VLF anomalies; adjacent short wavelength magnetic anomaly and close to major magnetic lineament; priority 1*

(a)

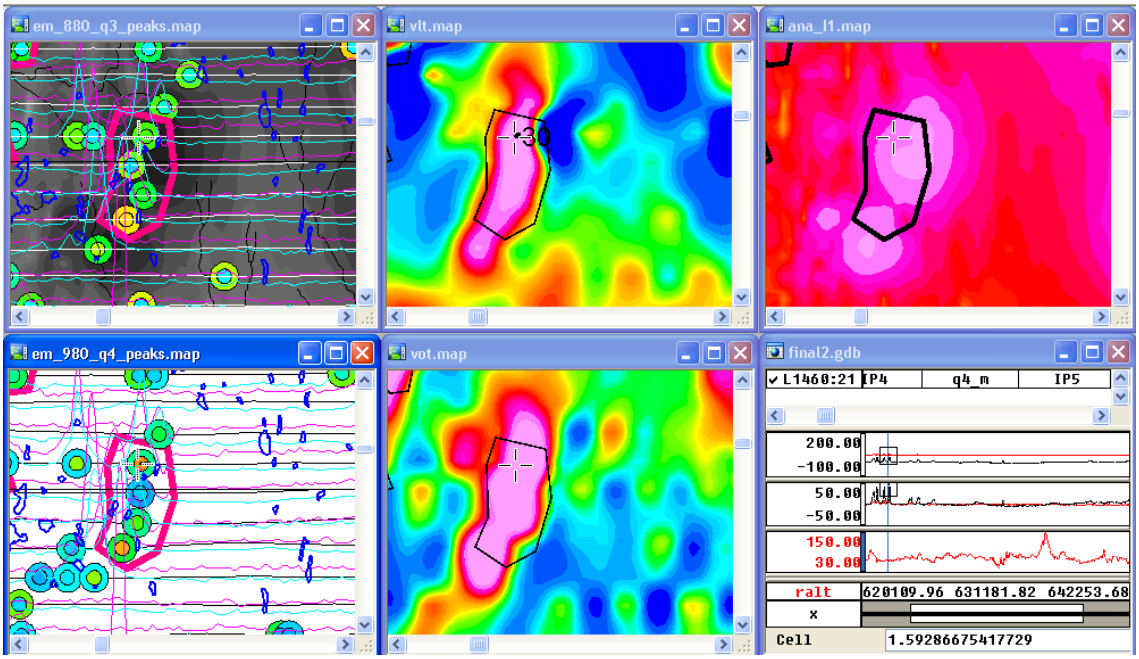

(b)

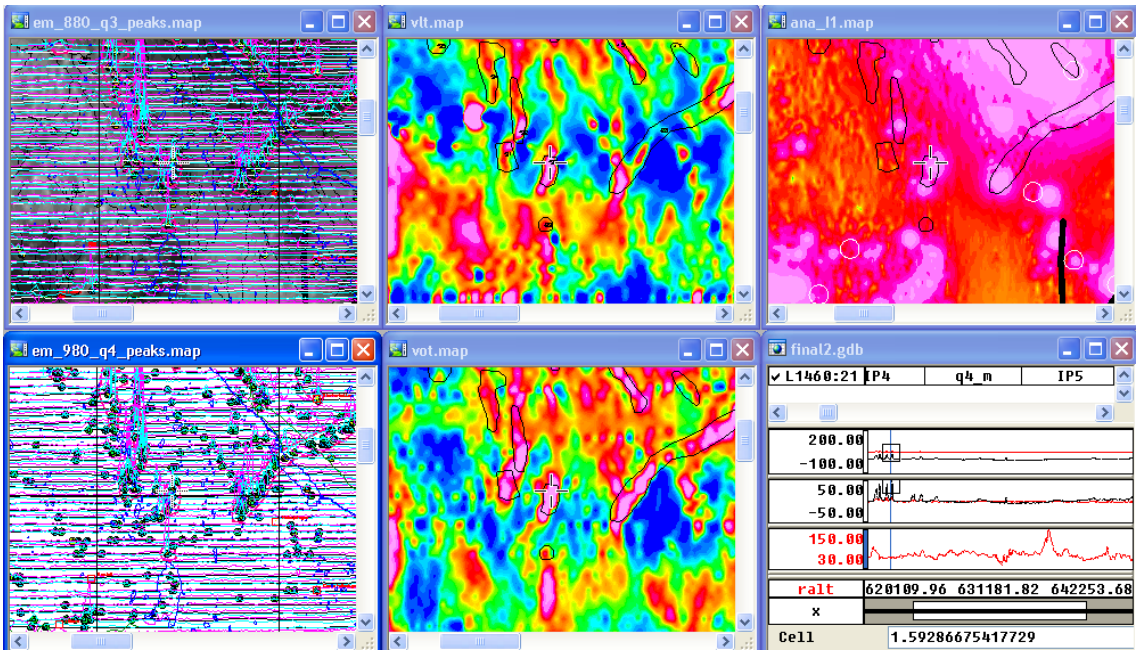

Figure 65. *Target Røros 30; elongated group of medium to large EM peaks; coincident VLF anomalies; adjacent short wavelength magnetic anomaly; priority 1*

(a)

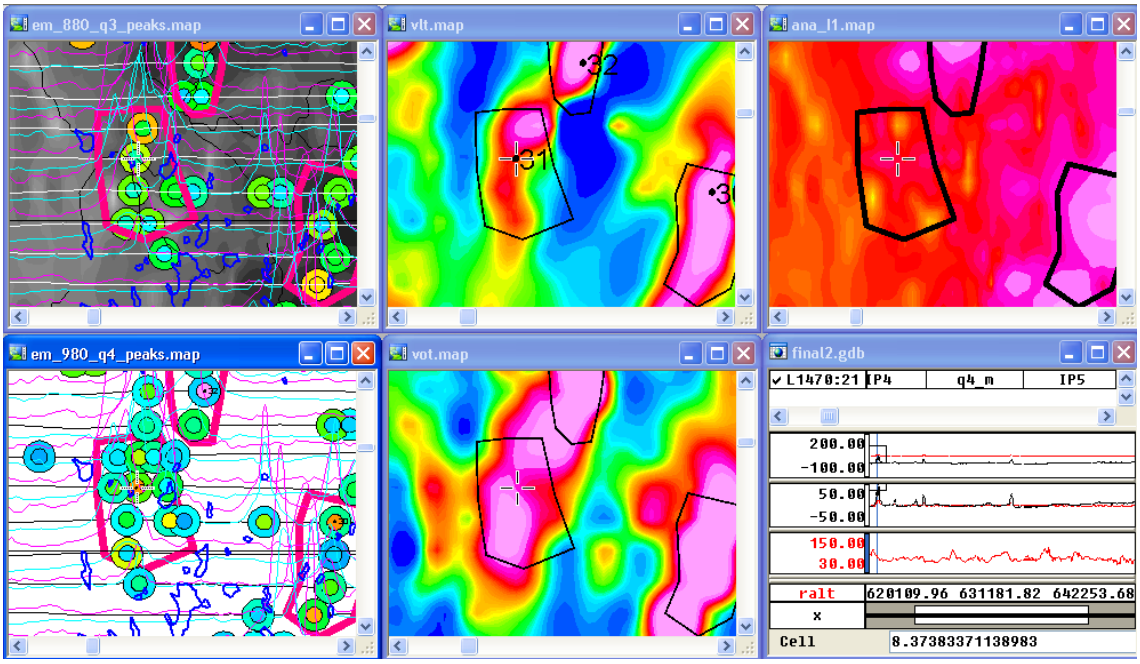

(b)

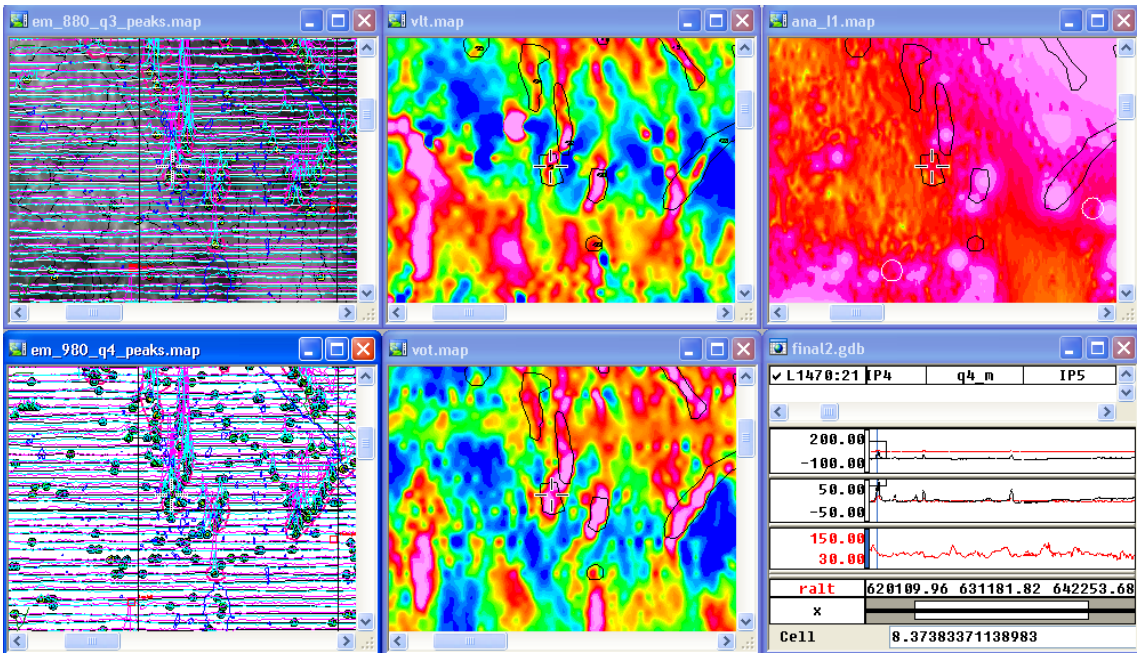

Figure 66. *Target Røros 31; group of medium to large EM peaks; coincident VLF anomalies; adjacent short wavelength magnetic anomaly; priority 1*

(a)

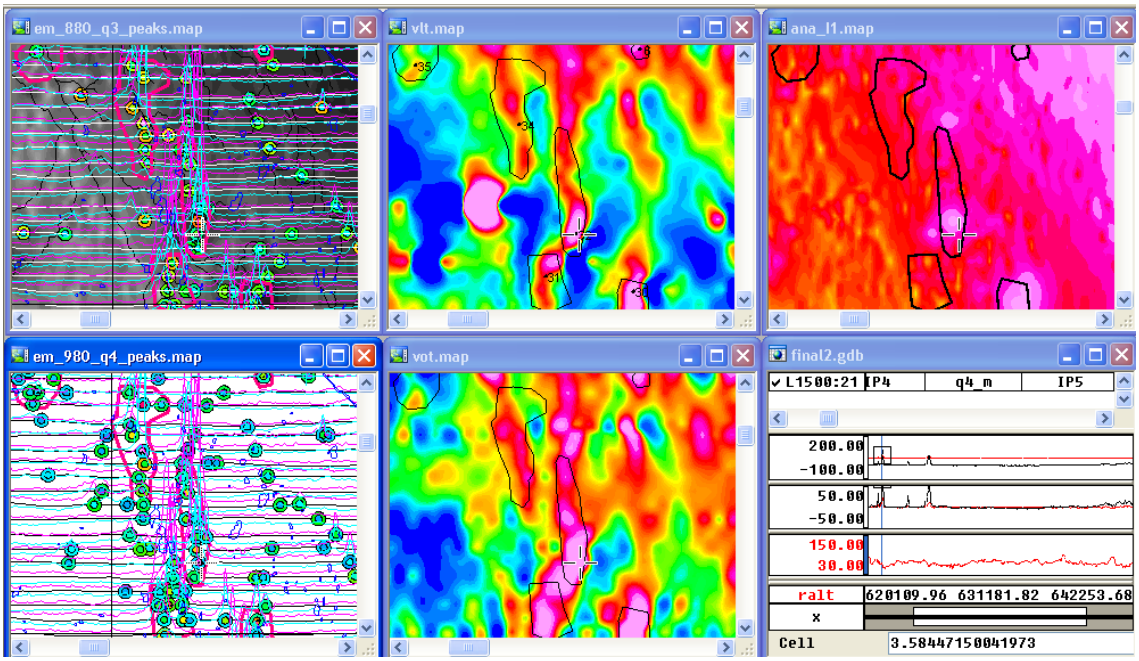

(b)

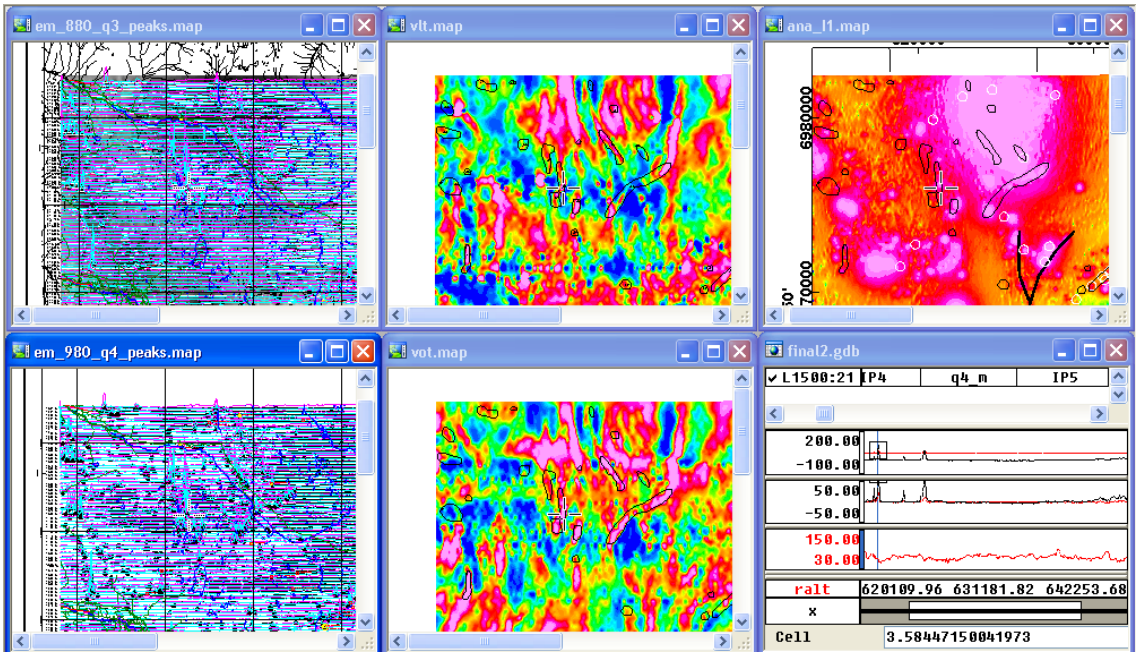

Figure 67. *Target Røros 32; elongated group of medium to large EM peaks; coincident VLF anomalies; adjacent short wavelength magnetic anomaly; priority 1*

(a)

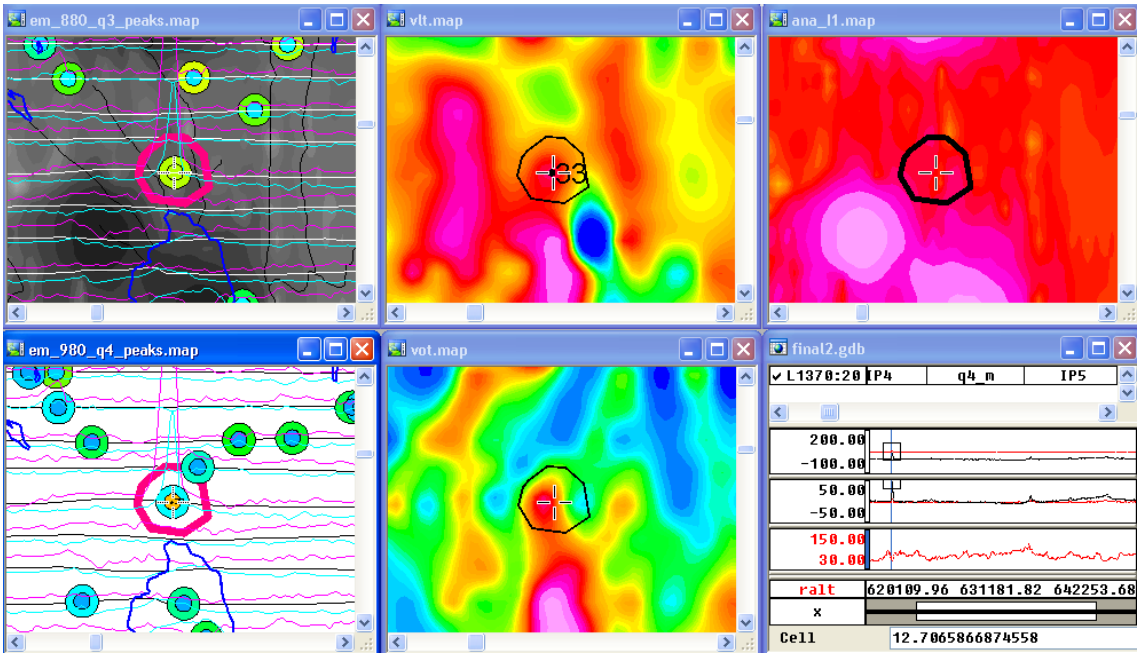

(b)

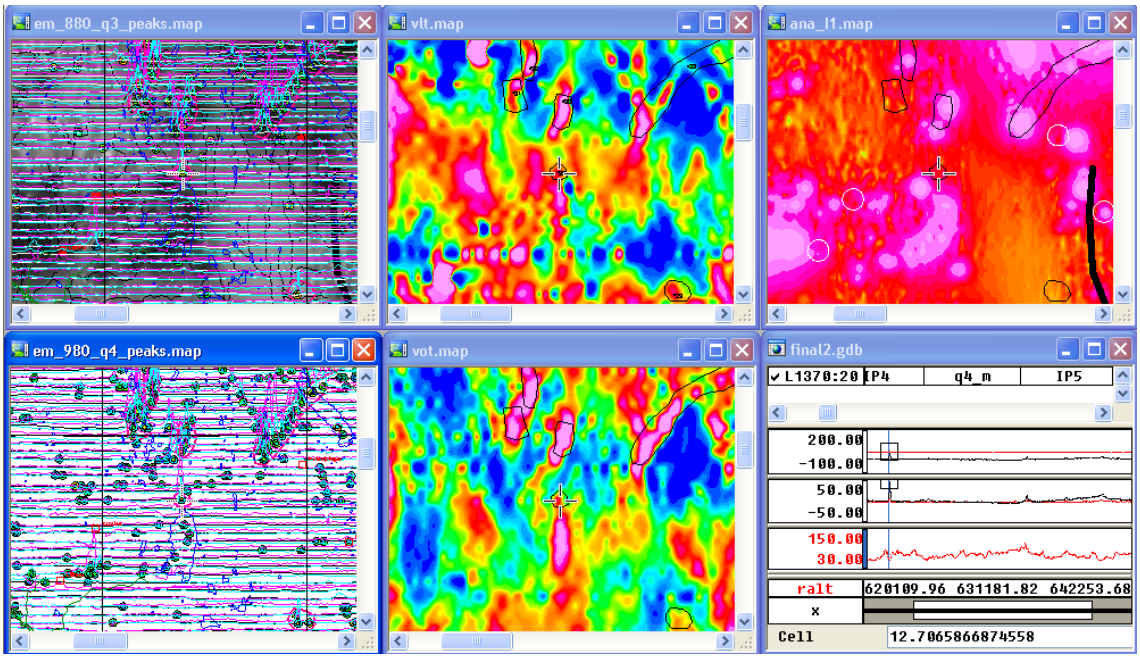

Figure 68. *Target Røros 33; single medium to large EM peas; coincident medium VLF anomalies; adjacent short wavelength magnetic anomaly; priority 2*

(a)

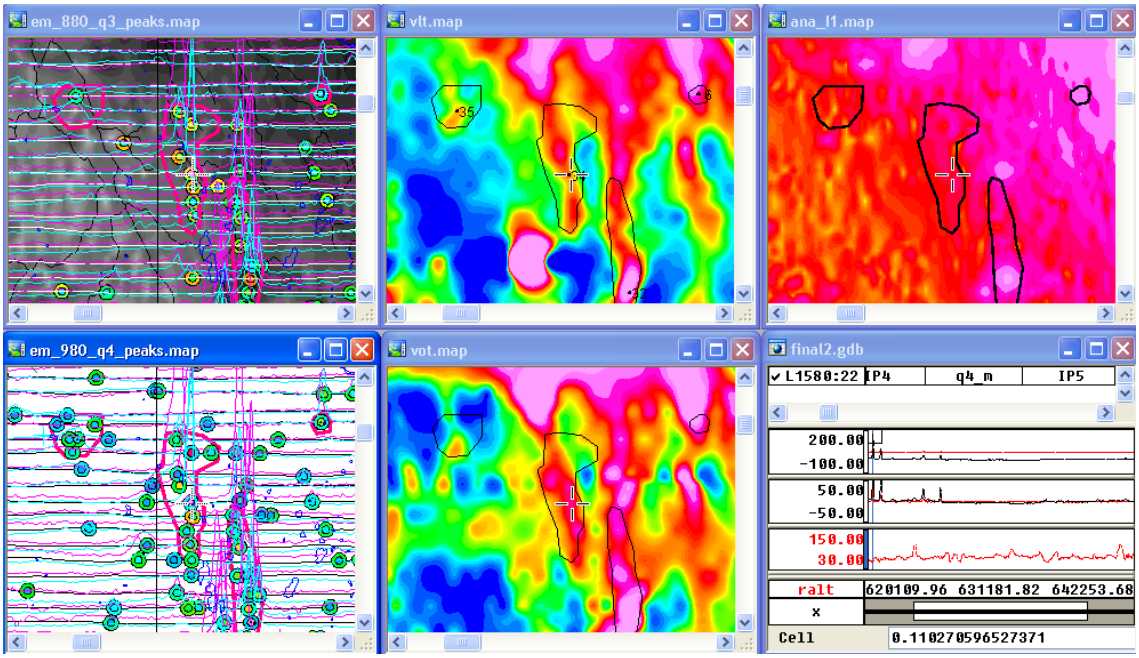

(b)

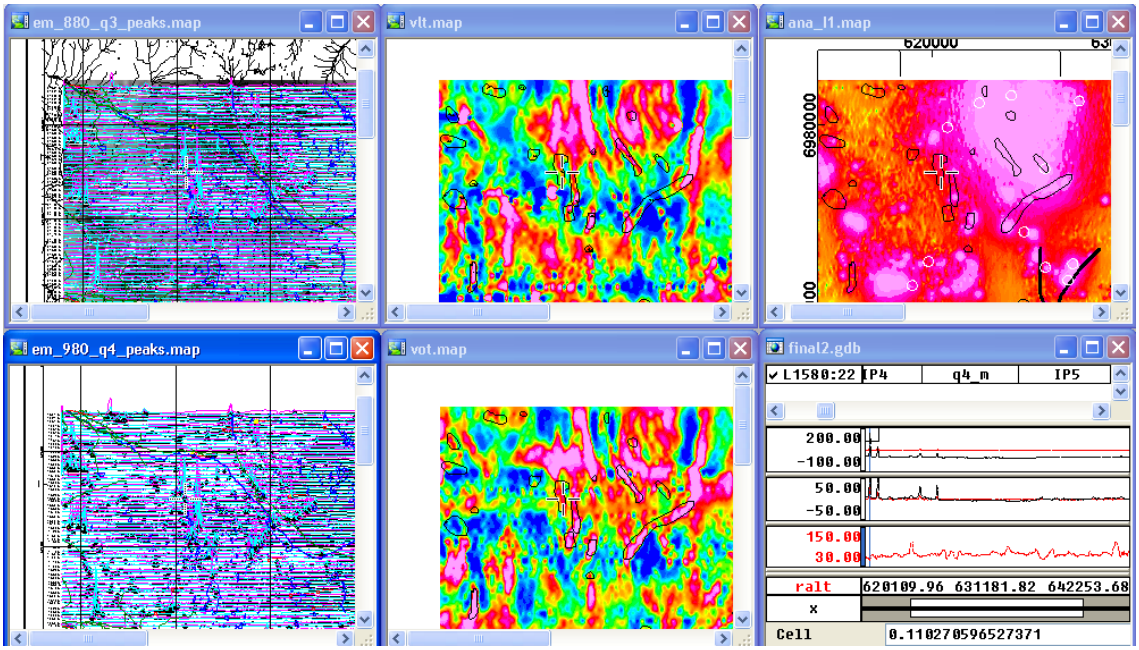

Figure 69. *Target Røros 34; elongated group of medium to large EM peaks; coincident VLF anomalies; adjacent short wavelength magnetic anomaly; priority 1*

(a)

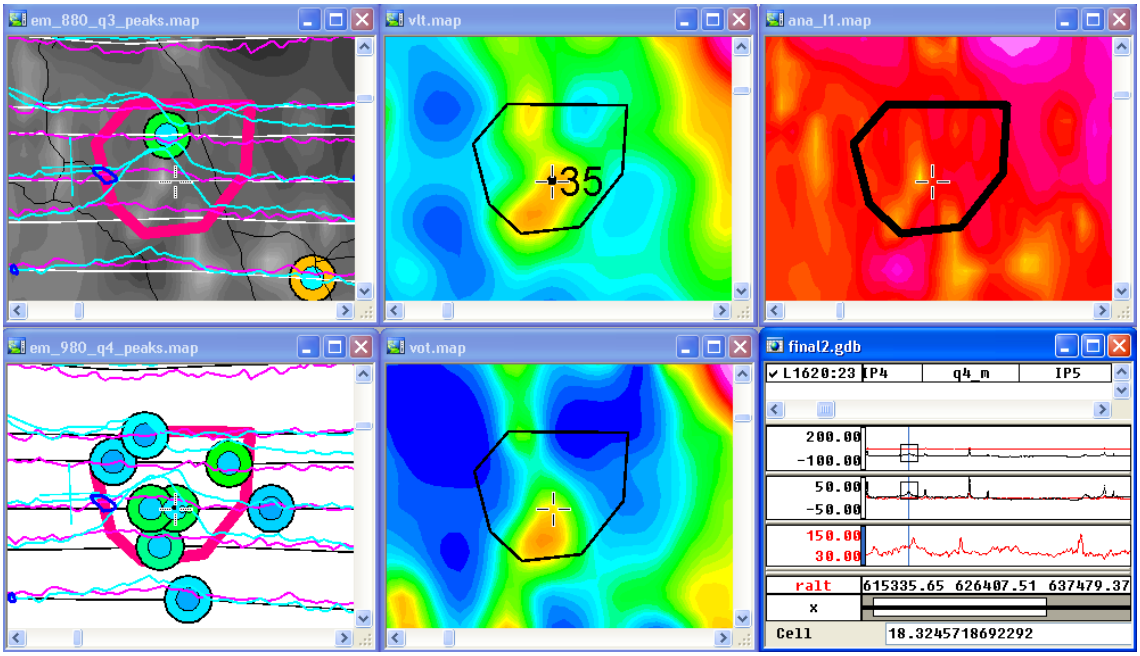

(b)

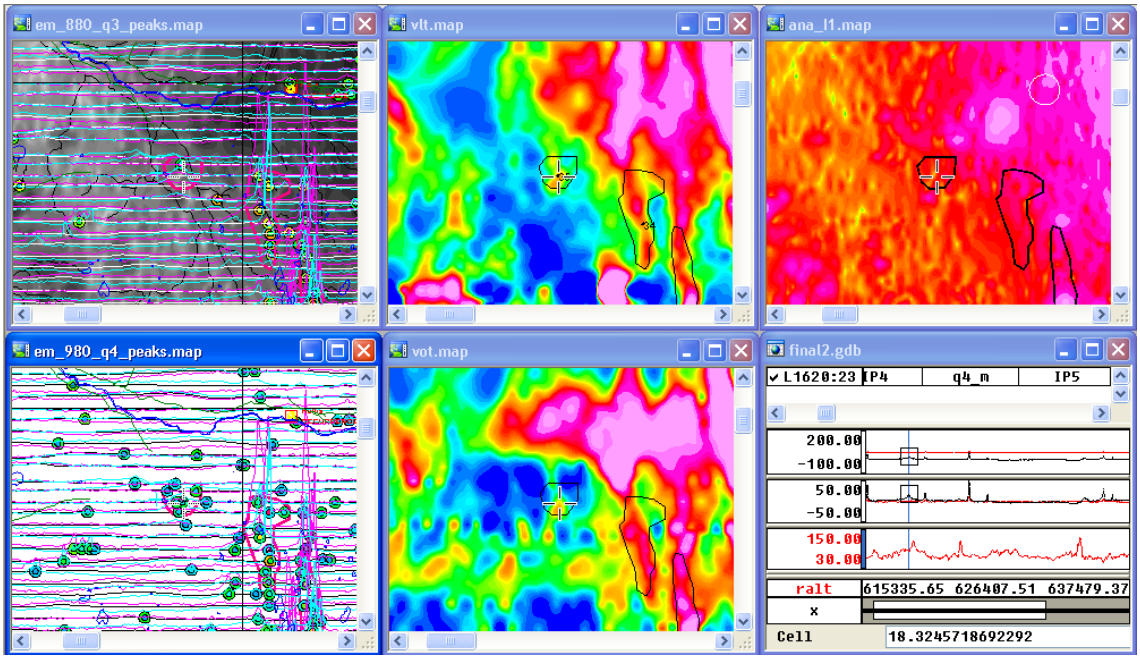

Figure 70. *Target Røros 35; group of medium EM peaks; coincident medium VLF anomalies; adjacent short wavelength magnetic anomaly; priority 3*

(a)

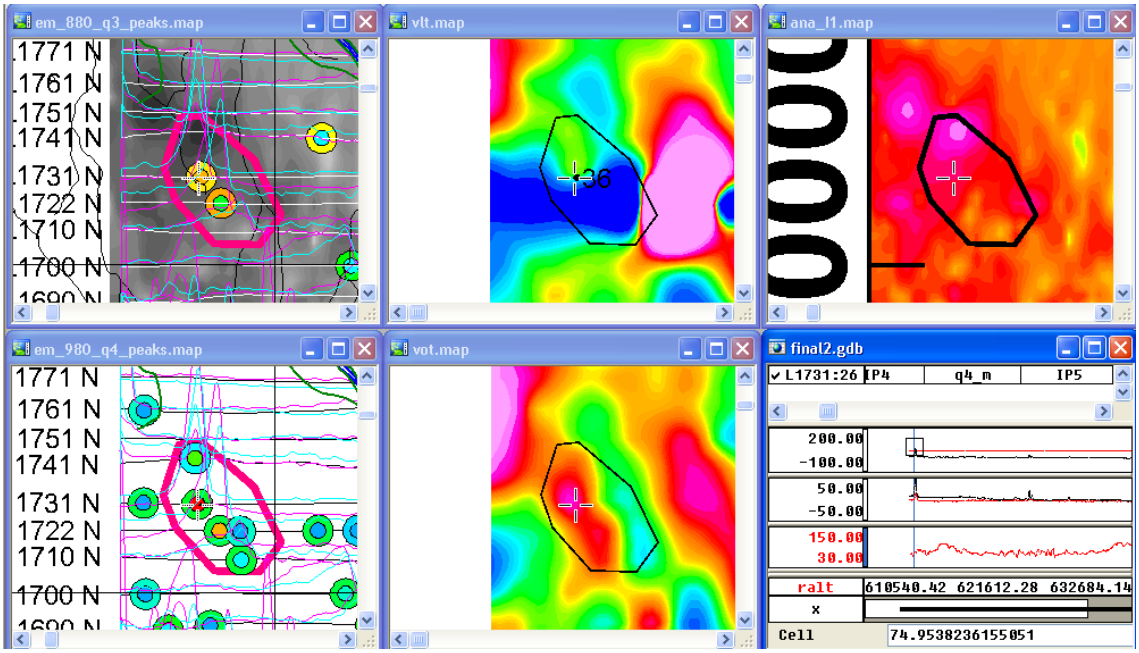

(b)

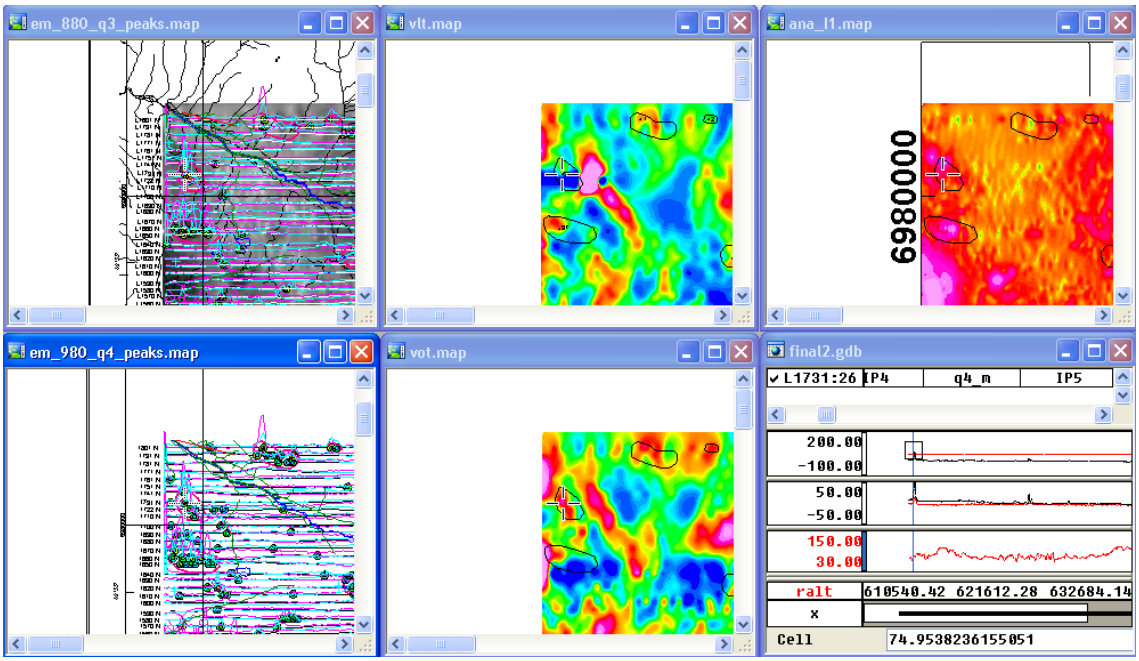

Figure 71. *Target Røros 36; a small group of medium to large EM peaks; coincident VLF anomalies; adjacent short wavelength magnetic anomaly; priority 2*

(a)

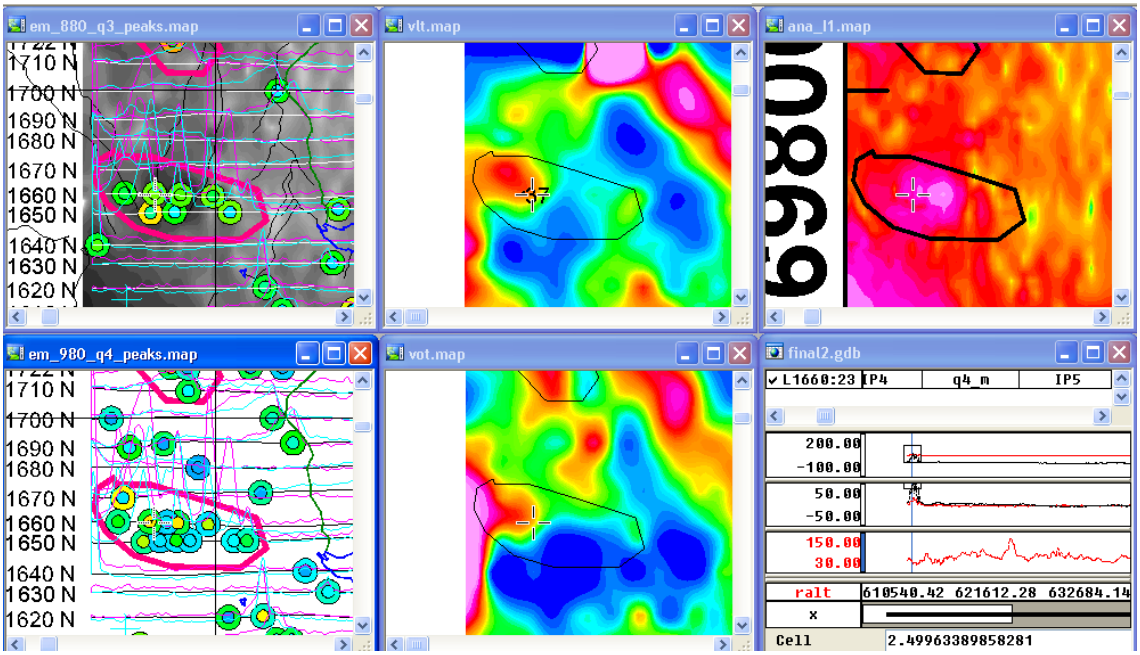

(b)

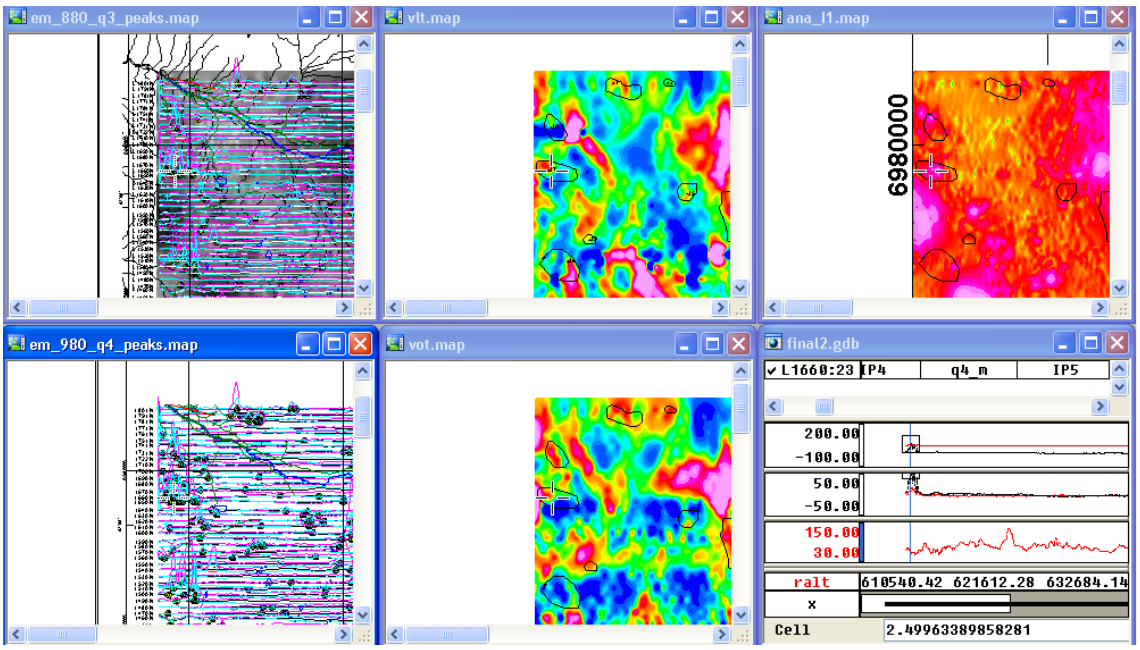

Figure 72. *Target Røros 37; group of medium EM peaks; variable VLF signature; adjacent short wave-length magnetic anomaly; priority 2*

(a)

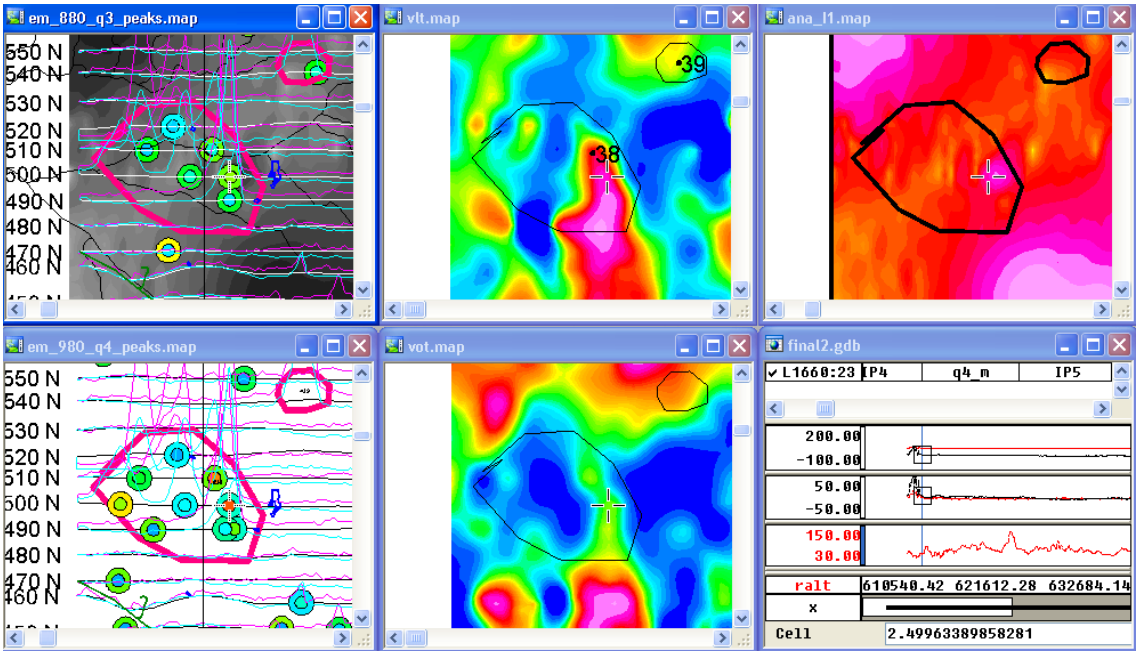

(b)

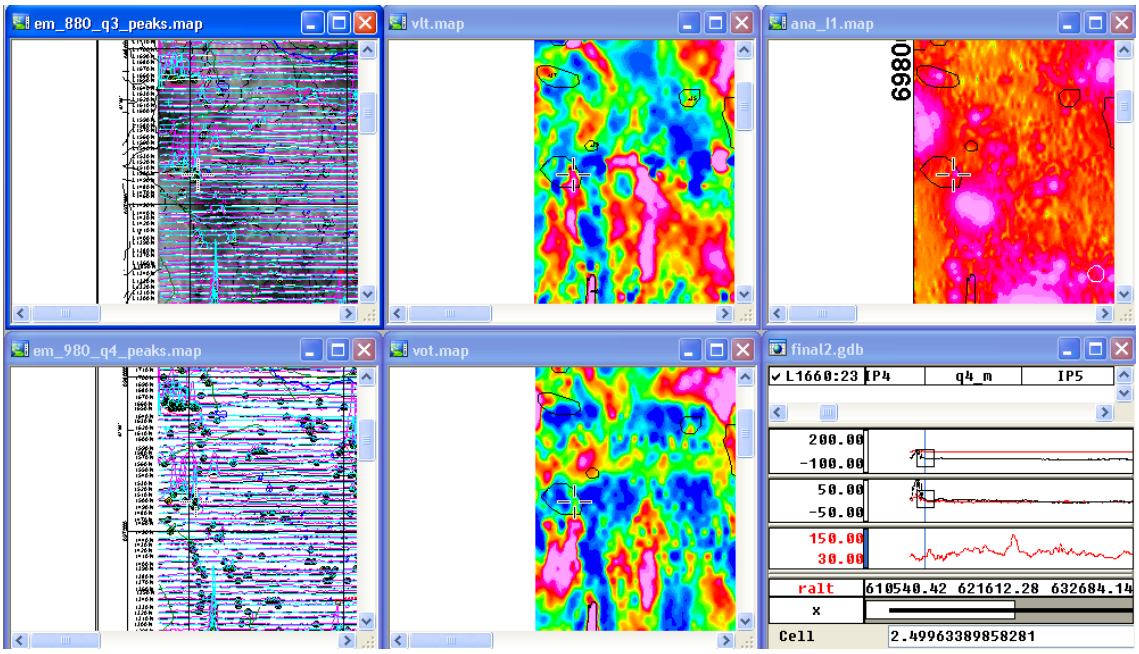

Figure 73. *Target Røros 38; group of medium to large EM peaks; variable VLF signature but high at eastern part; adjacent short wavelength magnetic anomaly; priority 2*

(a)

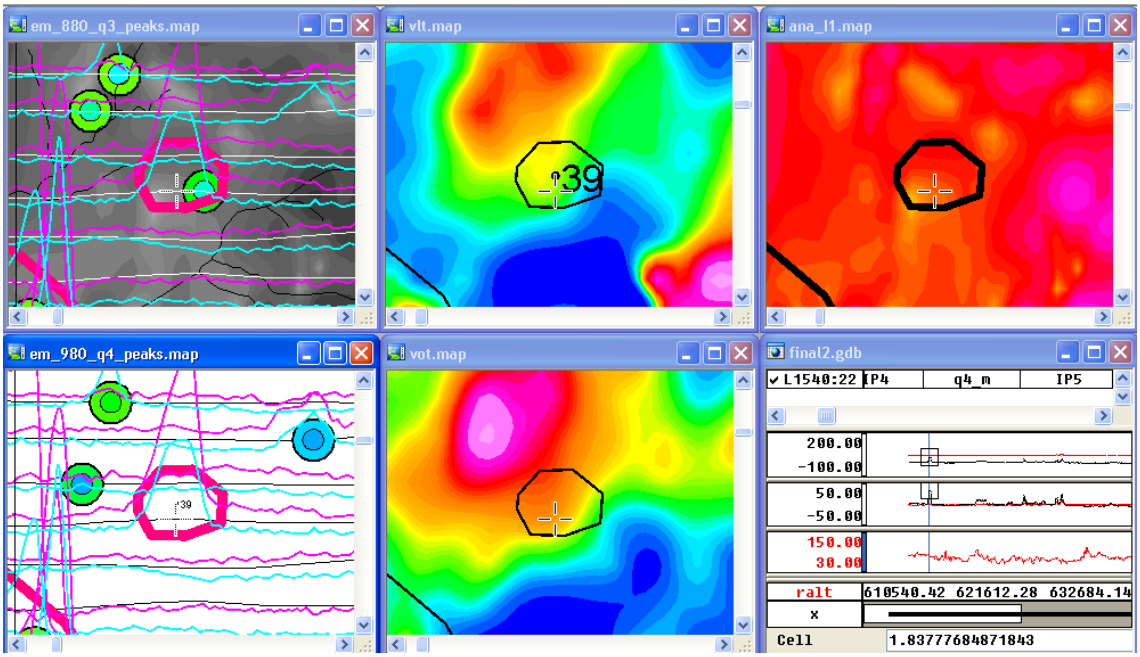

(b)

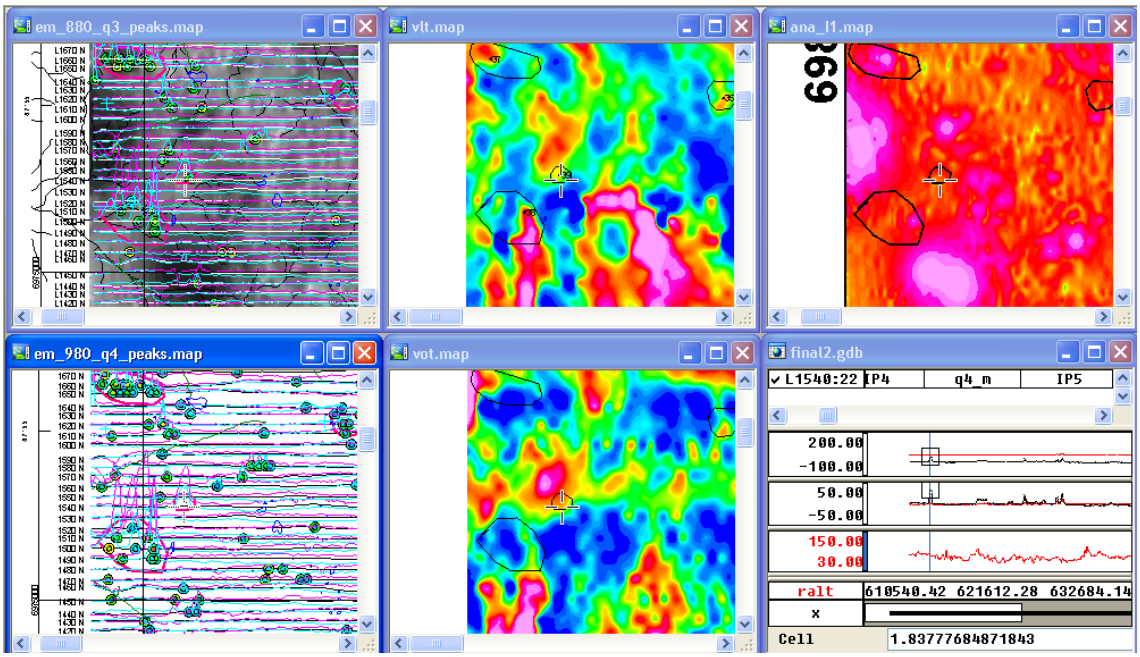

Figure 74. *Target Røros 39; isolated medium EM peaks; medium VLF anomaly; adjacent short wave-length magnetic anomaly; priority 4*

(a)

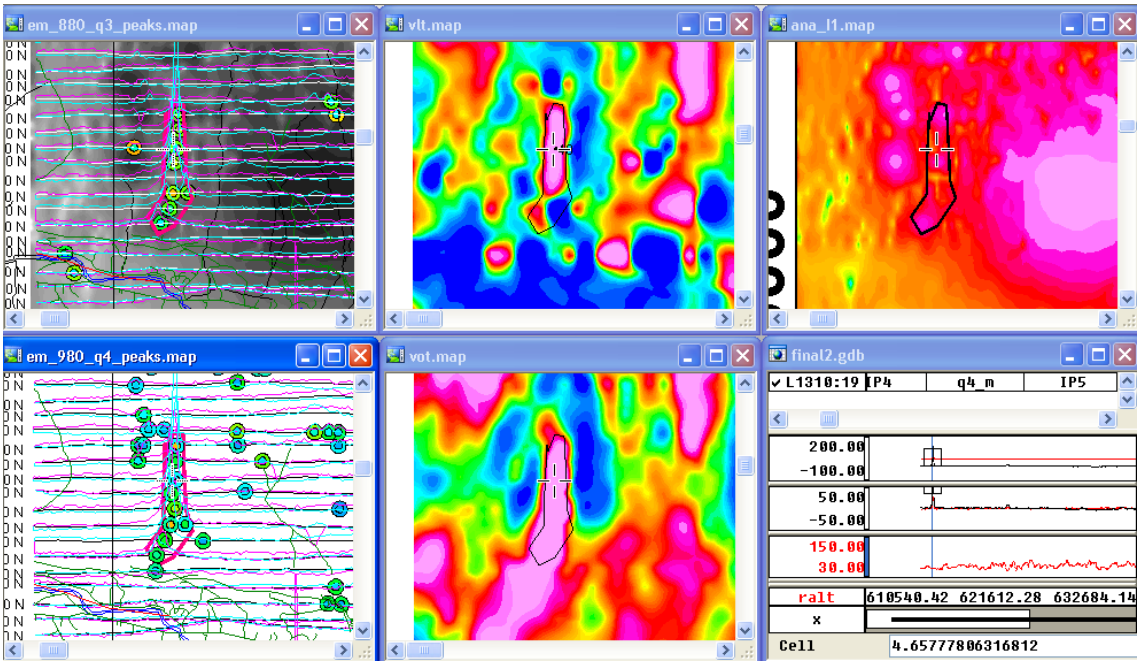

(b)

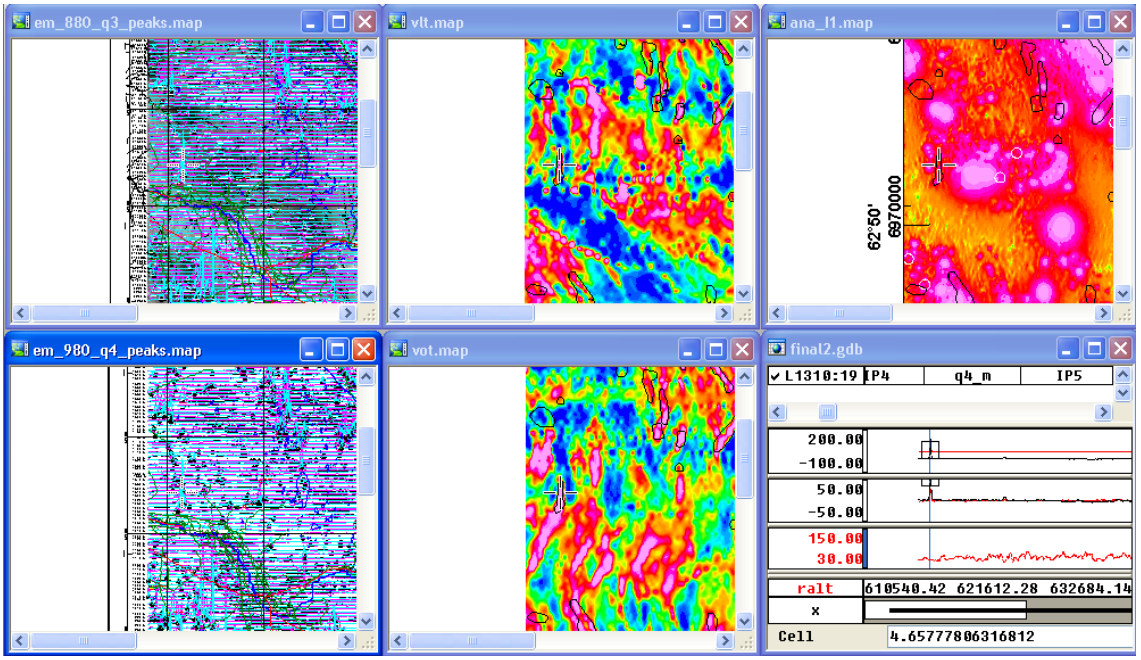

Figure 75. *Target Røros 40; elongated group of medium to large EM peaks; coincident VLF anomalies; adjacent short wavelength magnetic anomaly; priority 1*

(a)

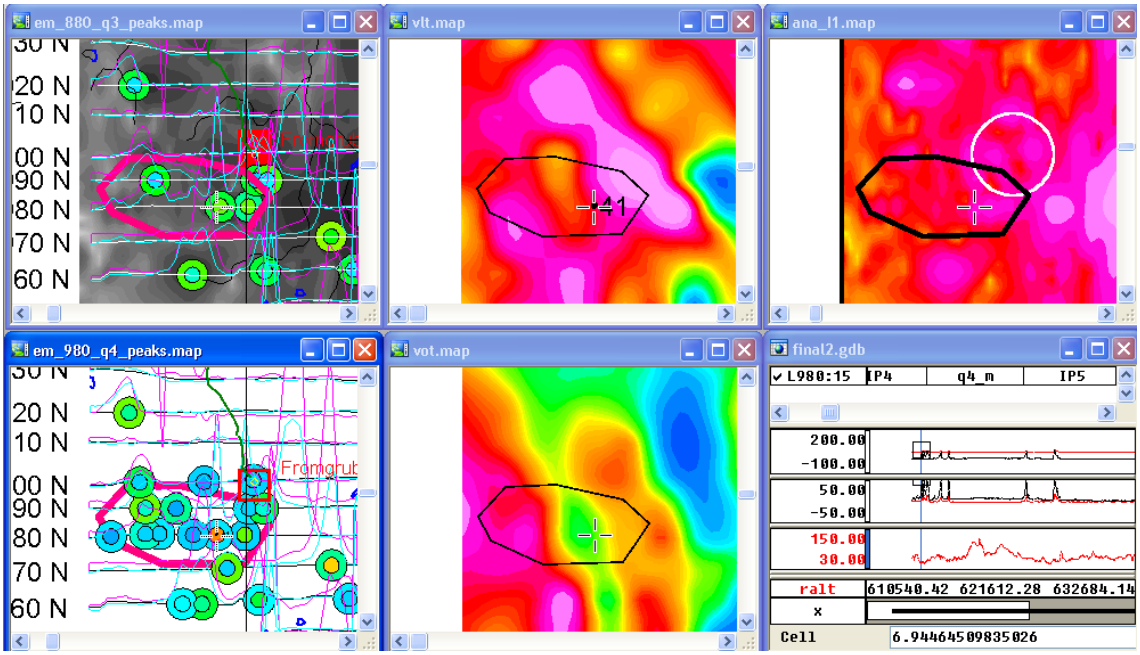

(b)

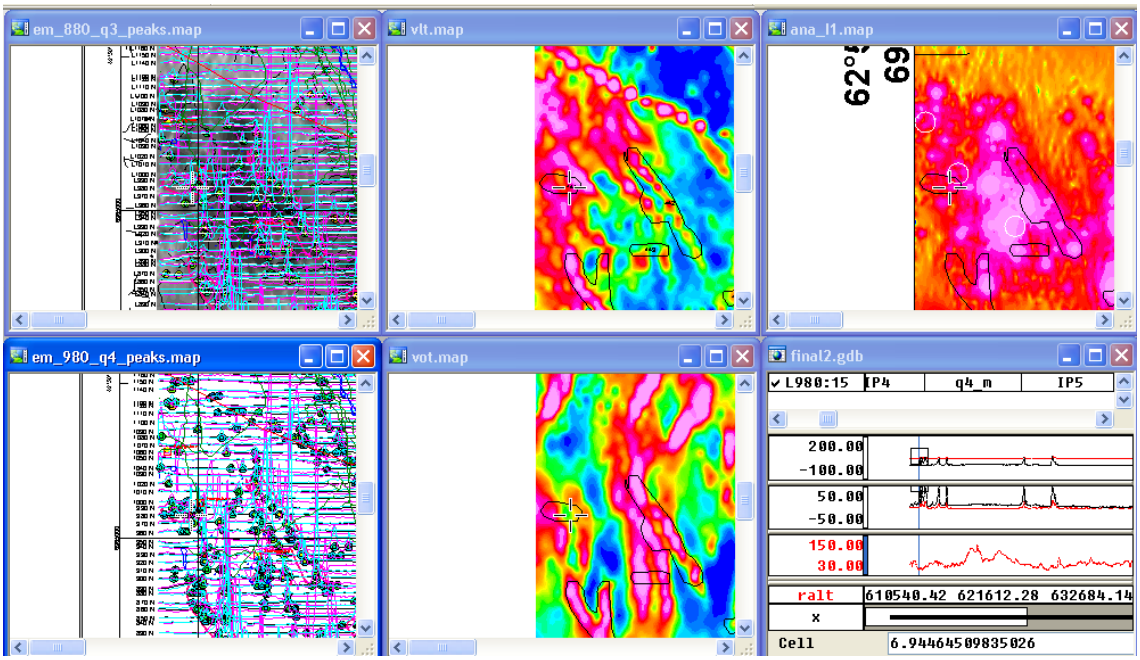

Figure 76. *Target Røros 41; group of medium to large EM peaks; coincident VLF anomalies; adjacent short wavelength magnetic anomaly; priority 2*

(a)

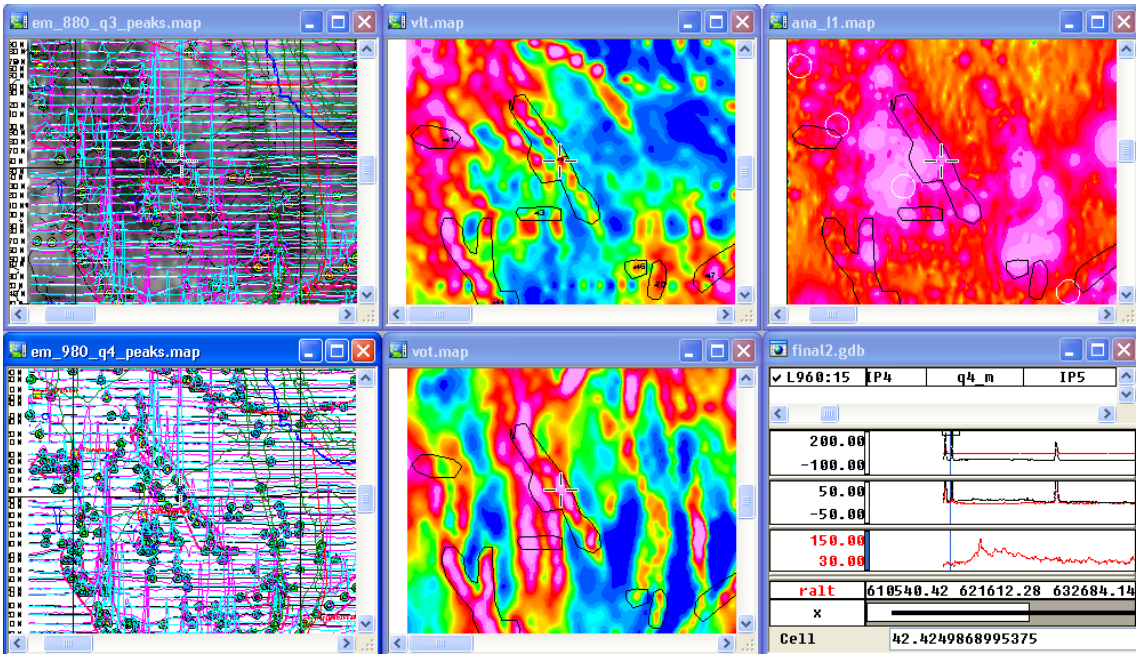

(b)

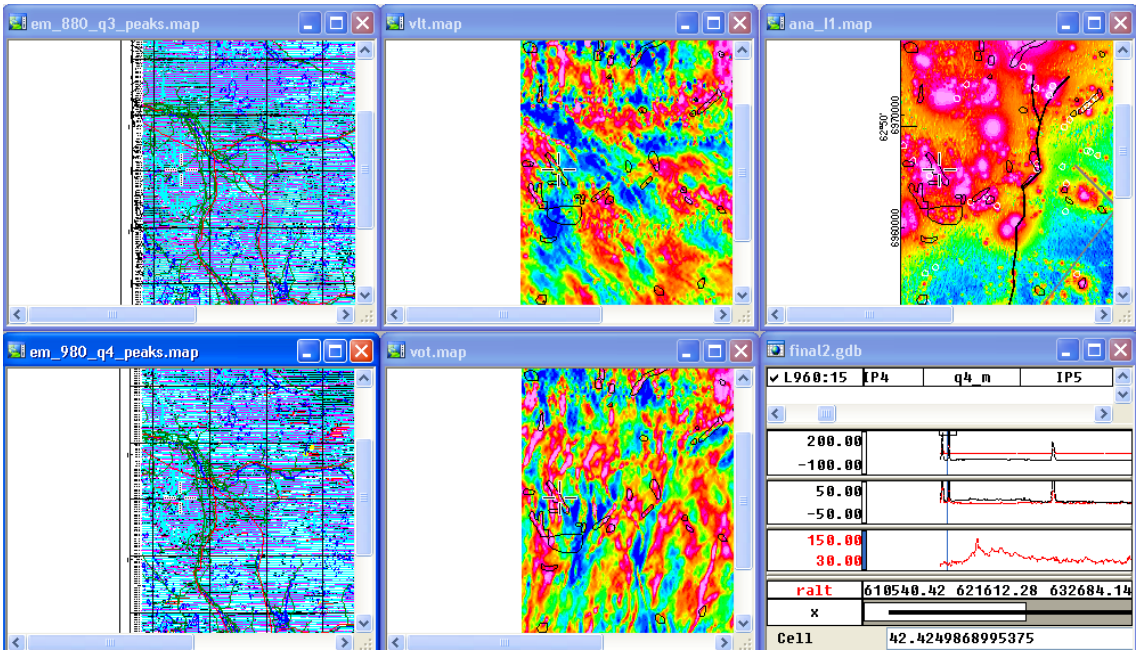

Figure 77. *Target Røros 42; large group of medium to large EM peaks; coincident VLF anomalies; adjacent short wavelength magnetic anomaly; priority 1*

(a)

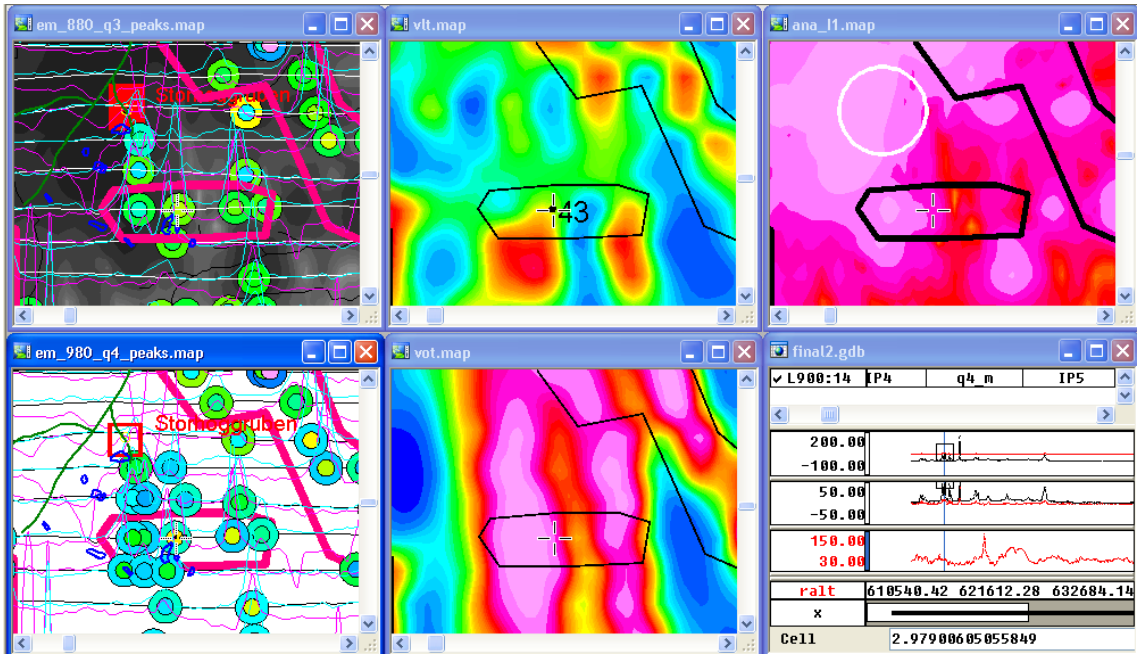

(b)

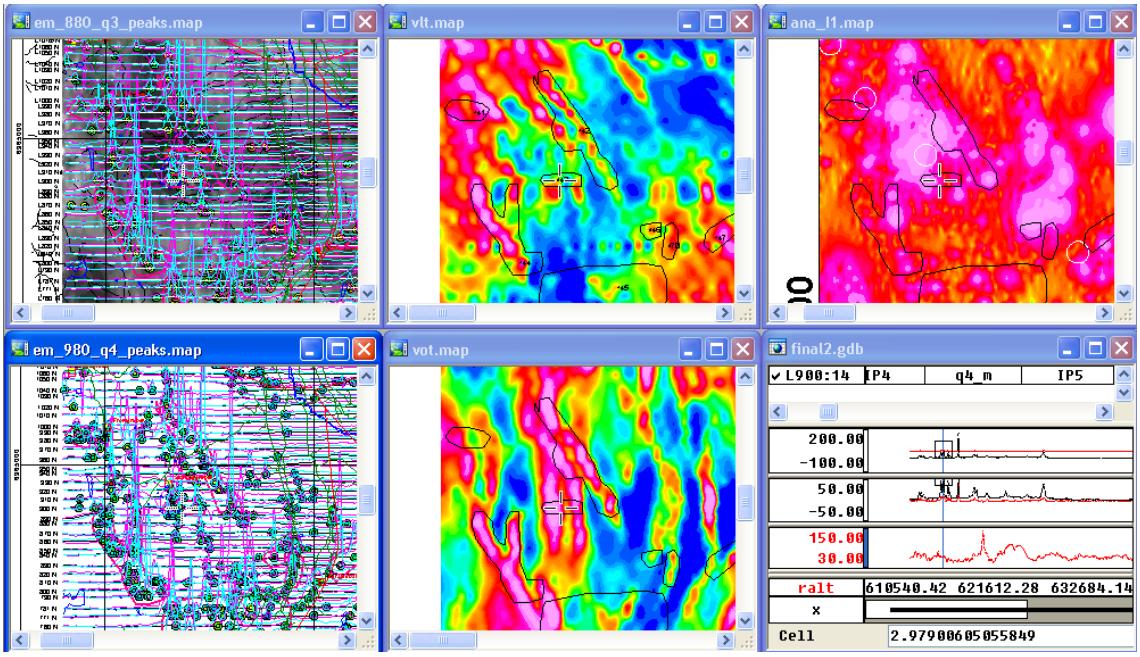

Figure 78. *Target Røros 43; group of medium to large EM peaks; coincident VLF anomalies; adjacent short wavelength magnetic anomaly; priority 1*

(a)

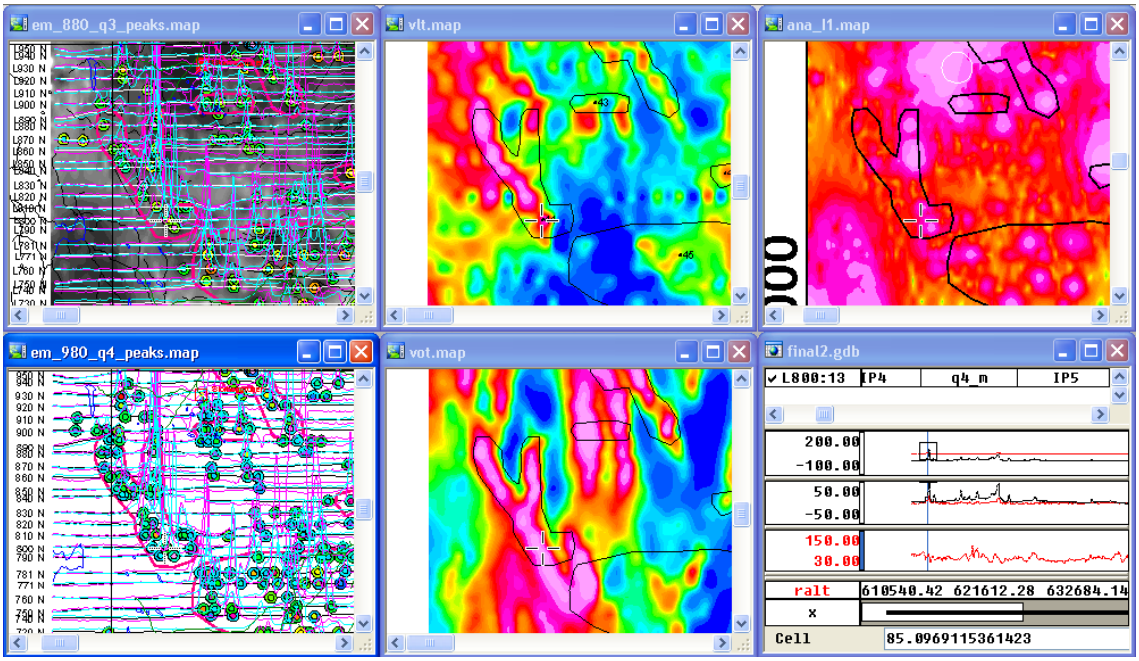

(b)

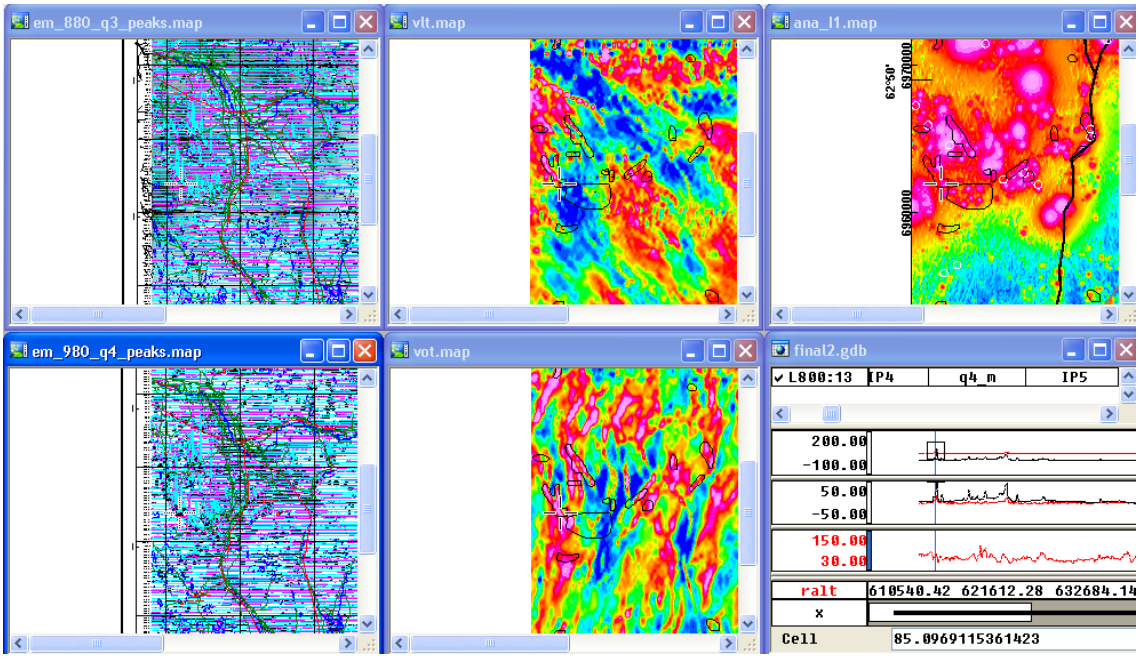

Figure 79. *Target Røros 44; large branching group of medium to large EM peaks; coincident VLF anomalies; adjacent short wavelength magnetic anomaly; priority 1*

(a)

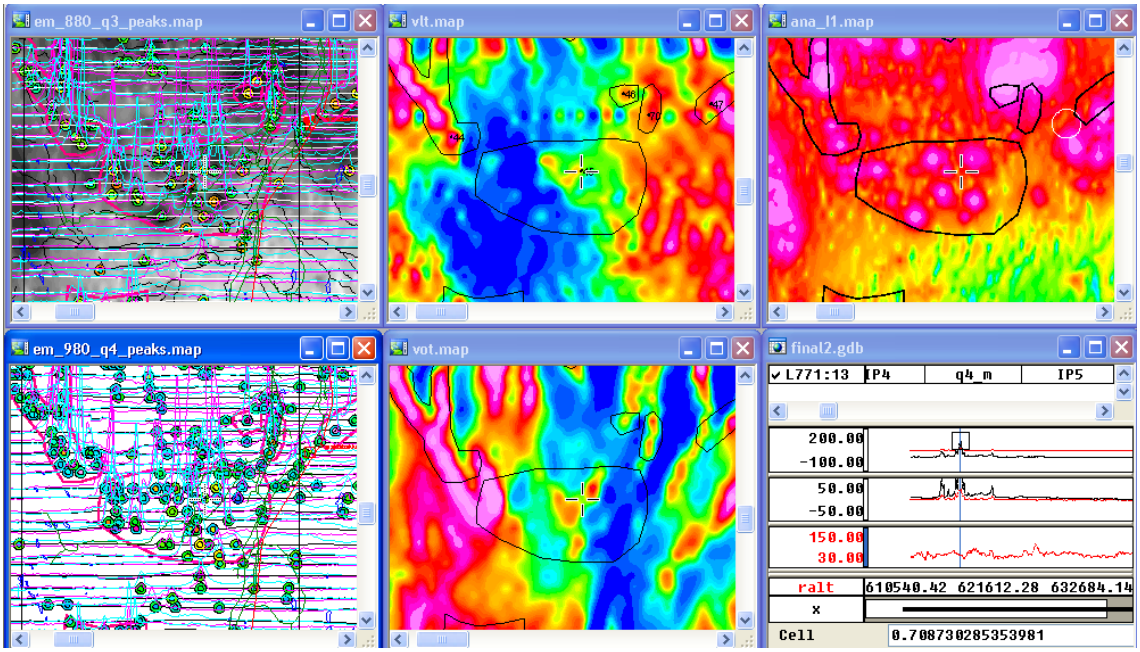

(b)

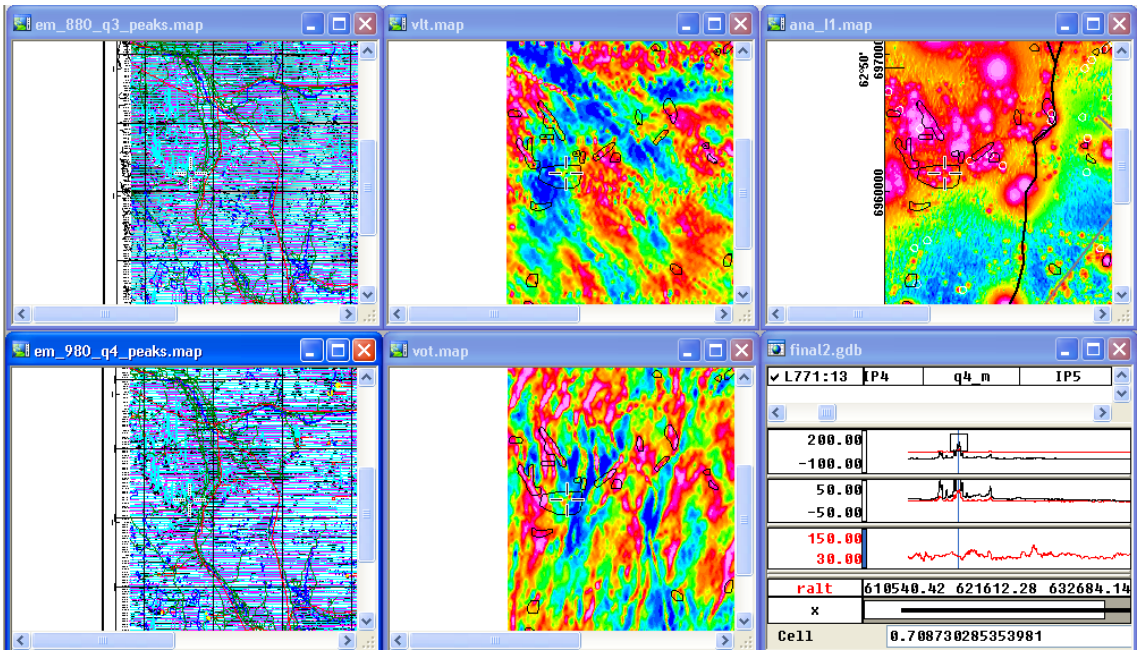

Figure 80. *Target Røros 45; large group of medium to large EM peaks; variable VLF anomalies but some positive; many adjacent short wavelength magnetic anomalies; priority 1*

(a)

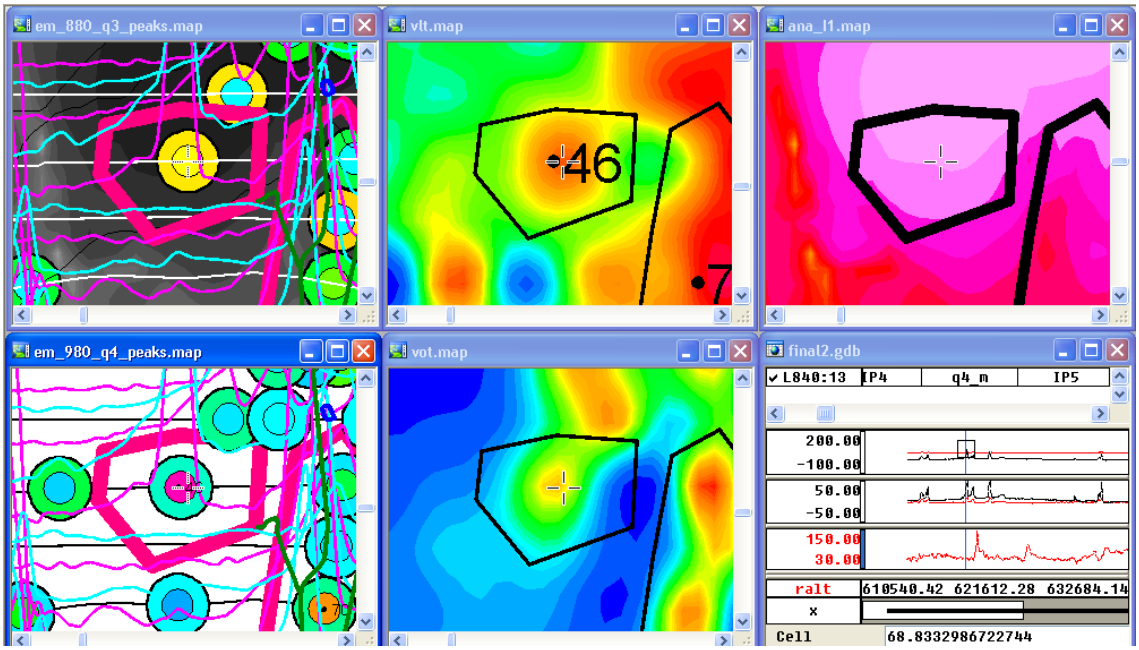

(b)

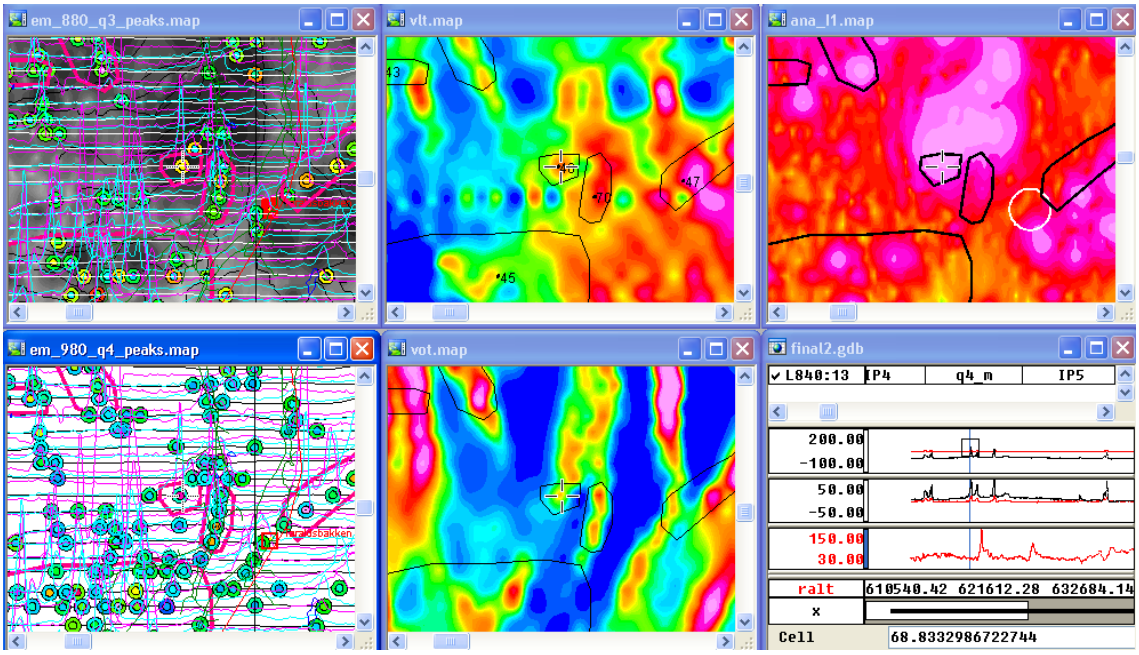

Figure 81. *Target Røros 46; small group of medium to large EM peaks; medium VLF anomalies; adjacent short wavelength magnetic anomaly; priority 3*

(a)

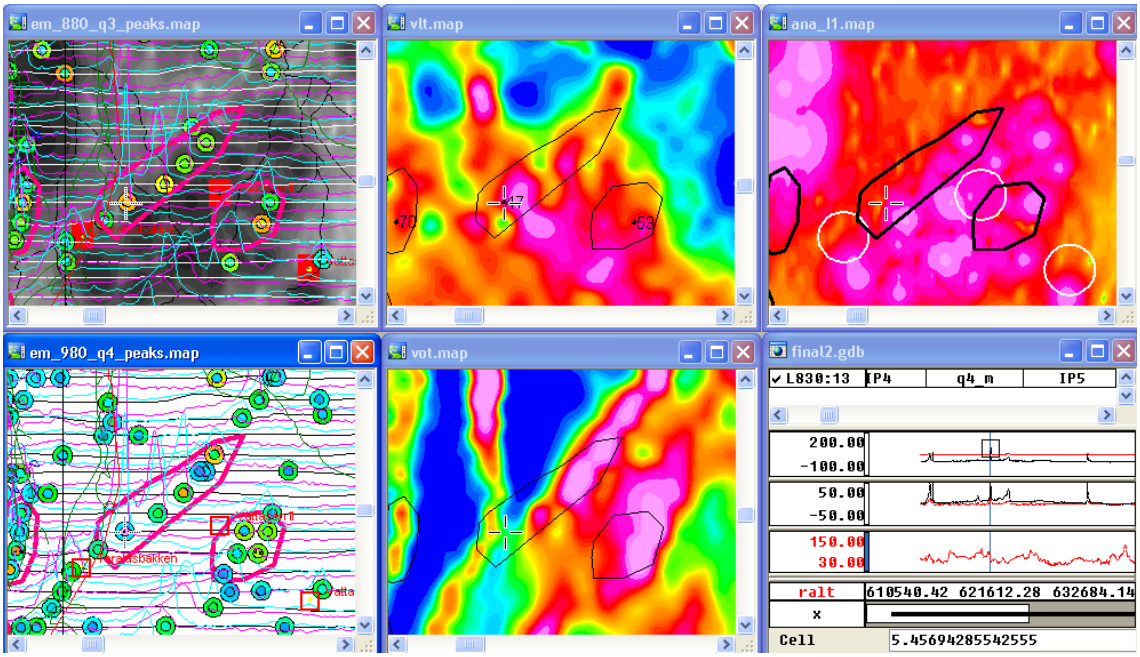

(b)

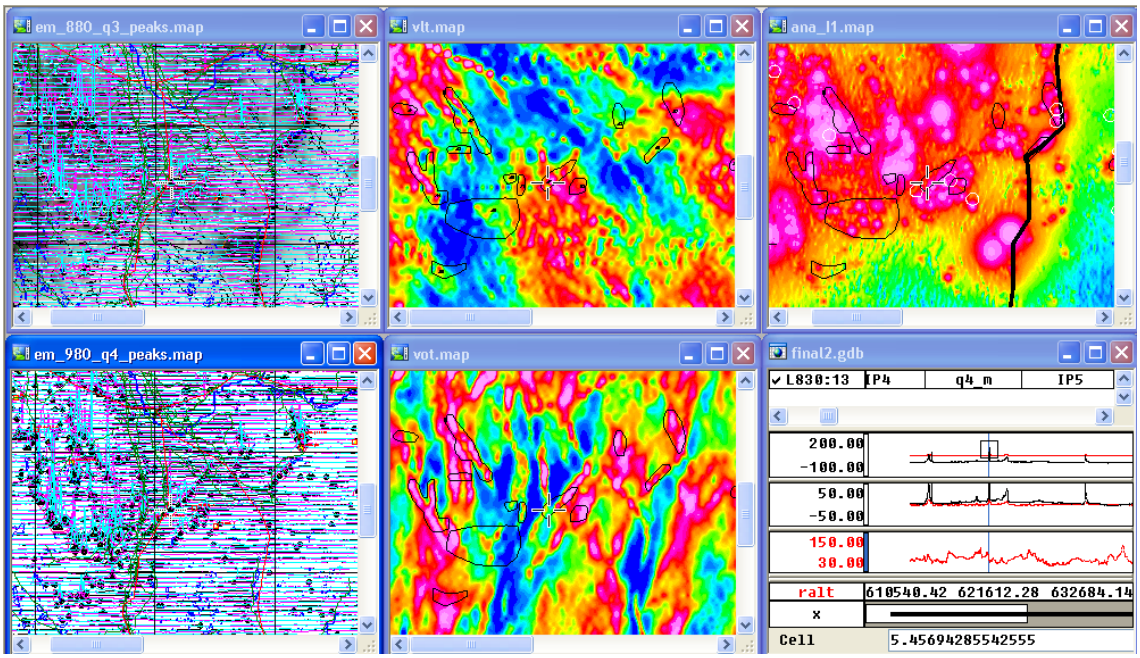

Figure 82. *Target Røros 47; elongated group of medium to large EM peaks; coincident VLF anomalies; adjacent short wavelength magnetic anomaly; priority 1*

(a)

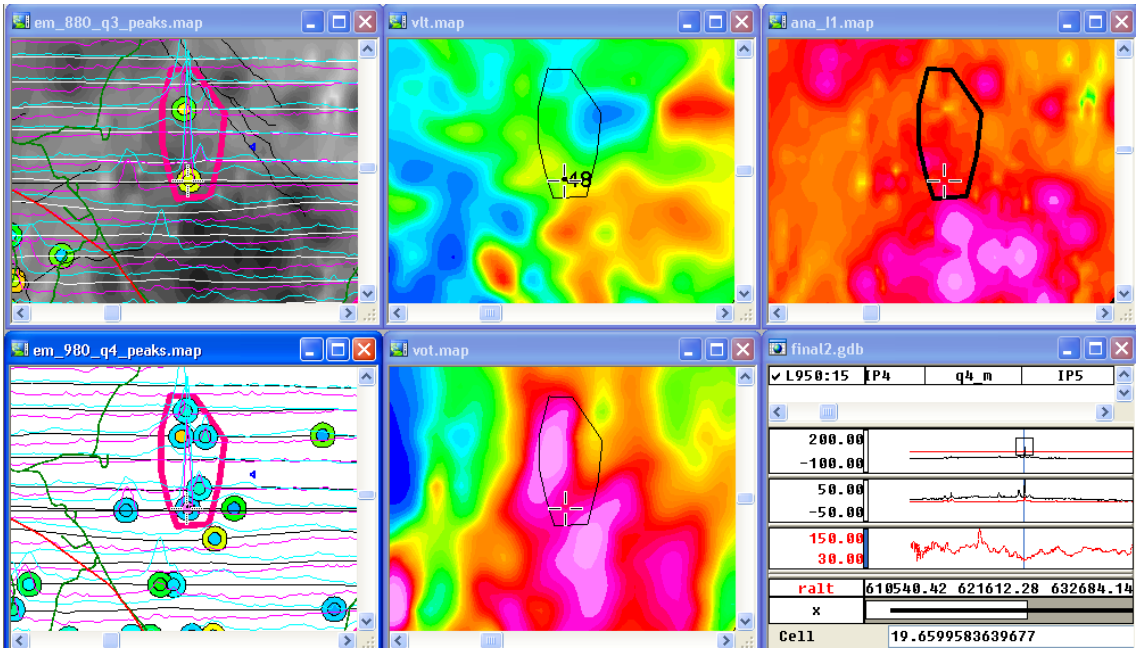

(b)

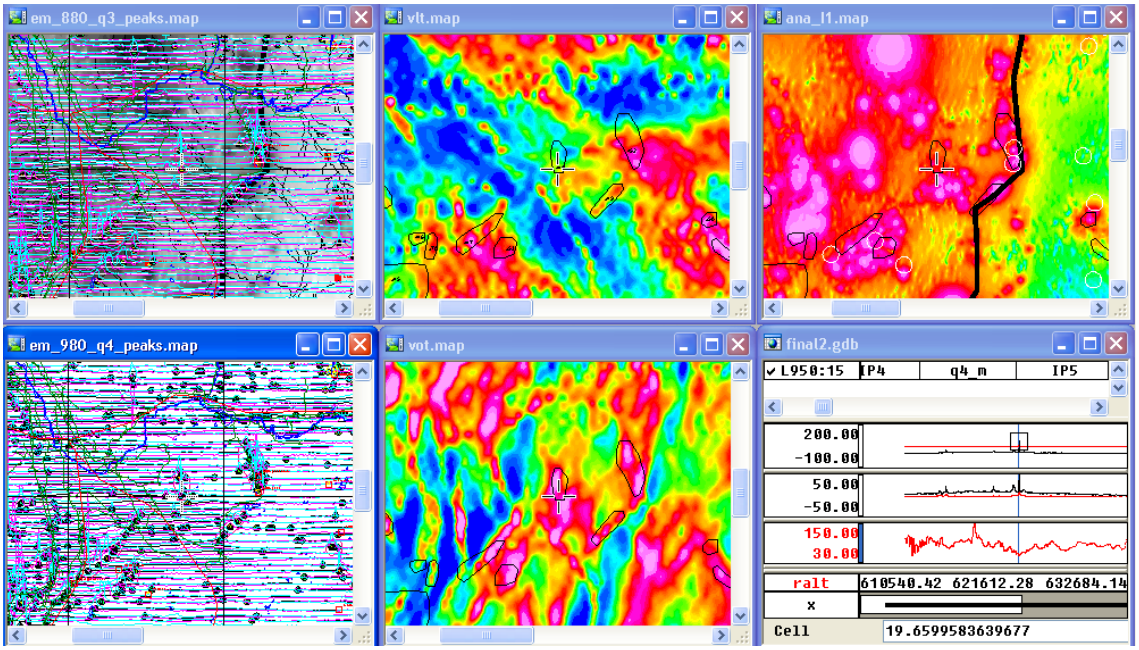

Figure 83. *Target Røros 48; a few medium to large EM peaks; coincident medium VLF anomalies; adjacent short wavelength magnetic anomaly; priority 2*

(a)

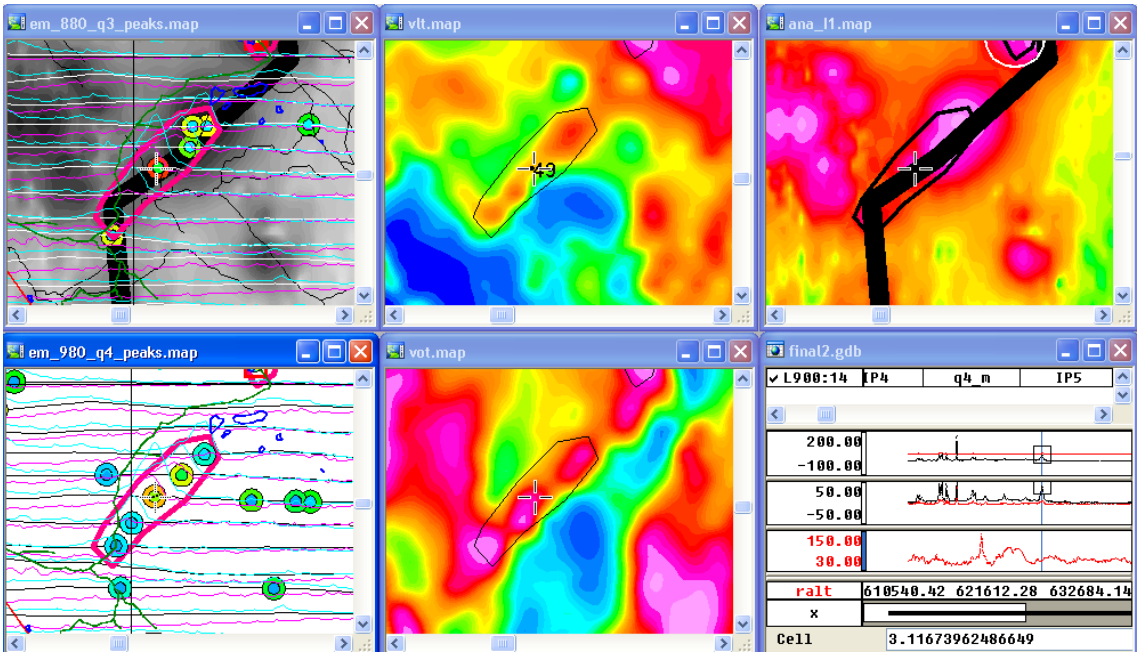

(b)

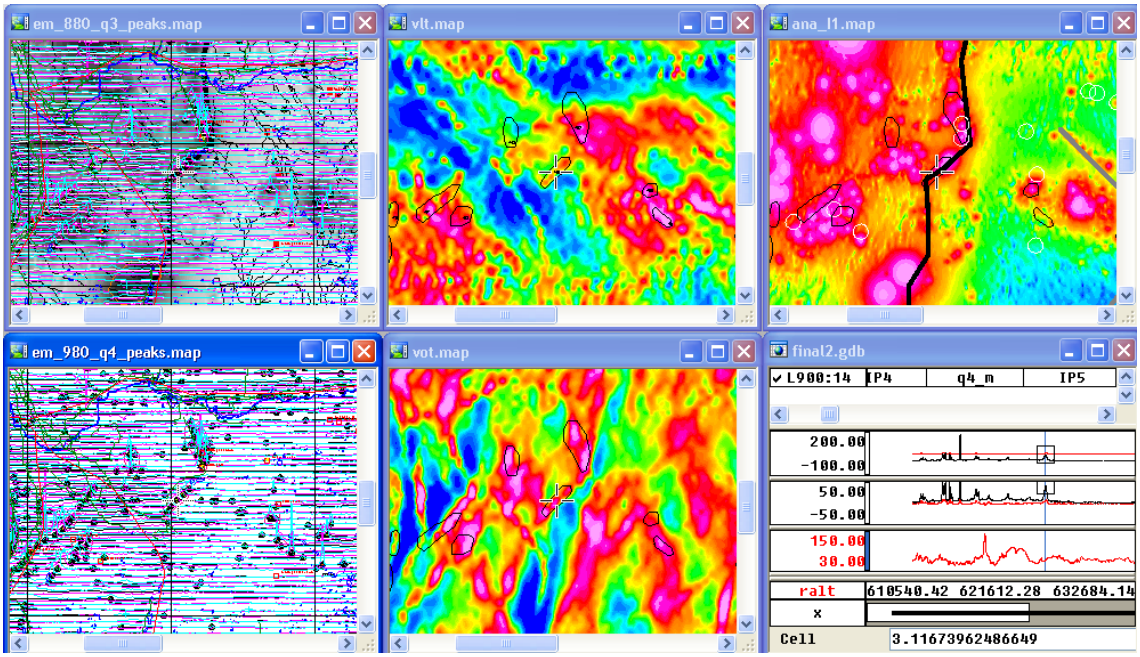

Figure 84. *Target Røros 49; elongated group of medium EM peaks; coincident VLF anomalies; adjacent short wavelength magnetic anomalies and on major magnetic boundary; priority 1*

(a)

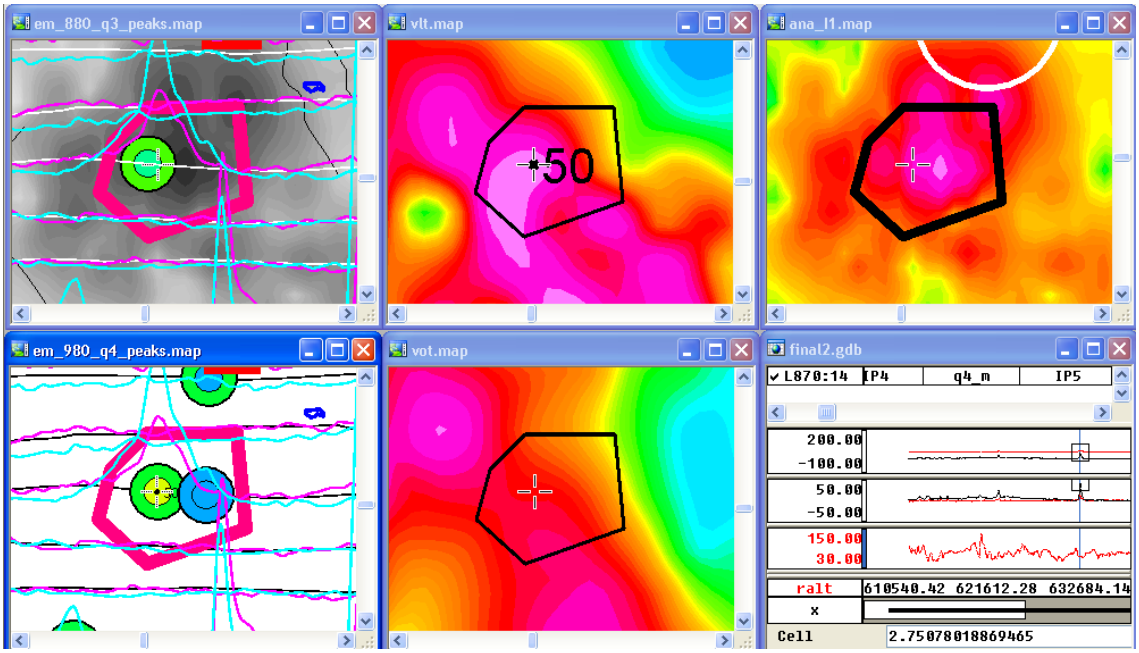

(b)

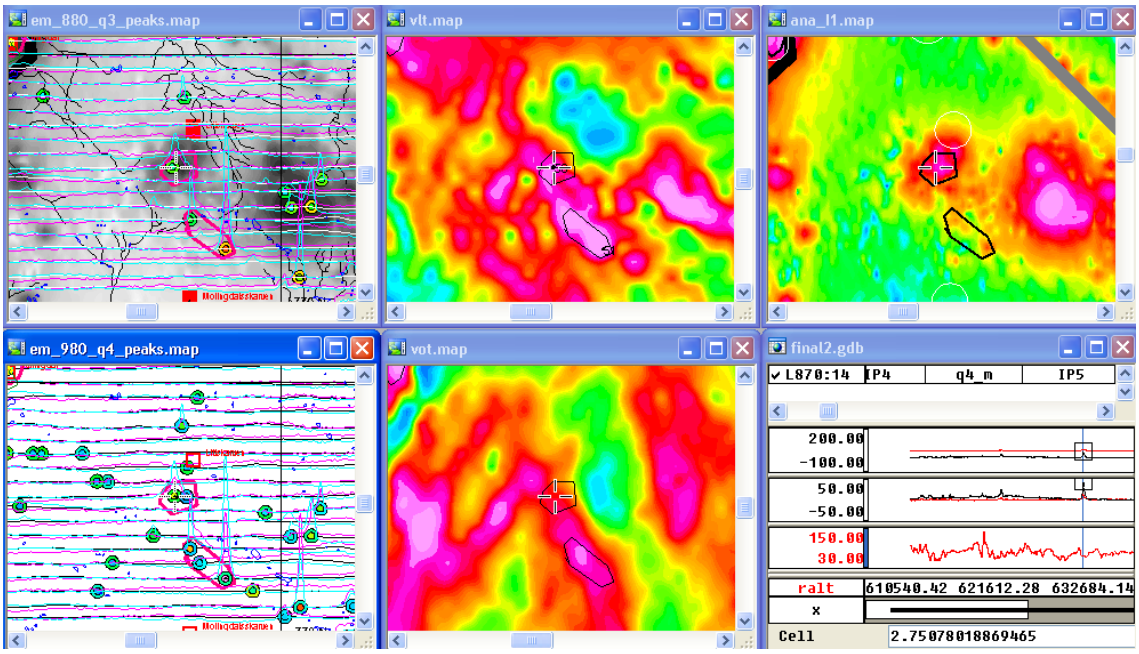

Figure 85. *Target Røros 50; a few medium to large EM peaks; coincident VLF anomalies; on top of short wavelength magnetic anomaly; priority 2*

(a)

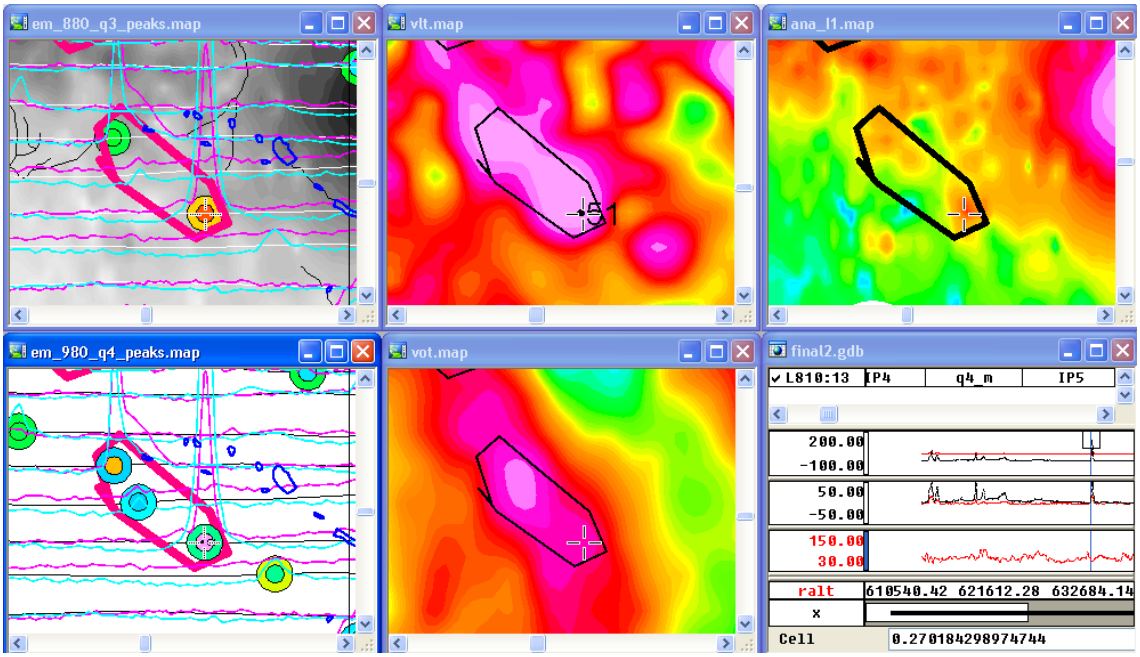

(b)

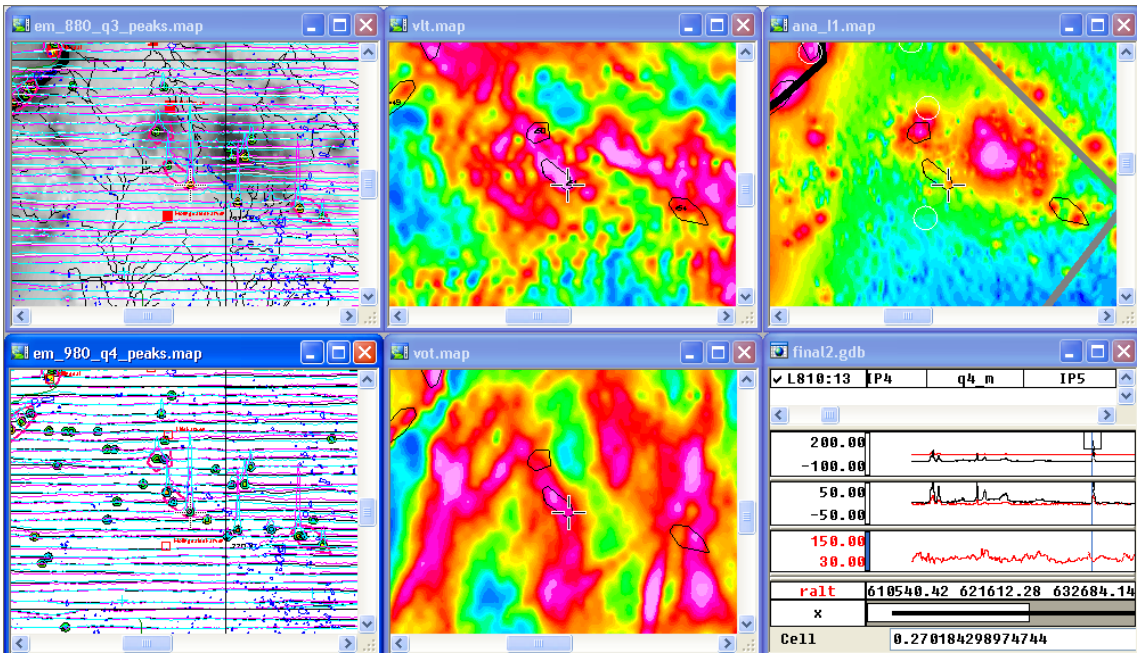

Figure 86. *Target Røros 51; small group of medium to large EM peaks; coincident VLF anomalies; adjacent short wavelength magnetic anomaly; priority 1*

(a)

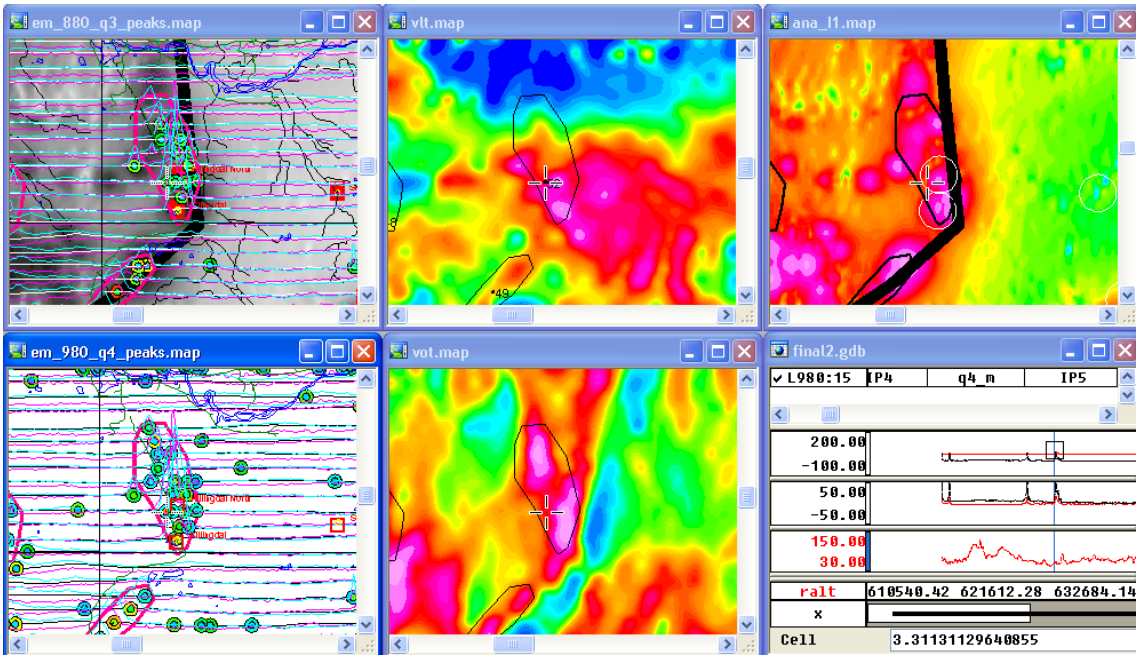

(b)

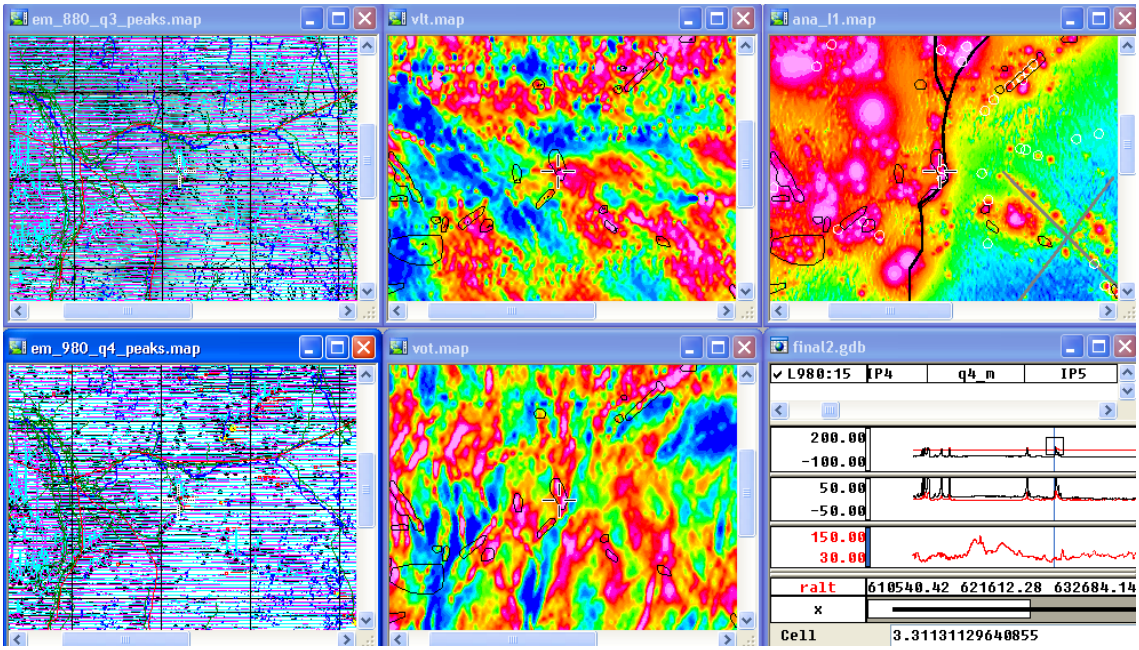

Figure 87. *Target Røros 52; group of medium to large EM peaks; coincident VLF anomalies; adjacent short wavelength magnetic anomalies and on major magnetic lineament; priority 1*

(a)

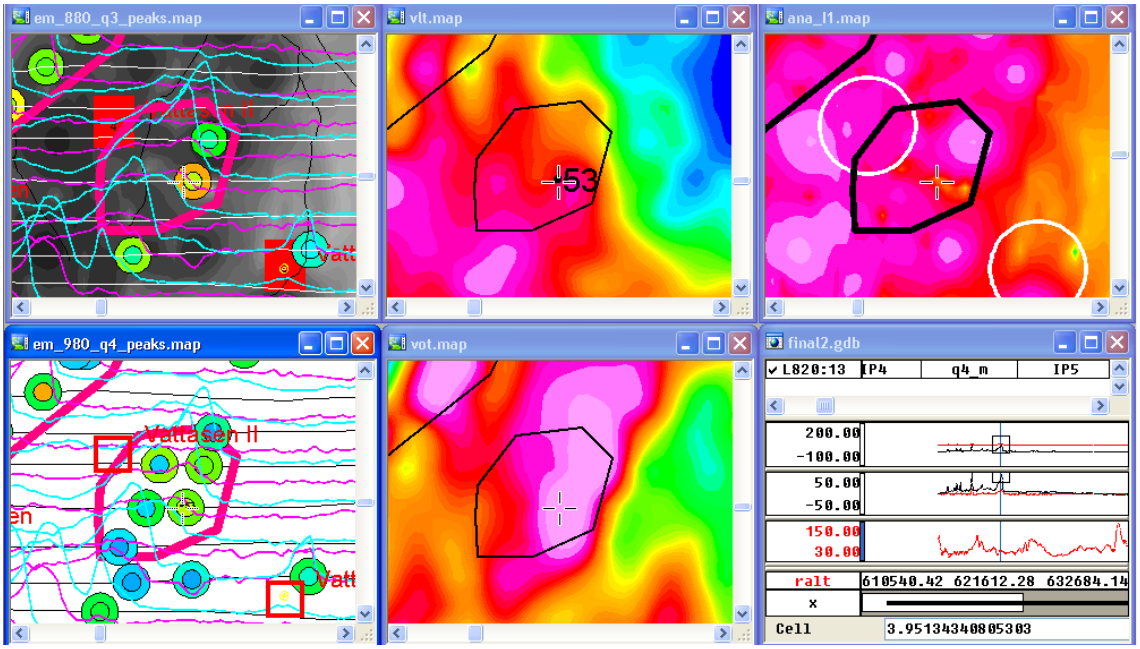

(b)

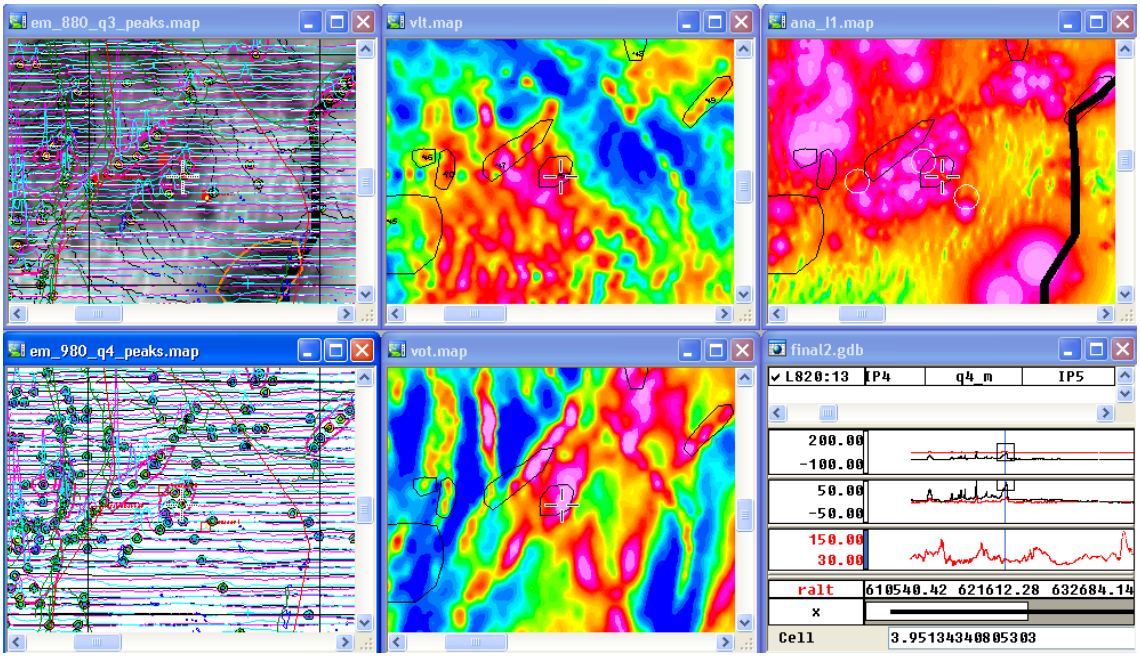

Figure 88. *Target Røros 53; elongated group of medium to large EM peaks; coincident VLF anomalies; adjacent short wavelength magnetic anomaly; priority 1*

(a)

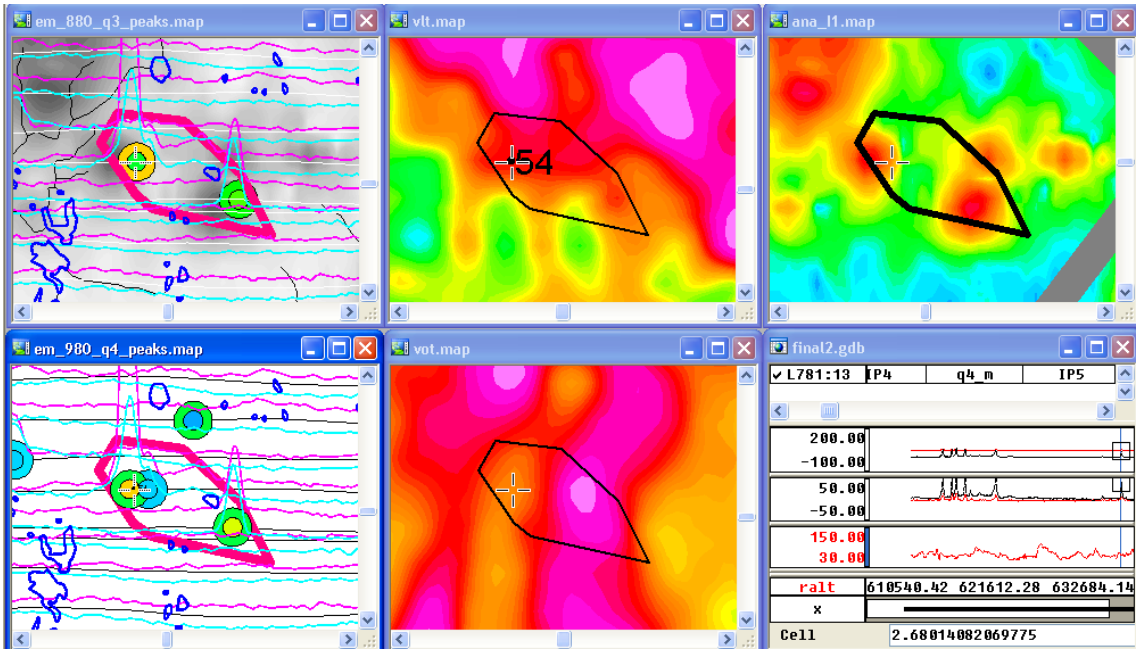

(b)

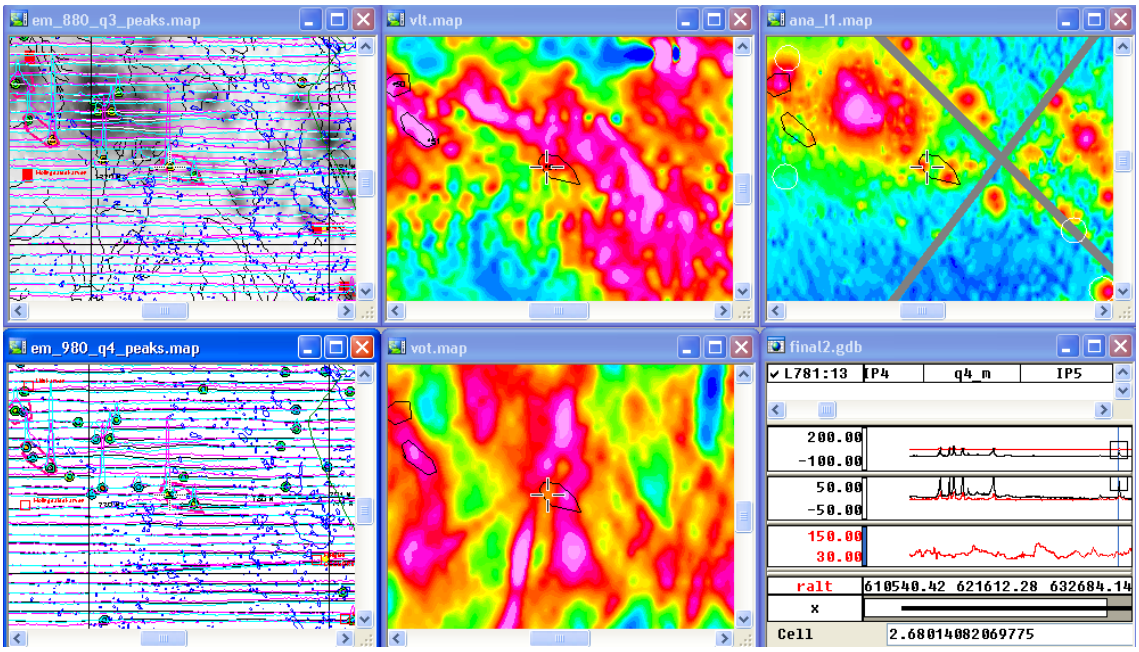

Figure 89. *Target Røros 54; elongated group of medium to large EM peaks; coincident VLF anomalies; adjacent short wavelength magnetic anomaly; priority 1*

(a)

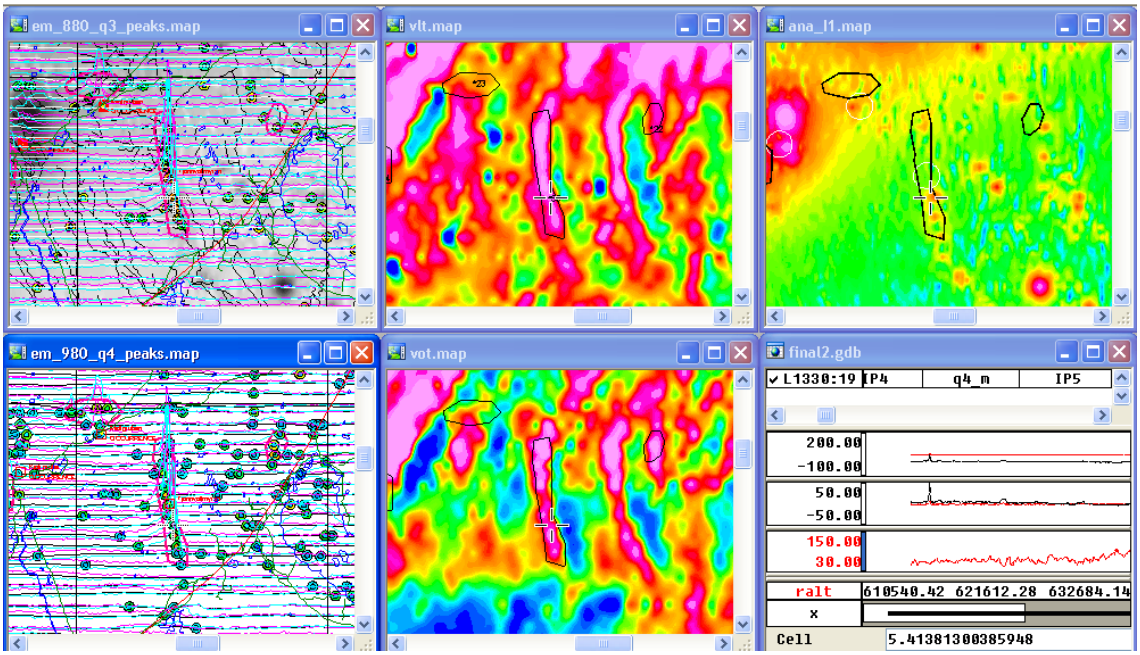

(b)

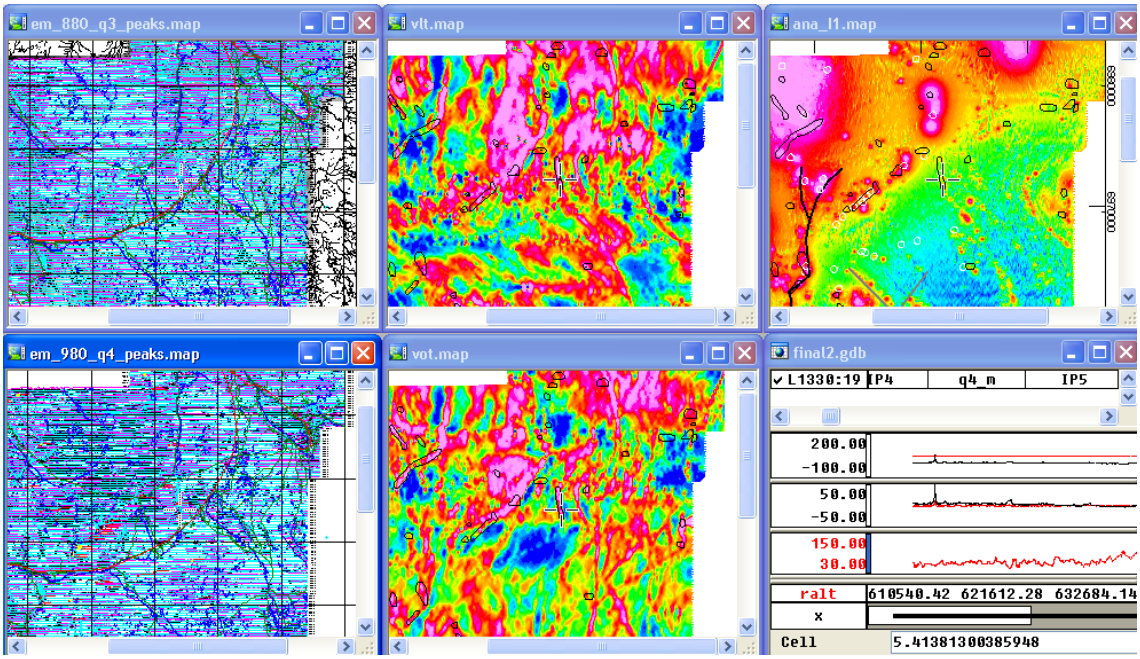

Figure 90. *Target Røros 55; large elongated group of medium to large EM peaks; coincident VLF anomalies; adjacent short wavelength magnetic anomalies trending along EM anomalies; priority 1*

(a)

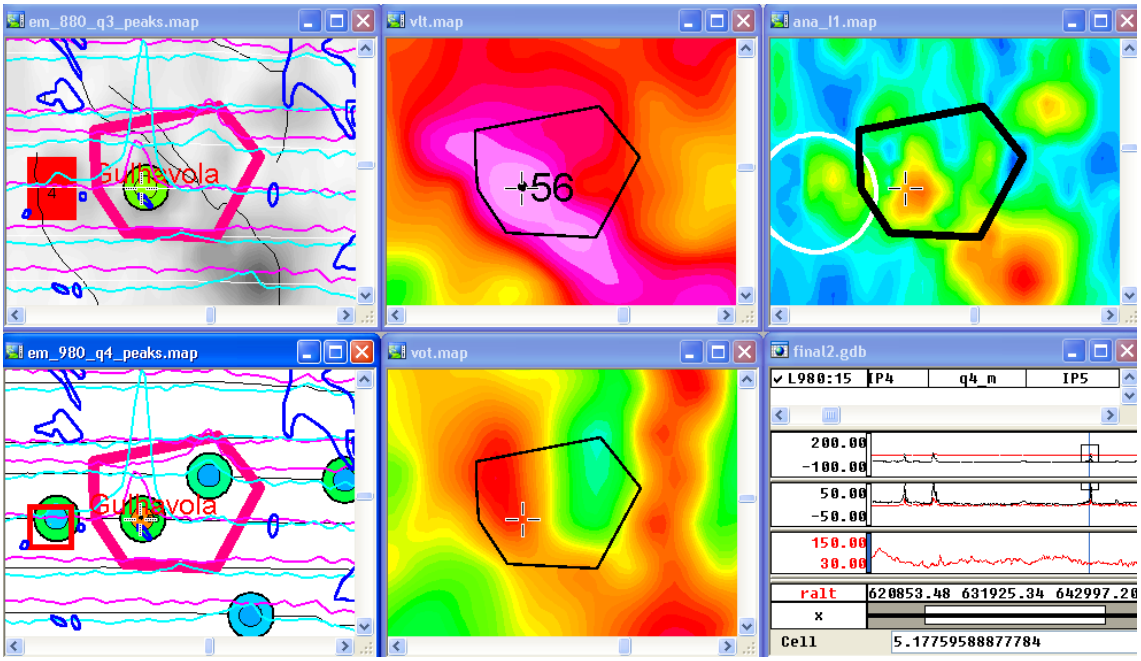

(b)

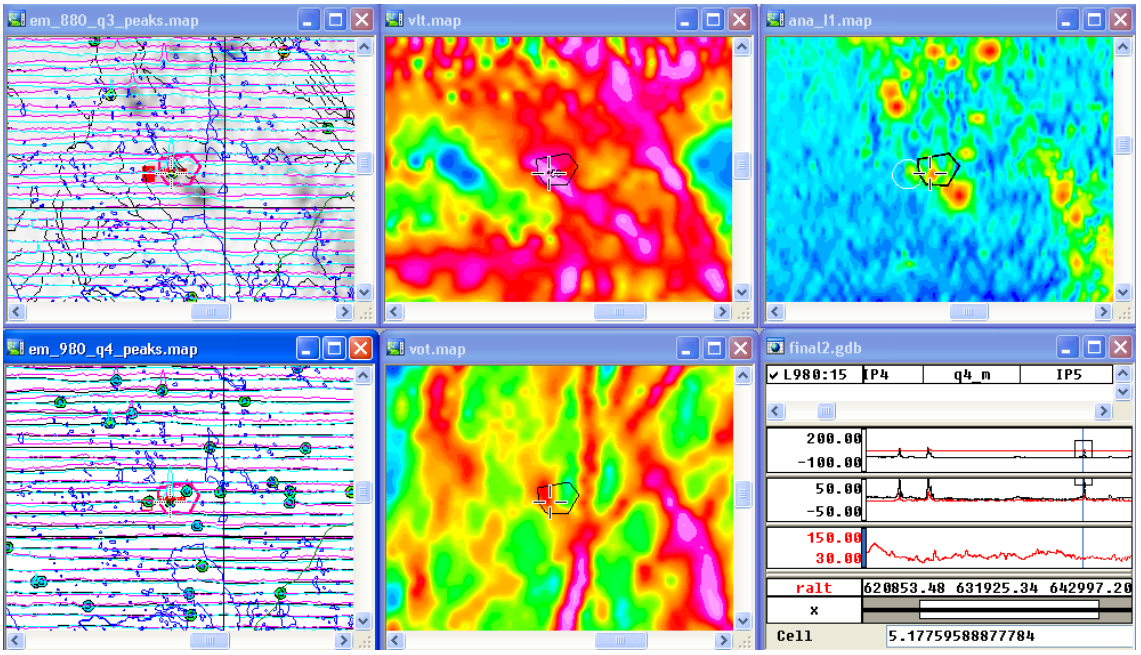

Figure 91. *Target Røros 56; small group of medium to large EM peaks; coincident VLF anomalies; adjacent short wavelength magnetic anomaly; priority 1*

(a)

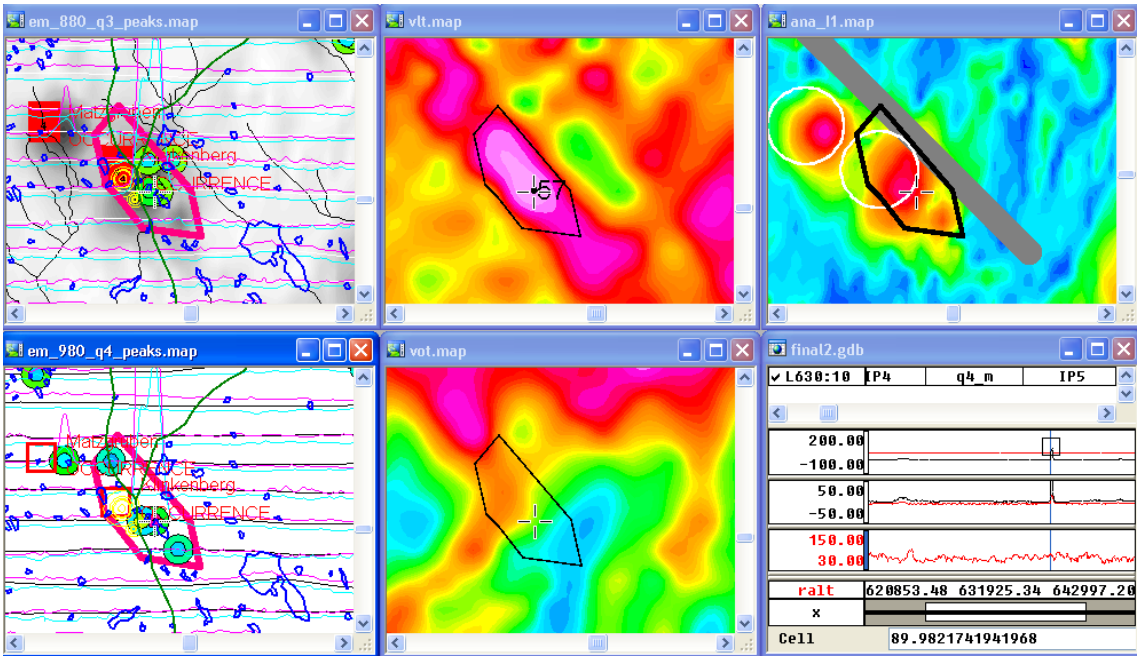

(b)

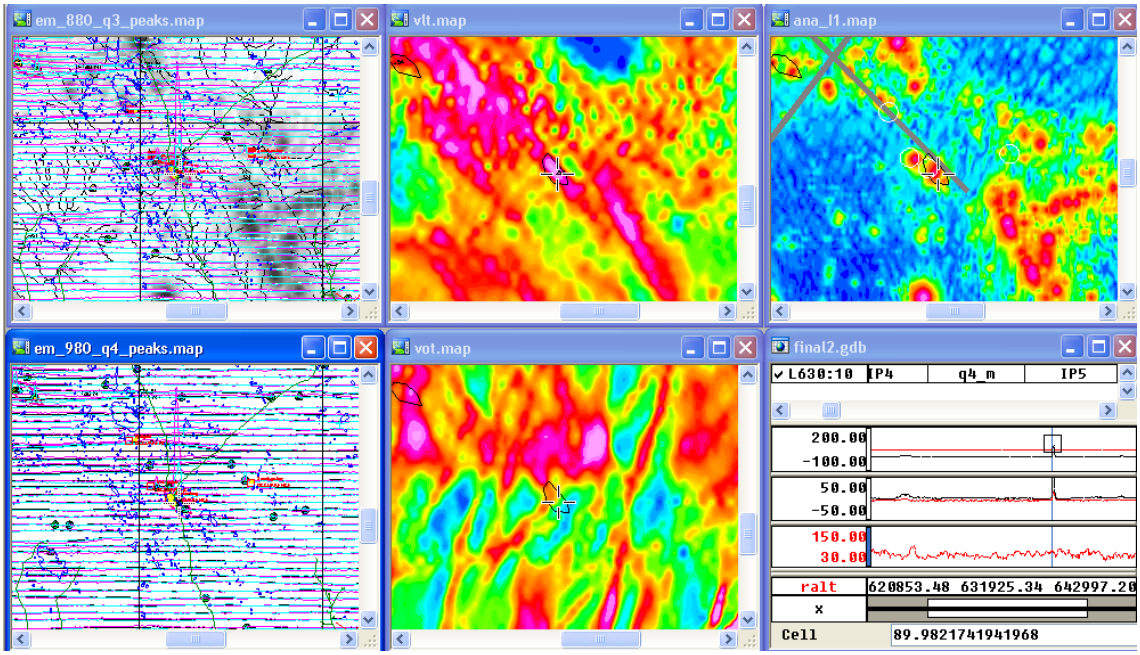

Figure 92. *Target Røros 57; elongated group of medium to large EM peaks; coincident VLF anomalies; adjacent short wavelength magnetic anomalies – on magnetic boundary; priority 1*

(a)

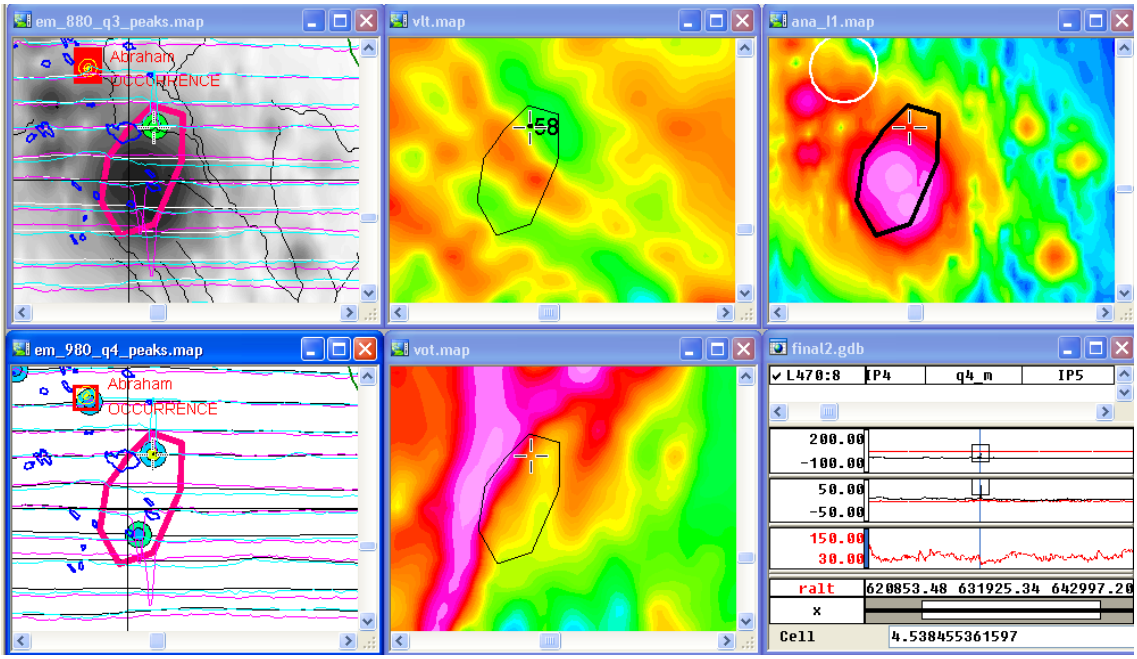

(b)

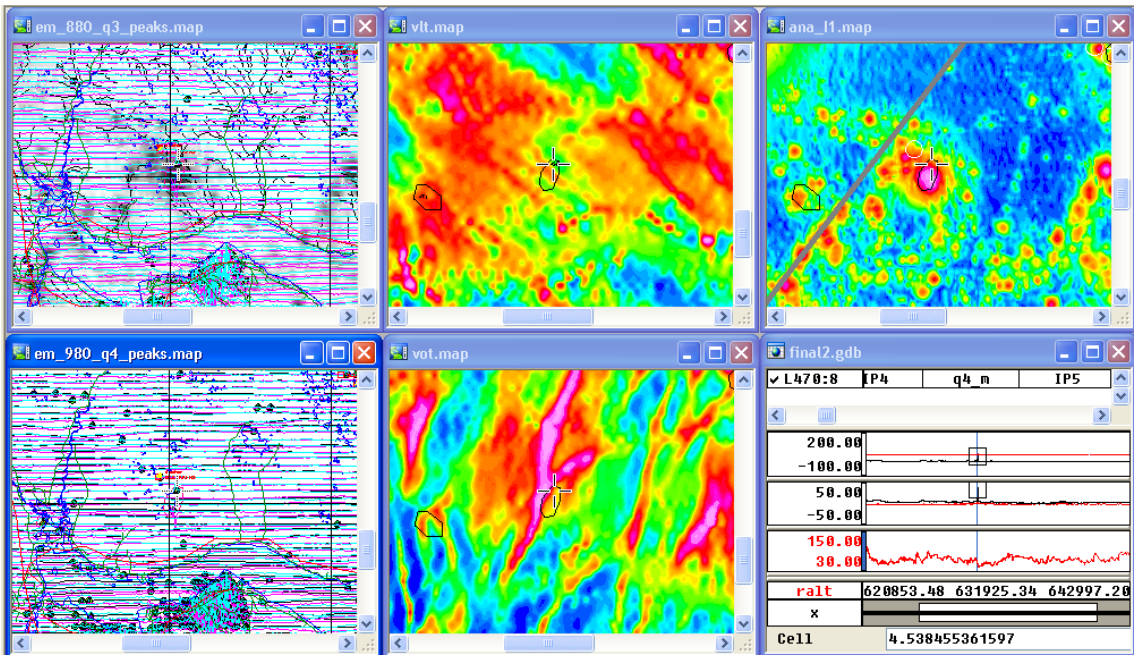

Figure 93. *Target Røros 58; a few medium to large EM peaks; coincident VLF anomalies; adjacent short wavelength magnetic anomaly with negative in-phase EM anomaly consistent with strong magnetic anomaly; priority 2*

(a)

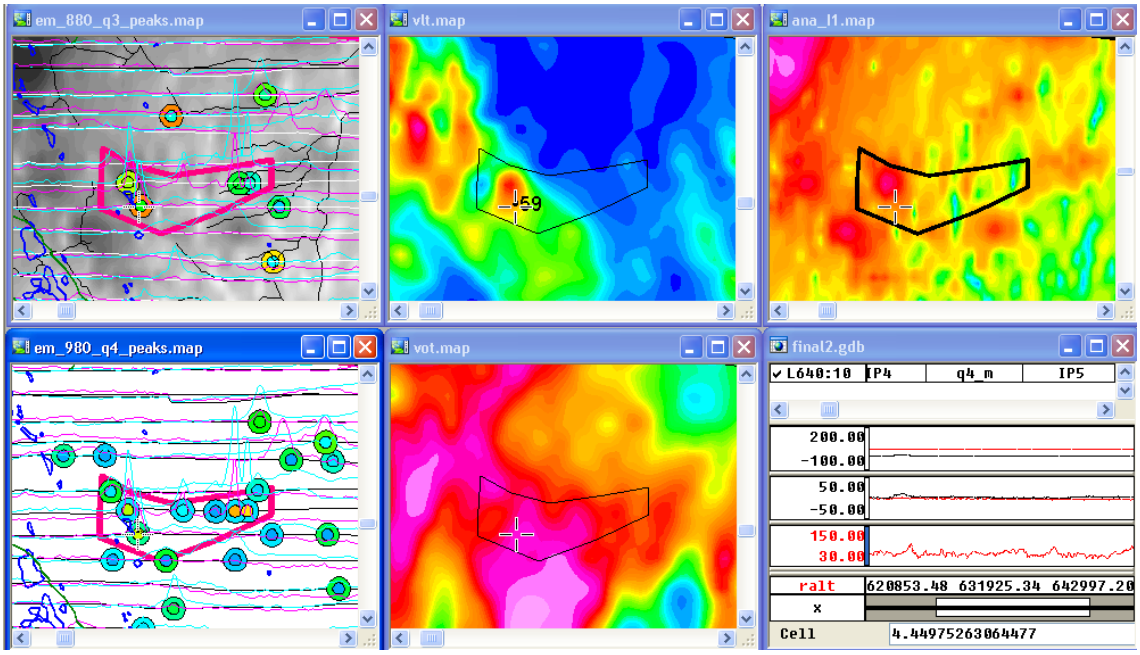

(b)

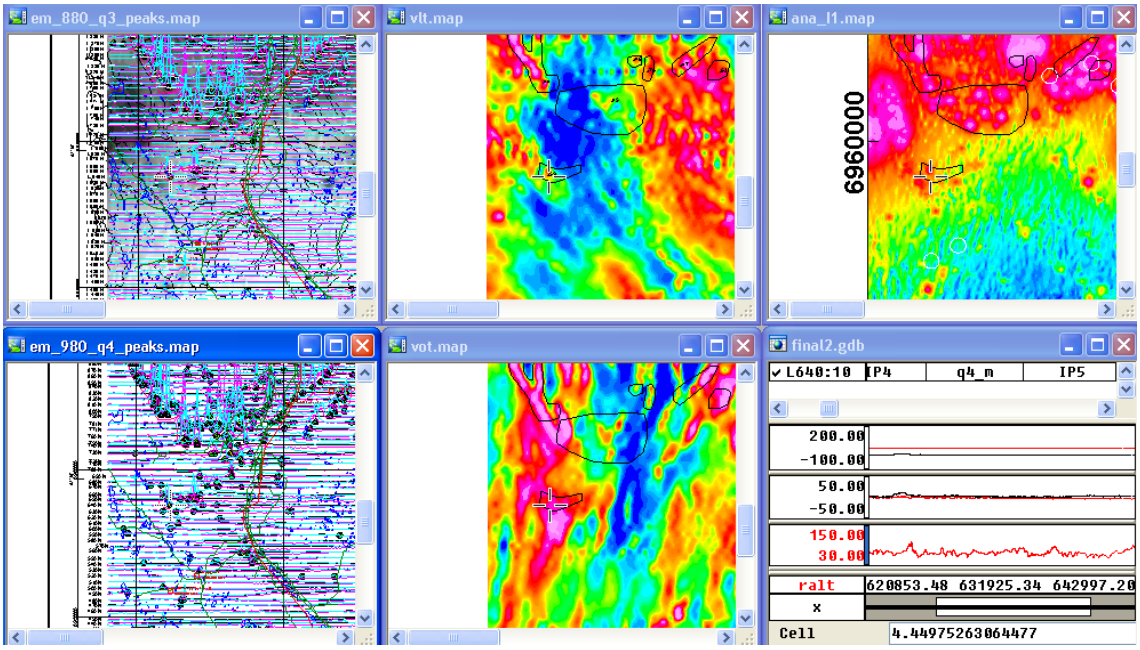

Figure 94. *Target Røros 59; elongated group of medium to large EM peaks; partly coincident VLF anomalies; adjacent short wavelength magnetic anomaly; priority 2*

(a)

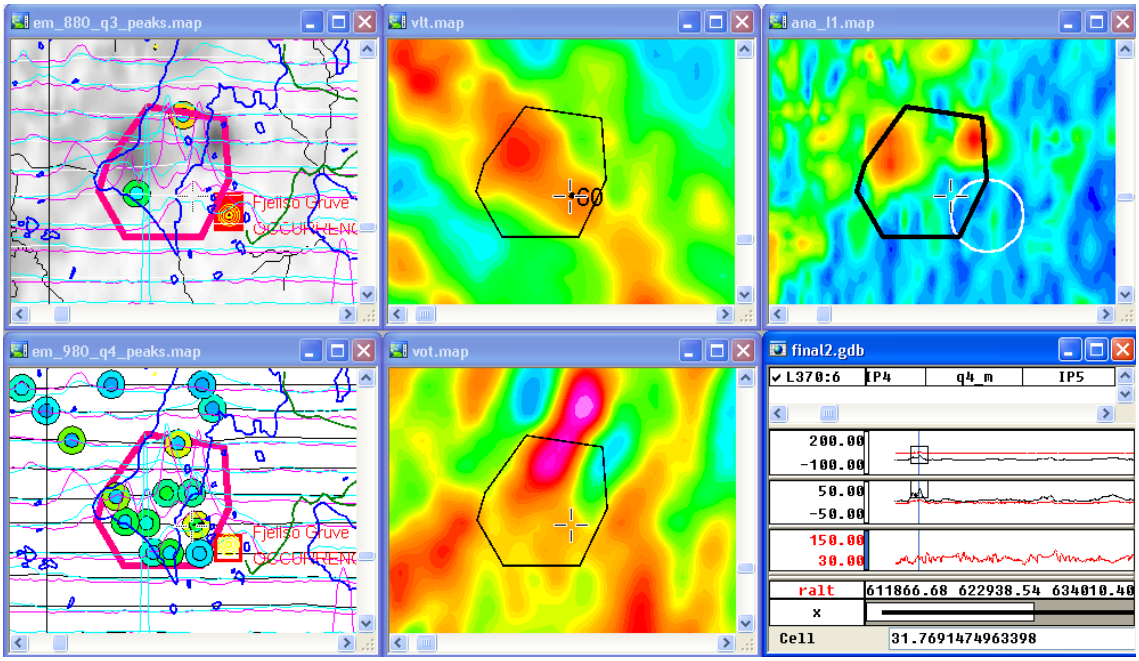

(b)

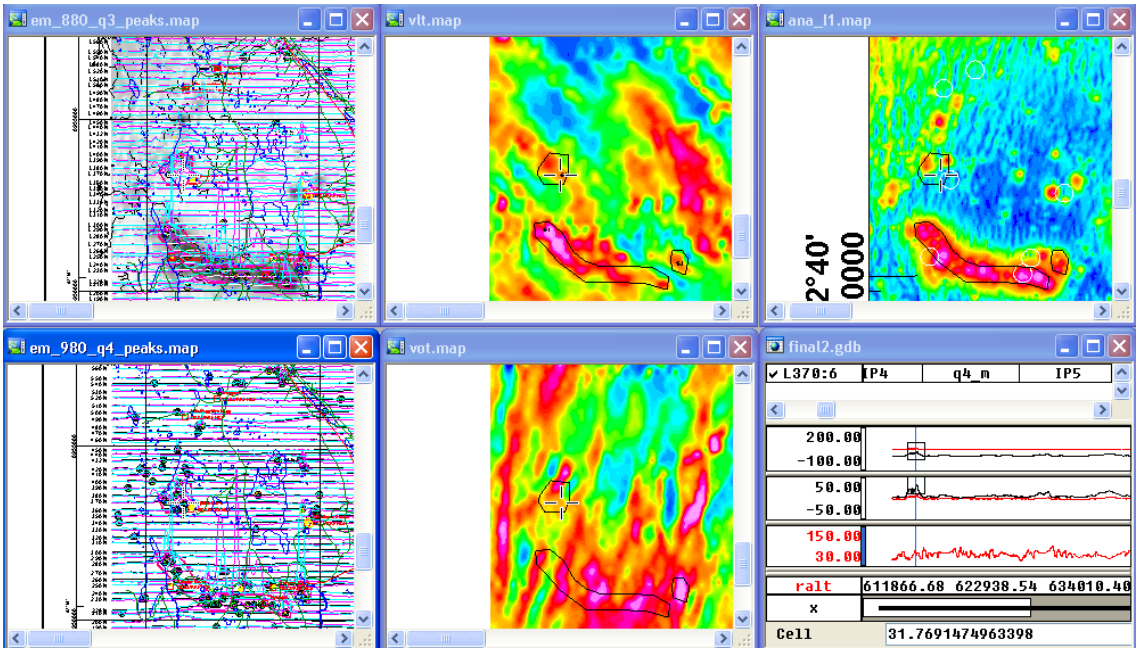

Figure 95. *Target Røros 60; group of medium to large EM peaks; coincident VLF anomalies; adjacent short wavelength magnetic anomaly; priority 2*

(a)

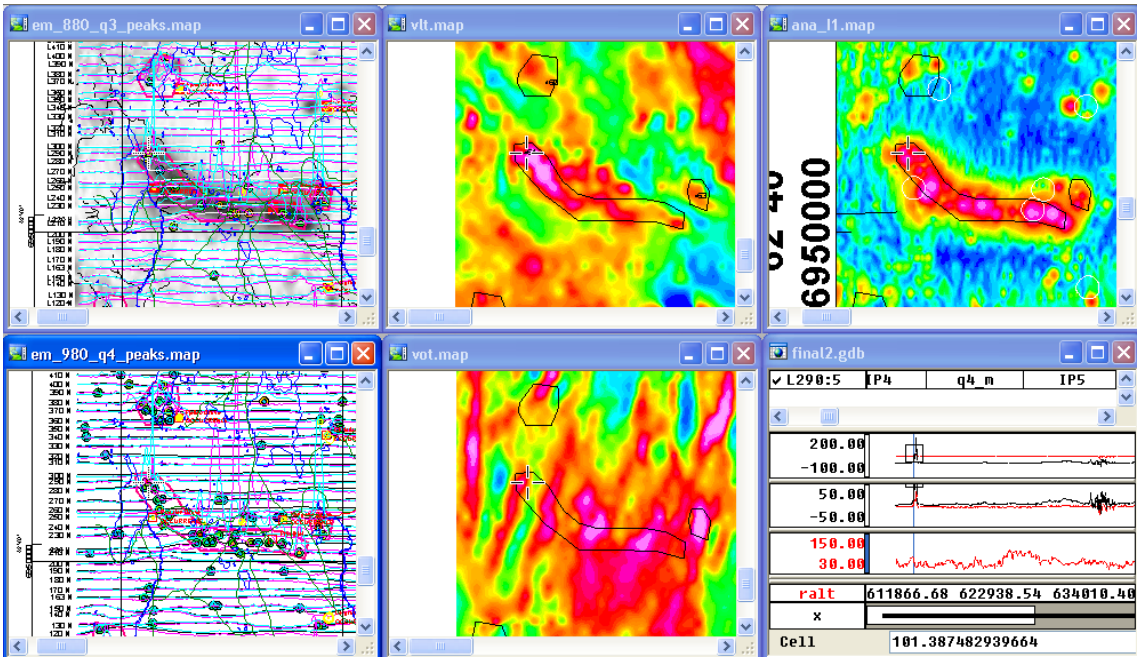

(b)

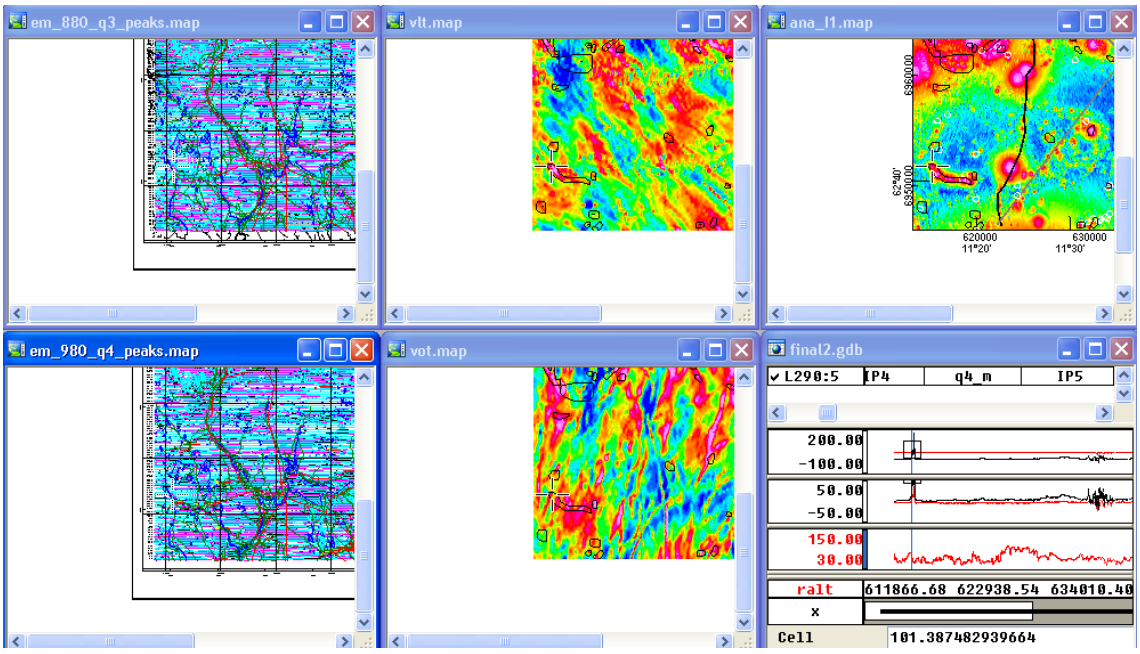

Figure 96. *Target Røros 61; elongated group of medium to large EM peaks; coincident VLF anomalies; adjacent short wavelength magnetic anomaly; priority 1*

(a)

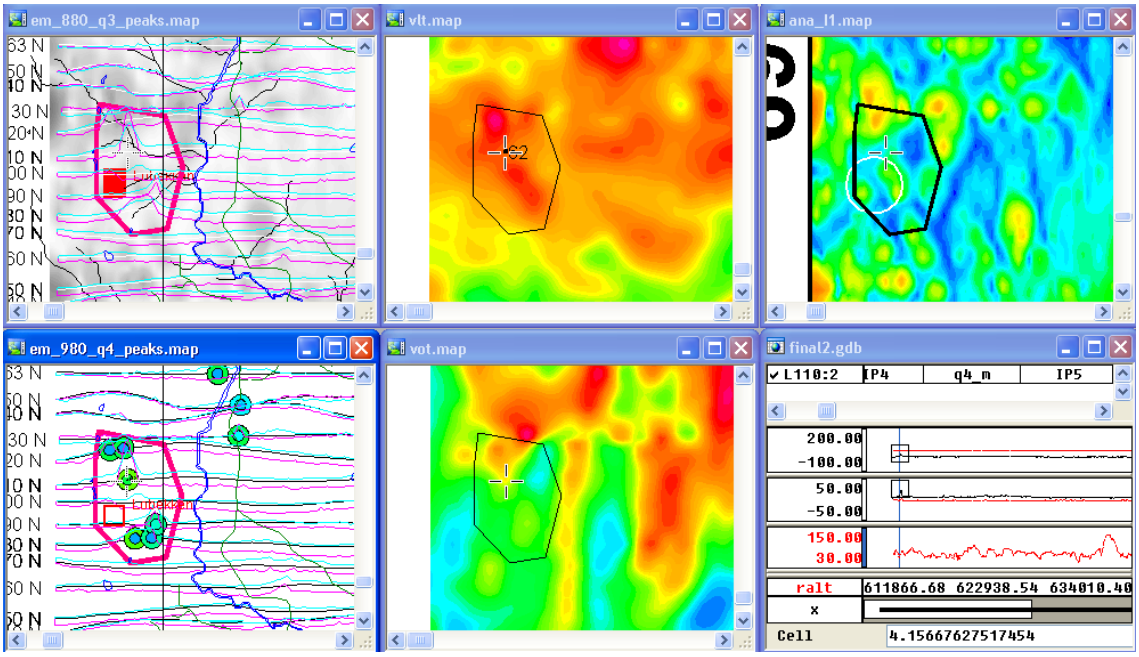

(b)

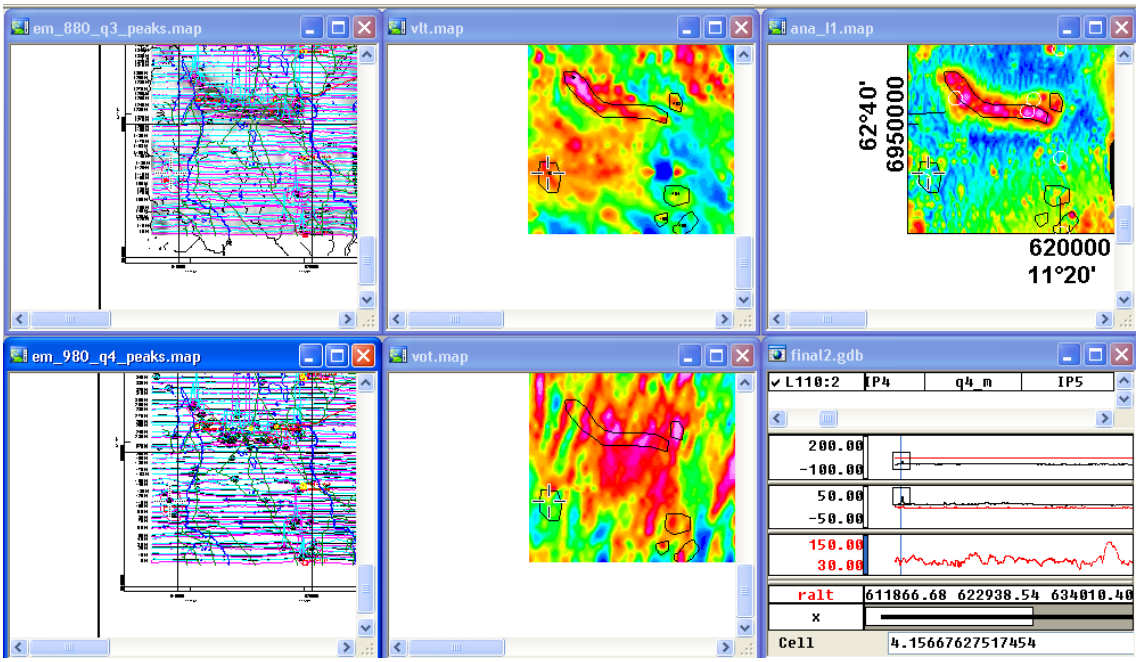

Figure 97. *Target Røros 62; a few medium EM peaks; coincident VLF anomalies; adjacent weak short wavelength magnetic anomaly; priority 3*

(a)

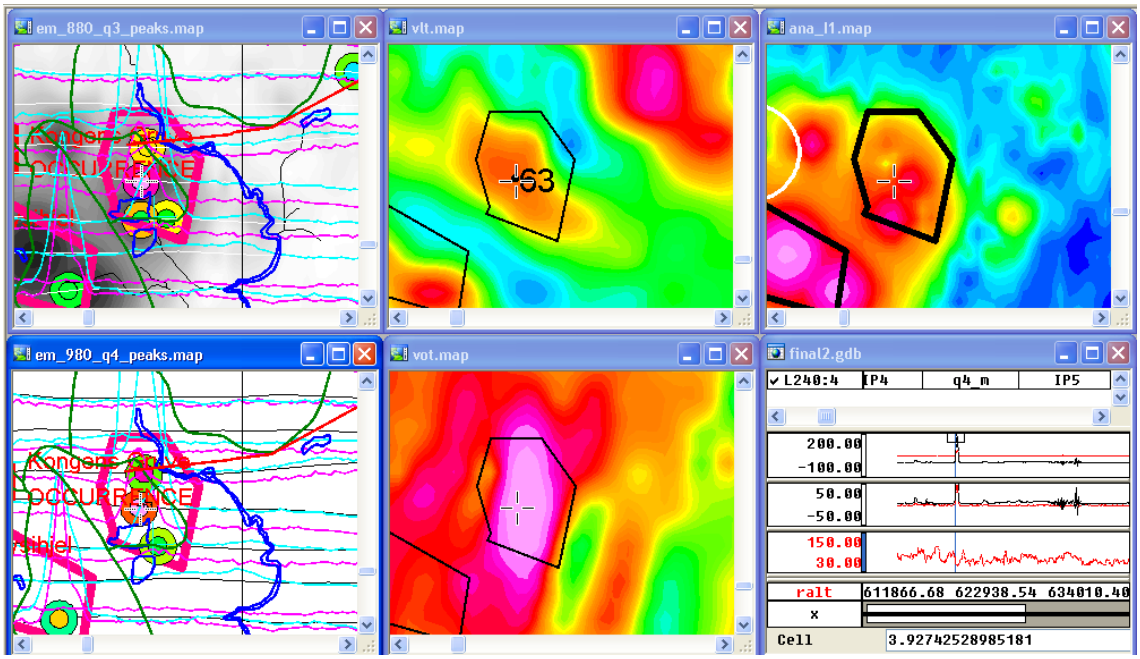

(b)

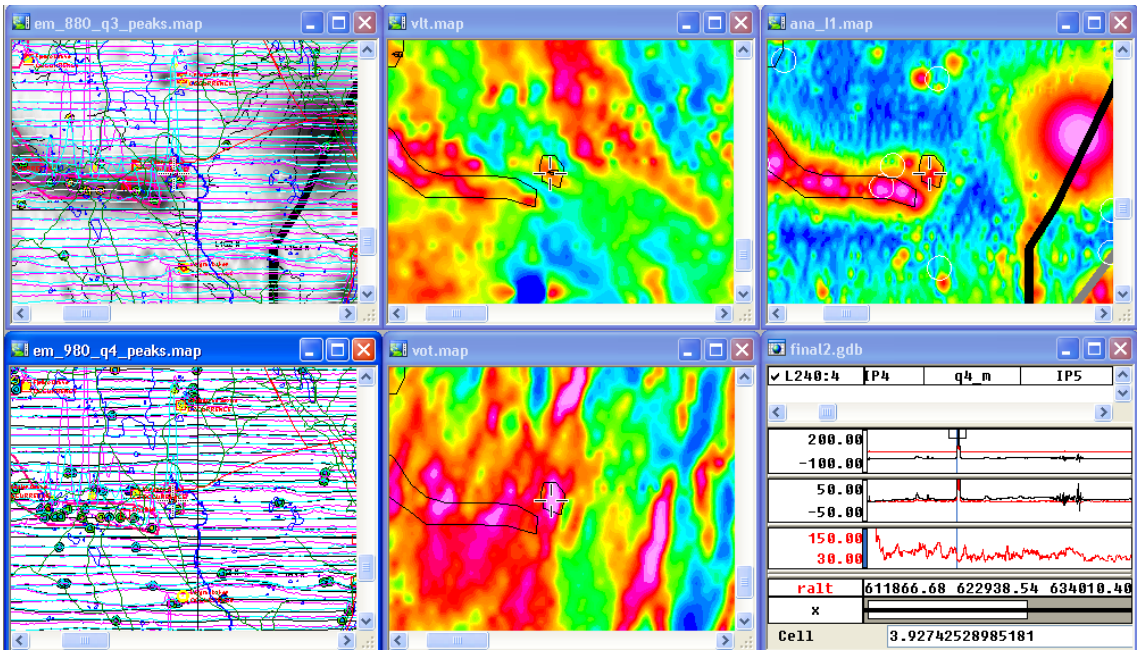

Figure 98. *Target Røros 63; small group of medium to large EM peaks; coincident VLF anomalies; adjacent short wavelength magnetic anomalies; priority 1*

(a)

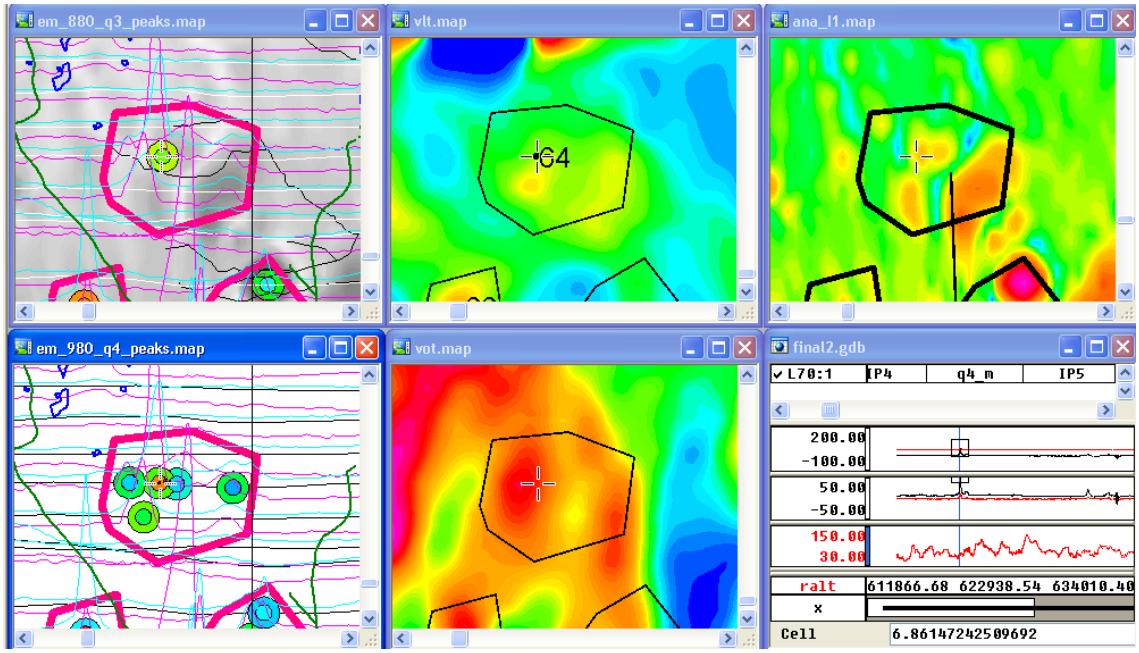

(b)

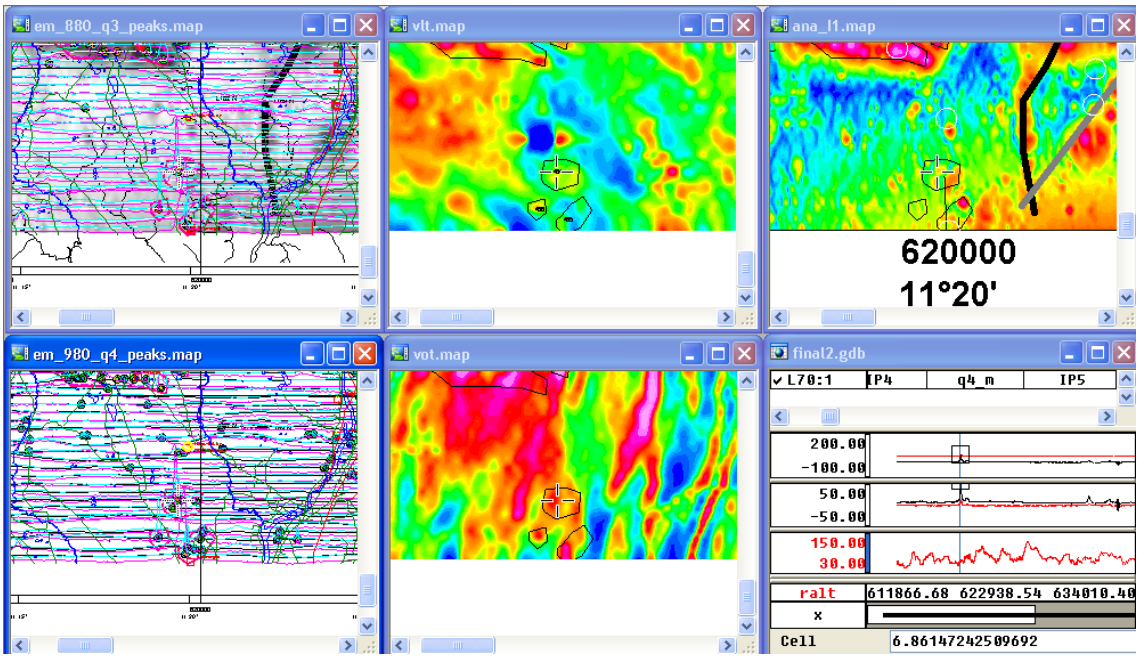

Figure 99. *Target Røros 64; a few medium to large EM peaks; coincident medium VLF anomalies; adjacent weak short wavelength magnetic anomaly; priority 3*

(a)

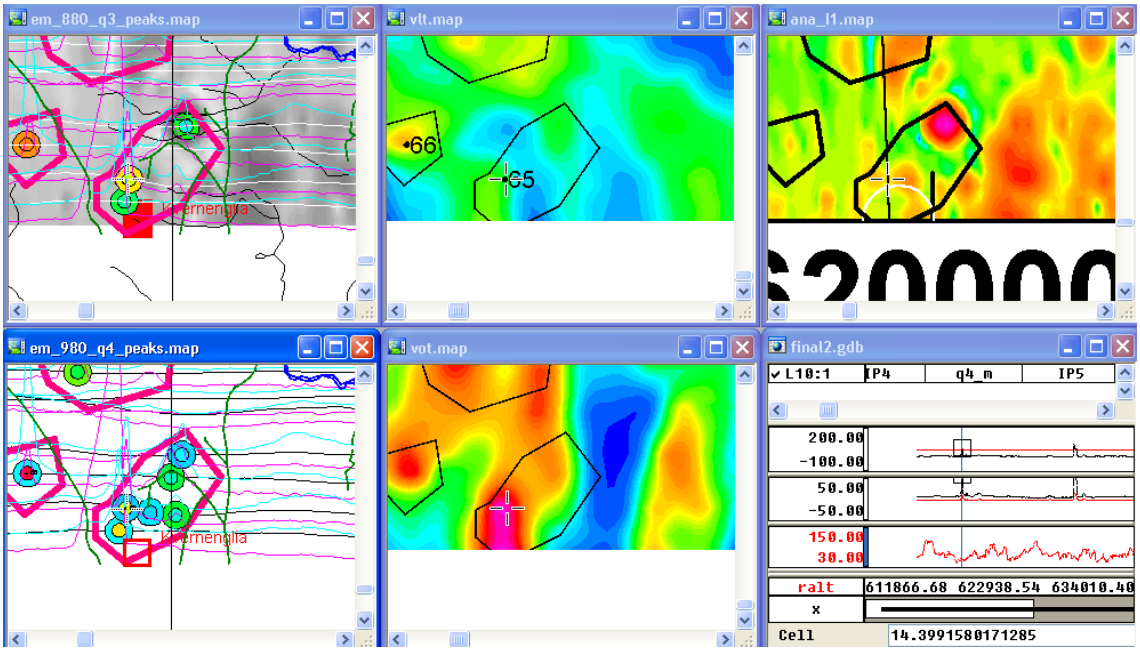

(b)

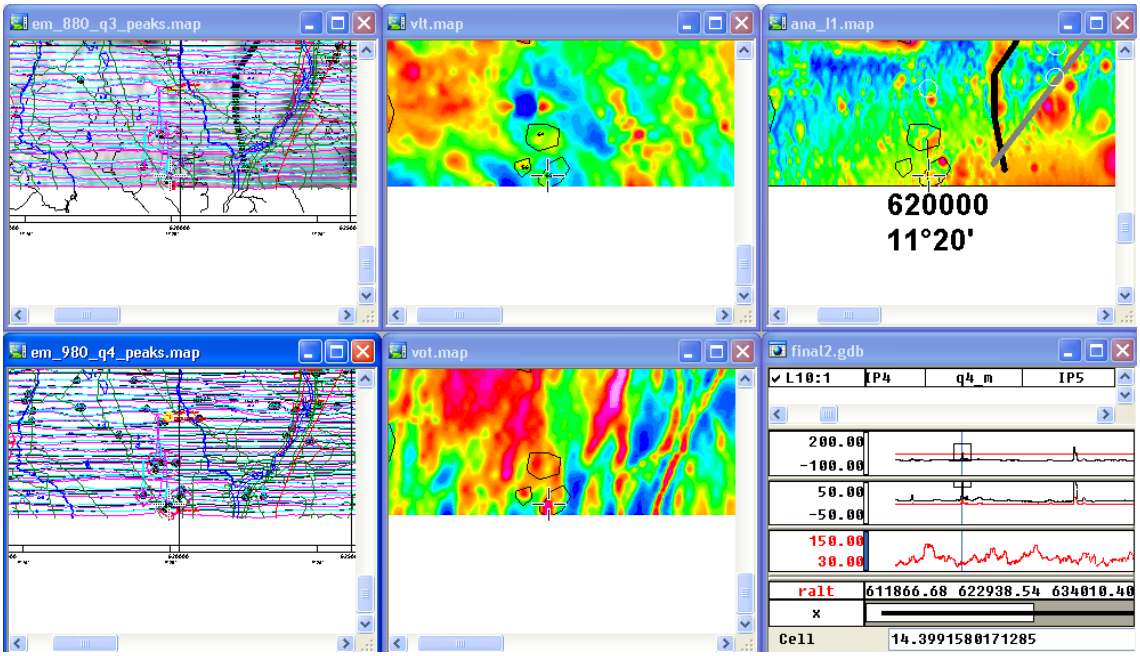

Figure 100. *Target Røros 65; a few medium to large EM peaks; coincident medium VLF anomalies; adjacent weak short wavelength magnetic anomaly; priority 3*

(a)

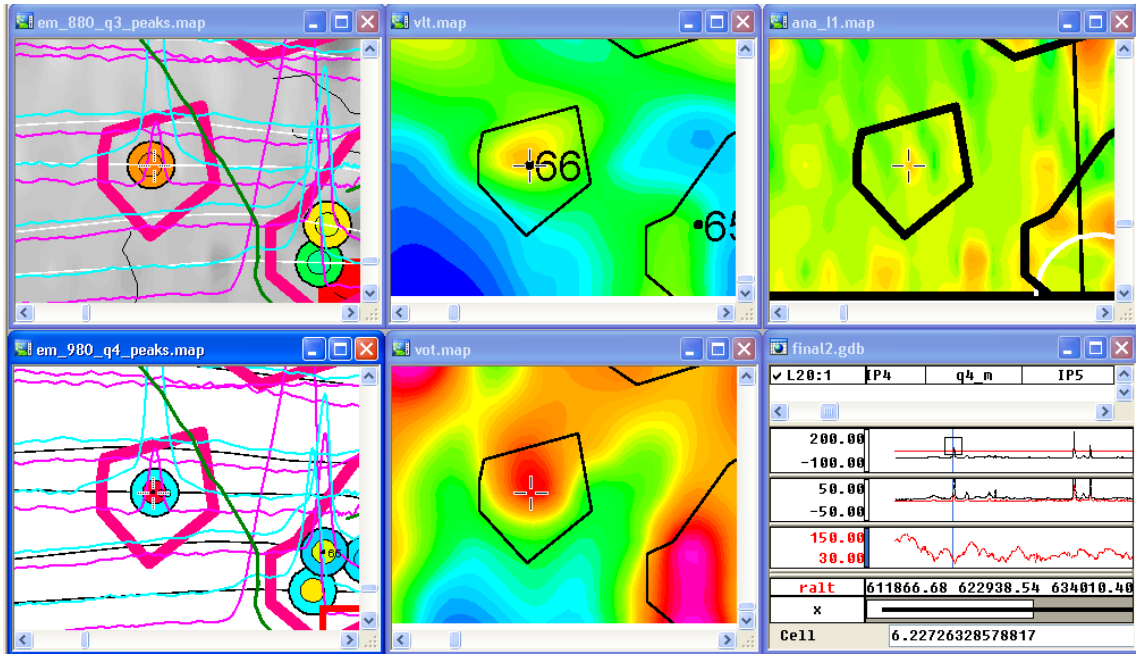

(b)

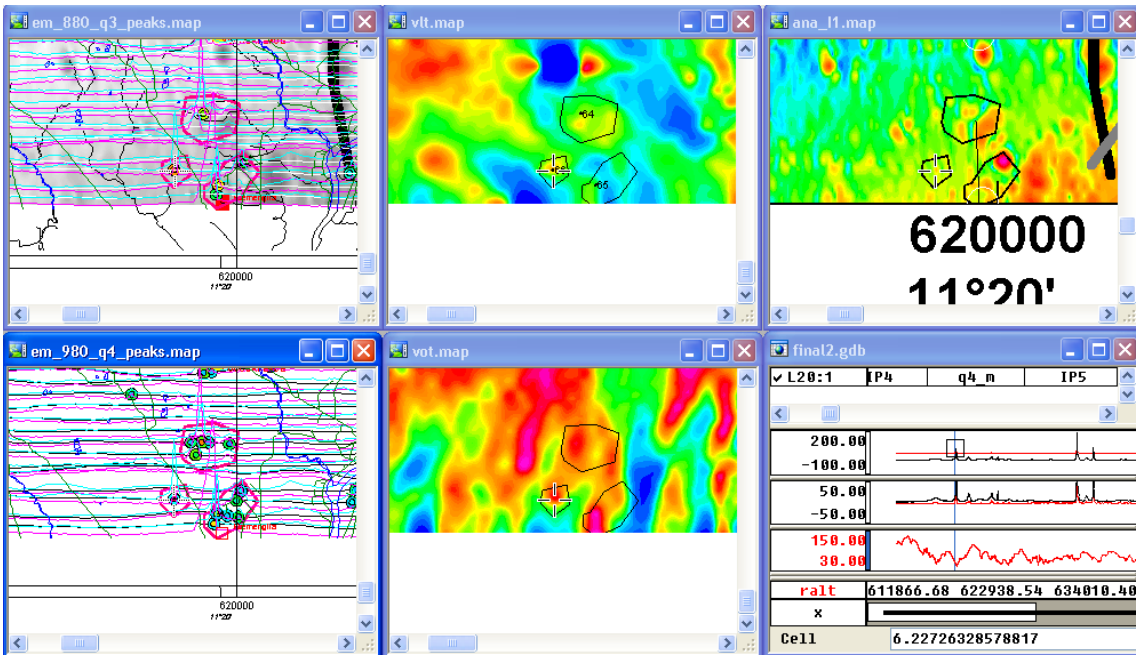

Figure 101. *Target Røros 66; large narrow EM peak; coincident VLF anomalies; adjacent weak short wavelength magnetic anomaly; priority 2*

(a)

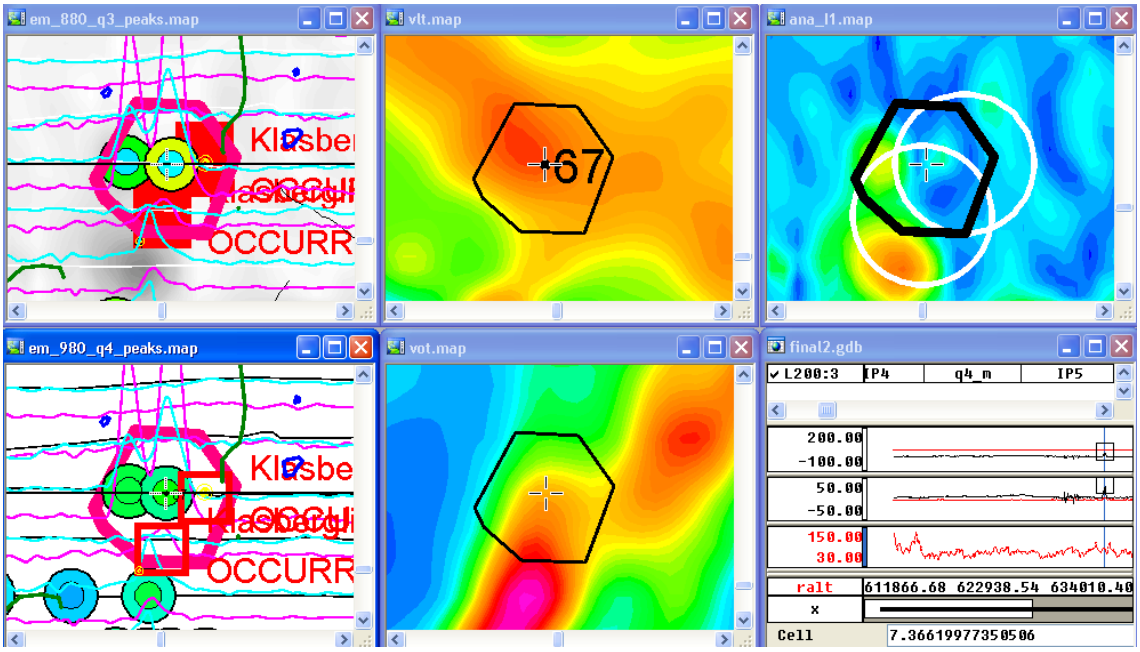

(b)

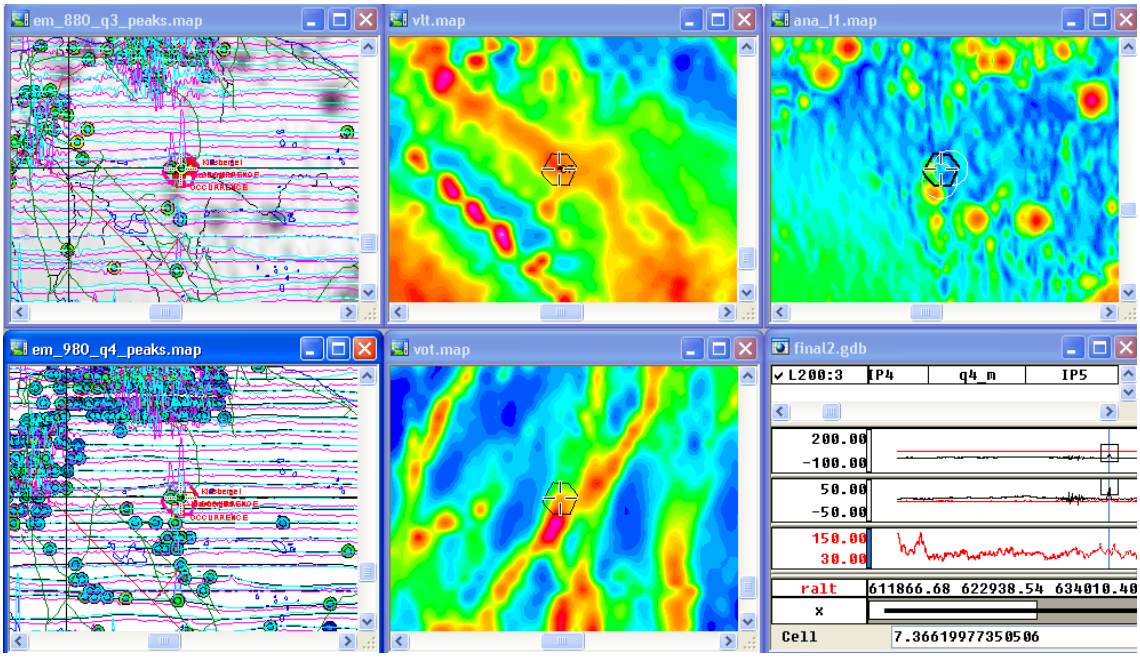

Figure 102. *Target Røros 67; small group of medium to large EM peaks; coincident VLF anomalies; adjacent short wavelength magnetic anomaly; priority 3.*

(a)

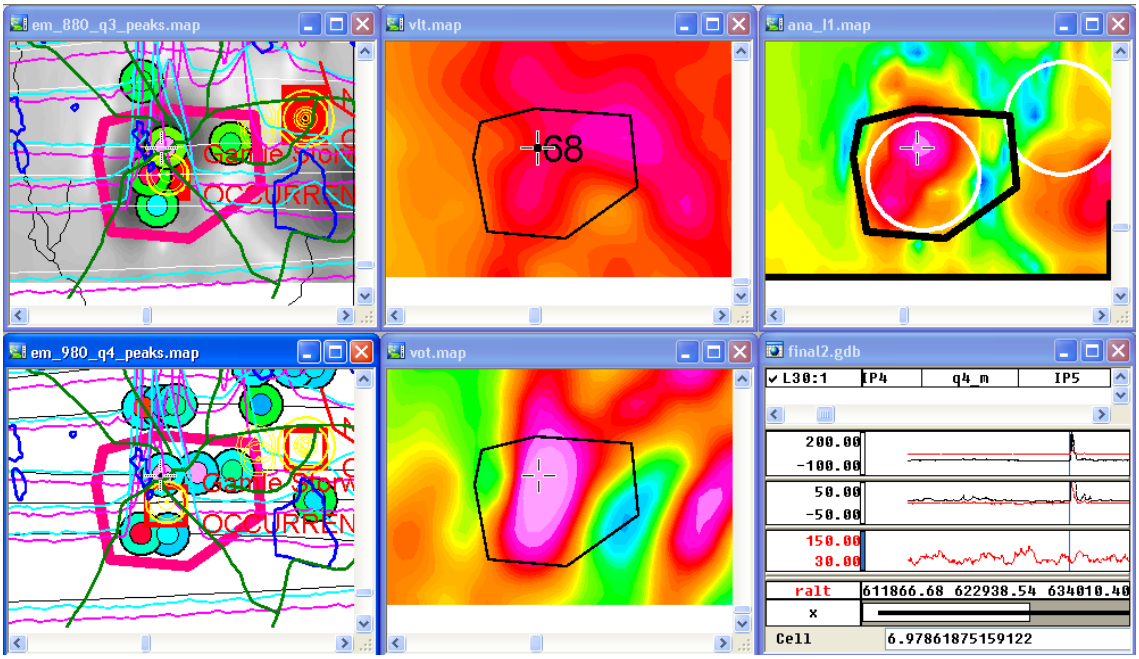

(b)

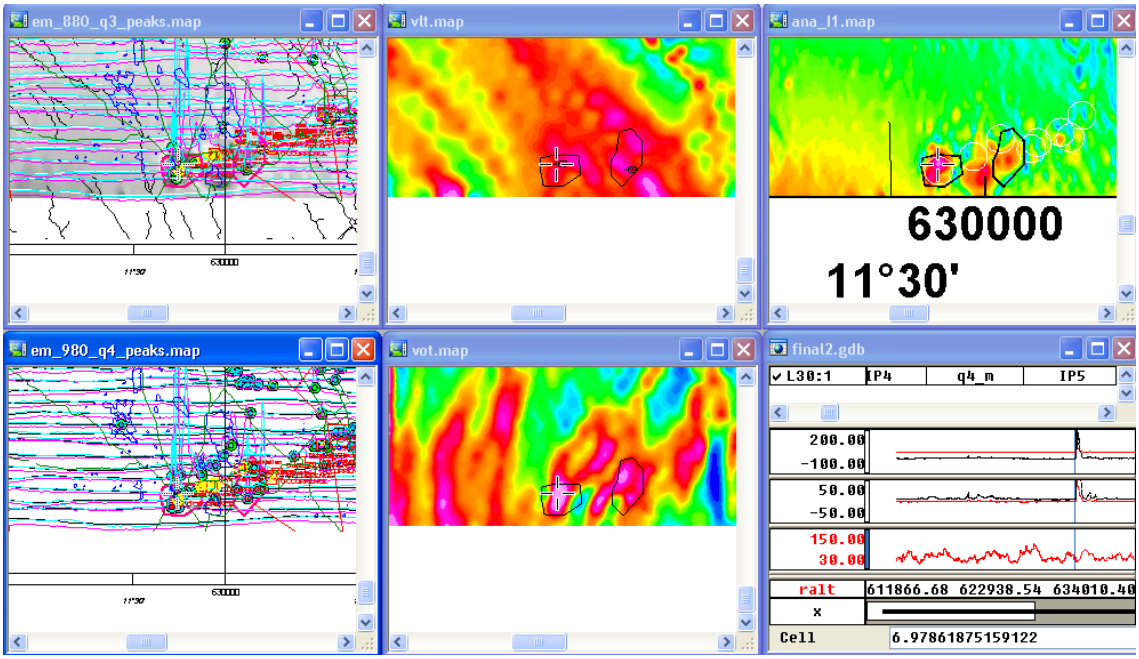

Figure 103. *Target Røros 68; group of medium to large EM peaks; coincident VLF anomalies; adjacent short wavelength magnetic anomalies; priority 1*

(a)

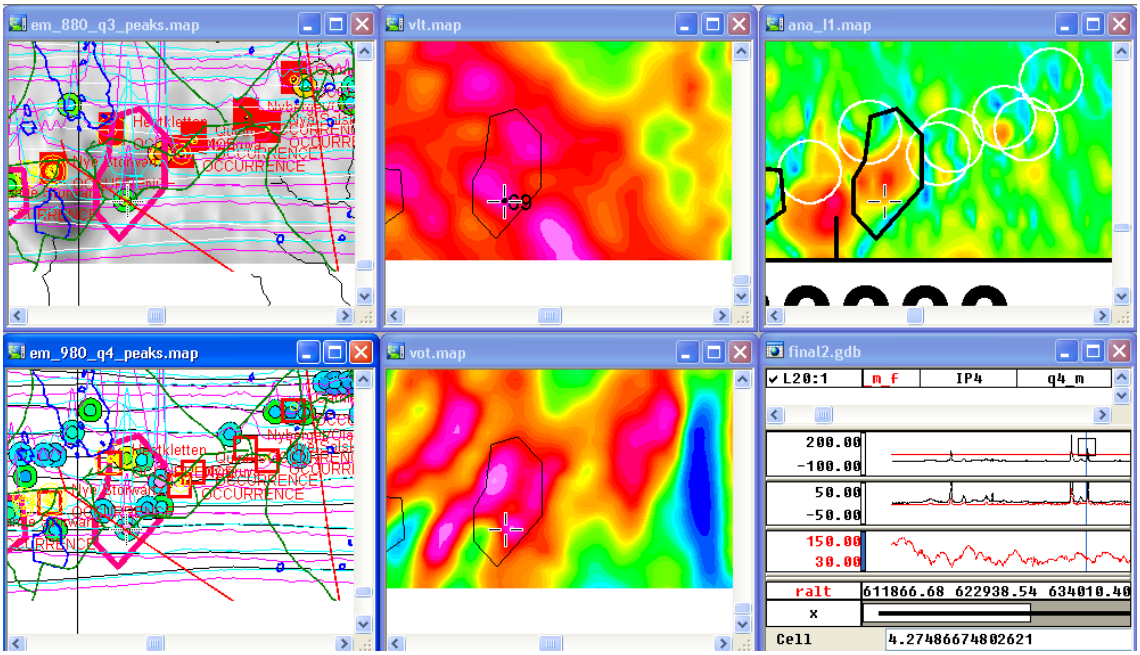

(b)

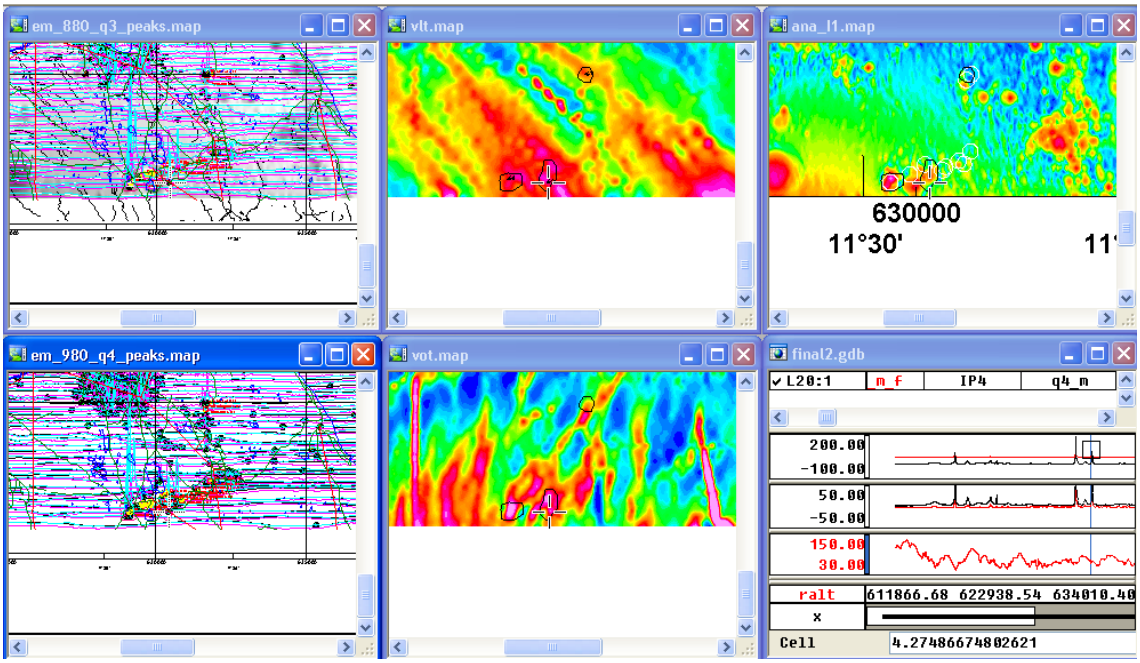

Figure 104. *Target Røros 69; elongated group of medium to large EM peaks; coincident VLF anomalies; adjacent short wavelength magnetic anomalies; priority 1*

(a)

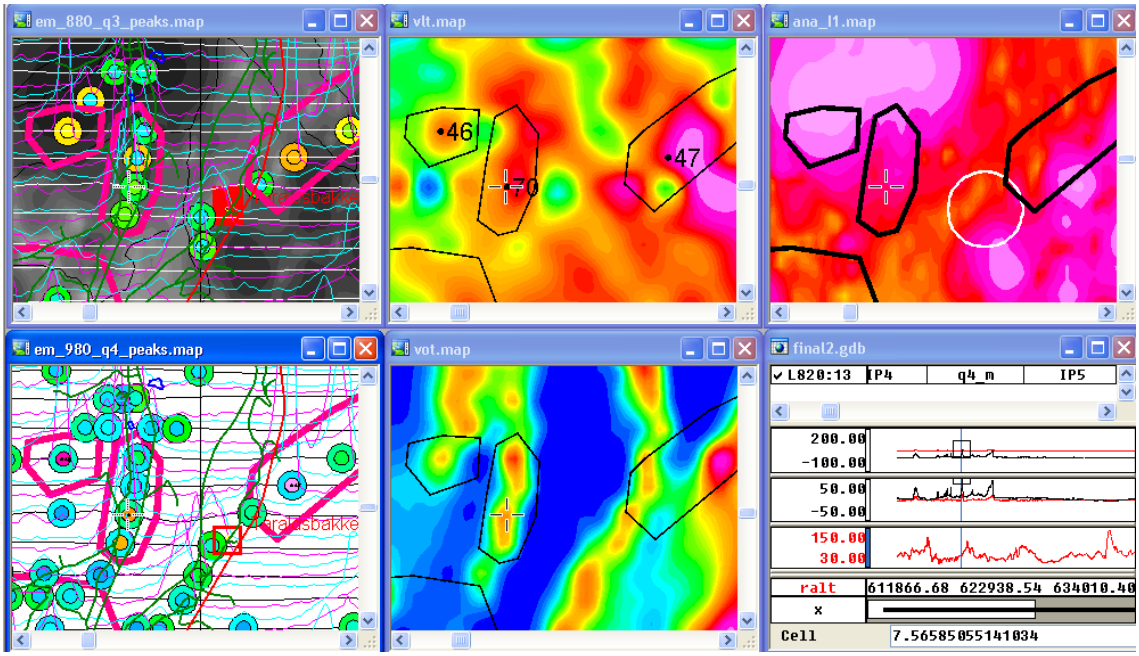

(b)

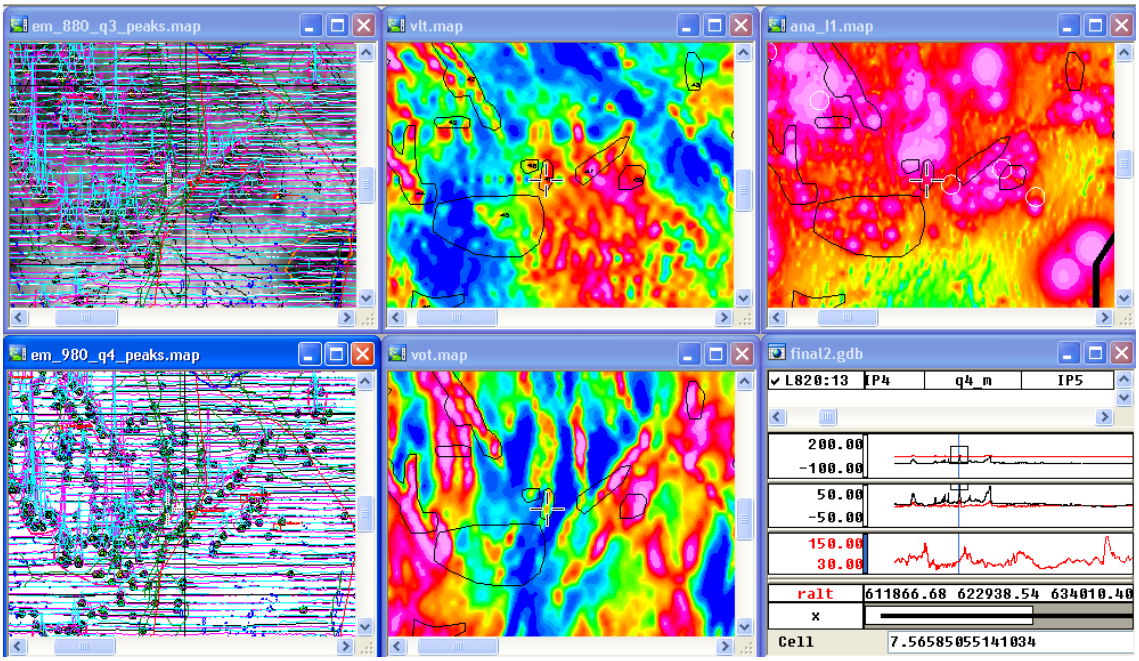

Figure 105. *Target Røros 70; elongated group of medium EM peaks; coincident VLF anomalies; adjacent short wavelength magnetic anomalies; priority 3*

(a)

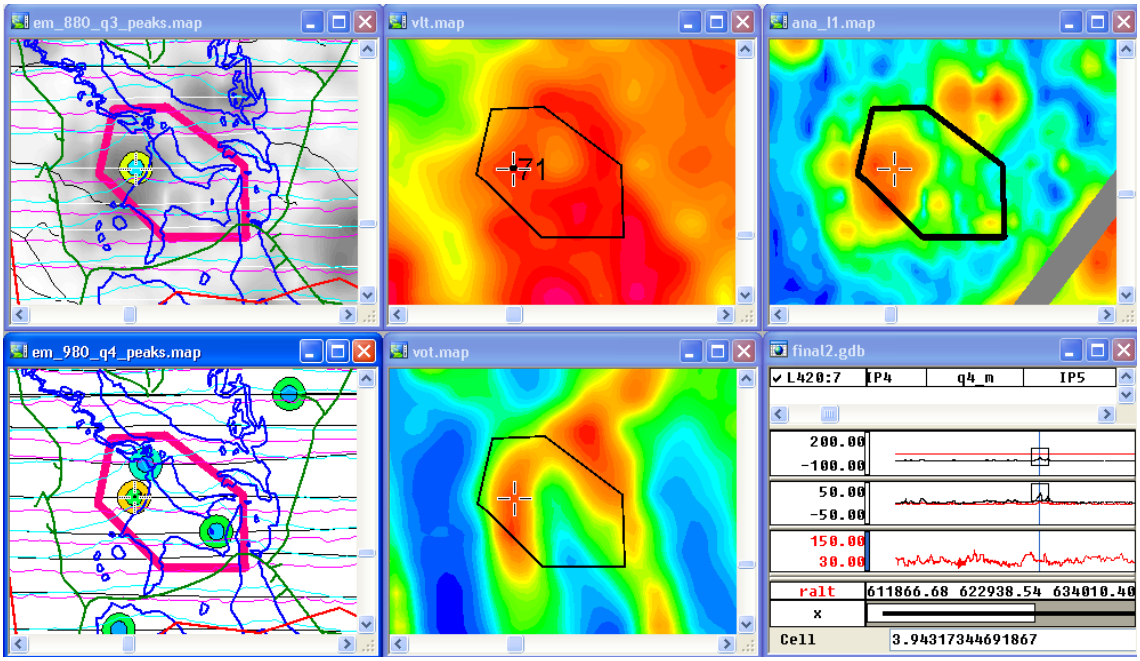

(b)

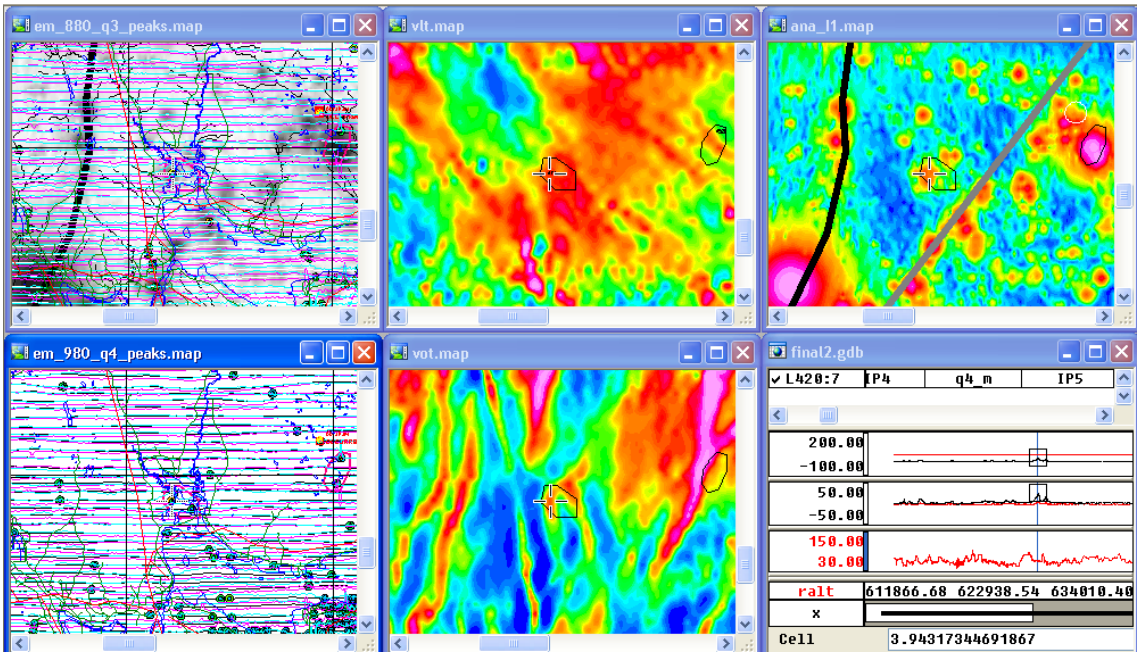

Figure 106. *Target Røros 71; a few medium EM peaks; coincident VLF anomalies; adjacent short wave-length magnetic anomalies and on magnetic boundary; priority 3*

(a)

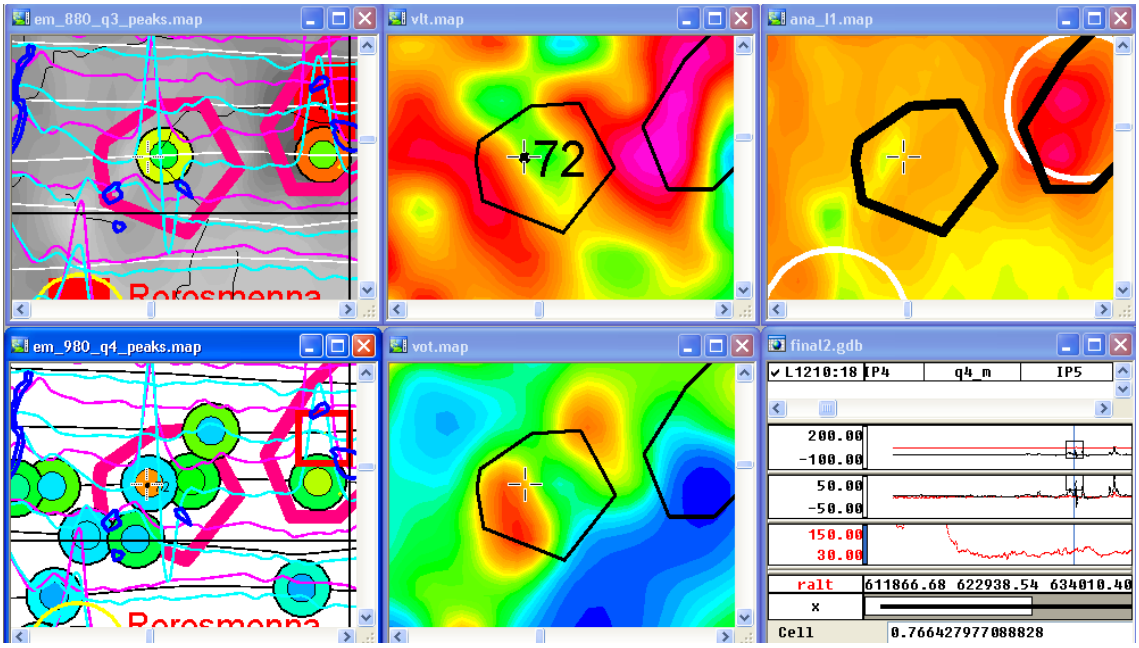

(b)

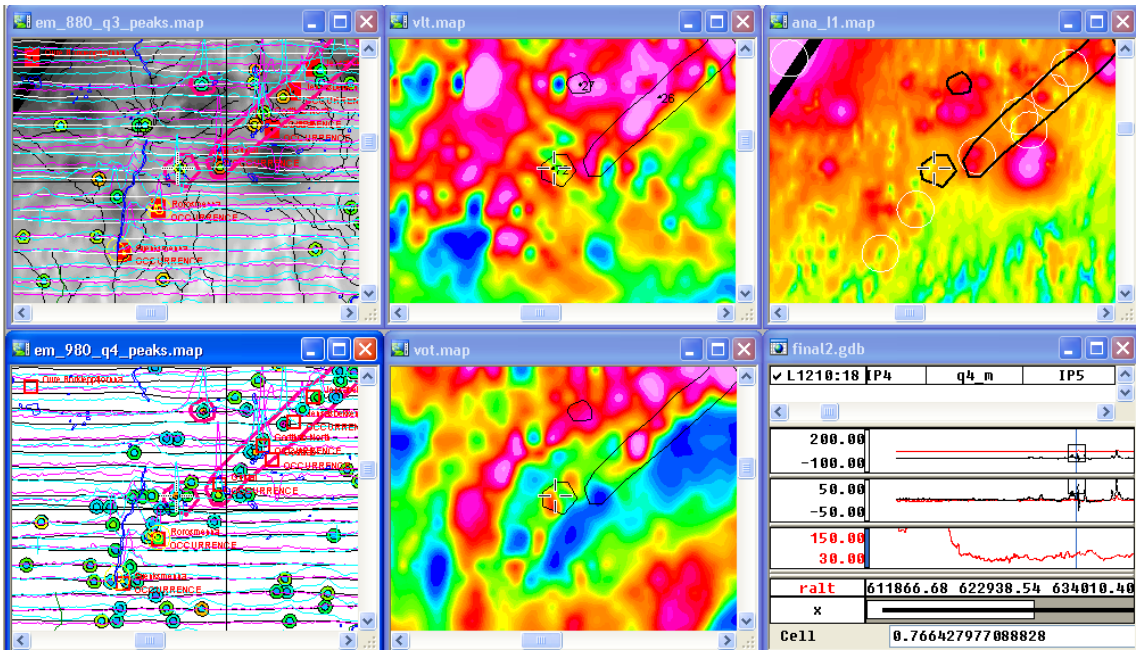

Figure 107. *Target Røros 72; elongated group of EM peaks; coincident VLF anomalies; adjacent short wavelength magnetic anomalies and on magnetic boundary; priority 1*